Check for updates

View Article Online
View Journal

ChemComm

Chemical Communications

Accepted Manuscript

This article can be cited before page numbers have been issued, to do this please use: Y. Li, Z. Sui, J. Zheng, H. Cui, Z. Yan, K. Jiang and L. Li, *Chem. Commun.*, 2026, DOI: 10.1039/D6CC01653G.

Volume 54
Number 1
4 January 2018
Pages 1-112

ChemComm
Chemical Communications
rsc.li/chemcomm

ISSN 1359-7345

ROYAL SOCIETY OF CHEMISTRY

COMMUNICATION
S. J. Connon, M. O. Senge *et al.*
Conformational control of nonplanar free base porphyrins: towards bifunctional catalysts of tunable basicity

This is an Accepted Manuscript, which has been through the Royal Society of Chemistry peer review process and has been accepted for publication.

Accepted Manuscripts are published online shortly after acceptance, before technical editing, formatting and proof reading. Using this free service, authors can make their results available to the community, in citable form, before we publish the edited article. We will replace this Accepted Manuscript with the edited and formatted Advance Article as soon as it is available.

You can find more information about Accepted Manuscripts in the Information for Authors.

Please note that technical editing may introduce minor changes to the text and/or graphics, which may alter content. The journal's standard Terms & Conditions and the Ethical guidelines still apply. In no event shall the Royal Society of Chemistry be held responsible for any errors or omissions in this Accepted Manuscript or any consequences arising from the use of any information it contains.

ROYAL SOCIETY
OF CHEMISTRY

rsc.li/chemcomm

View Article Online
DOI: 10.1039/D6CC01653G

Platinum-Based High-Entropy Alloys for Electrocatalysis: Preparation, Applications and Prospects

Yehao Li[a,e], Zhuyin Sui[b,*], Jinghe Zheng[c], Hongzhi Cui[a,*], Zhenhua Yan[d], Kun Jiang[e,*], Leigang Li[a,*]

[a]College of Materials Science and Engineering, Ocean University of China, Qingdao 266100, China.

[b]School of Chemistry & Chemical Engineering, Yantai University, Yantai 264005, China.

[c]China Special Equipment Inspection and Research Institute, Chaoyang District, Beijing 100029, China.

[d]Key Laboratory of Advanced Energy Materials Chemistry (Ministry of Education), College of Chemistry, Nankai University, Tianjin 300071, China.

[e]Shanghai Key Laboratory of Electrochemical and Thermochemical Conversion for Resources Recycling, Collaborative Innovation Center of Chemistry for Energy Materials, Department of Chemistry, Fudan University, Shanghai 200438, China.

[*]E-mail: suizy@ytu.edu.cn; cuihongzhi@ouc.edu.cn; kunjiang@fudan.edu.cn; lilg@ouc.edu.cn

View Article Online
DOI: 10.1039/D6CC01653G

Abstract

Platinum-based high-entropy alloys (Pt-HEAs), composed of multiple principal elements in near-equiatomic ratios, have emerged as a transformative class of electrocatalysts that overcome the long-standing activity-stability-cost trade-off associated with conventional Pt catalysts. The unique high-entropy effect, severe lattice distortion, sluggish atomic diffusion, and synergistic multi-metal interactions endow Pt-HEAs with tunable electronic structures, abundant heterogeneous active sites, and exceptional resistance to corrosion and sintering. This review systematically summarizes recent advances in the rational design, synthesis, and electrocatalytic applications of Pt-HEAs. We first outline the thermodynamic and kinetic fundamentals governing entropy-stabilized solid-solution formation, followed by a comprehensive comparison of state-of-the-art synthetic strategies, including electrodeposition, laser-based manufacturing, carbothermal shock, high-temperature liquid shock, spray-drying-assisted reduction, Joule heating, and microwave-assisted processes. We then discuss the electrocatalytic behavior of Pt-HEAs in key reactions including hydrogen evolution reaction, oxygen evolution reaction, hydrogen oxidation reaction, and oxygen reduction reaction. Particular emphasis is placed on mechanistic insights revealed by advanced in situ/operando characterization and density functional theory calculation. Finally, we propose the remaining challenges and future opportunities in composition design, precise structural control, entropy-defect coupling, machine-learning-assisted discovery, and industrial-scale catalyst integration. This review aims to provide a mechanistic framework and design principles for advancing Pt-HEAs toward next-generation, high-performance, and durable electrocatalysts for clean-energy conversion technologies.

Keywords: Platinum; High-entropy alloys; Electrocatalysis; Water splitting; Fuel cell

View Article Online
DOI: 10.1039/D6CC01653G

1. Introduction

In the exploration of clean energy conversion and utilization technologies, electrocatalytic materials have always been the "core engine" driving key reactions.[1] Since the wide application of Pt in catalyzing oxygen reduction reaction (ORR) at the cathode of fuel cells in the 1960s, Pt-based catalysts have long been regarded as the benchmark in the electrocatalysis field due to their unique electronic structures and high activity. However, the high cost and limited reserves of Pt, coupled with the degradation of structure and performance during long-term operation, have posed bottlenecks for its large-scale applications.[2] Early studies mainly focused on reducing Pt dosage through alloying strategies, for example, forming binary or ternary alloys with transition metals such as Ni,[3] Co,[4] and Fe[5] to achieve the regulation of surface electronic structures and optimization of strain effects. Although this strategy has made certain progress, the limited component combinations make it difficult to balance catalytic activity and stability simultaneously. Against this backdrop, the proposal of high-entropy alloys (HEAs) has opened up a new path for the design of catalytic materials. The concept of HEAs was first proposed by Yeh et al. in 2004, with the core concept of forming a highly disordered solid solution structure using five or more elements in near-equiatomic ratios.[6] Thermodynamically and kinetically, the unique properties of HEAs can be rationalized by four interrelated core effects: the high configurational entropy effect, severe lattice distortion, sluggish atomic diffusion, and the cocktail (synergistic) effect.[7] These effects are intrinsically coupled rather than independent, collectively governing the phase stability, electronic structure, and catalytic behavior of HEAs (Fig. 1).

View Article Online
DOI: 10.1039/D6CC01653G

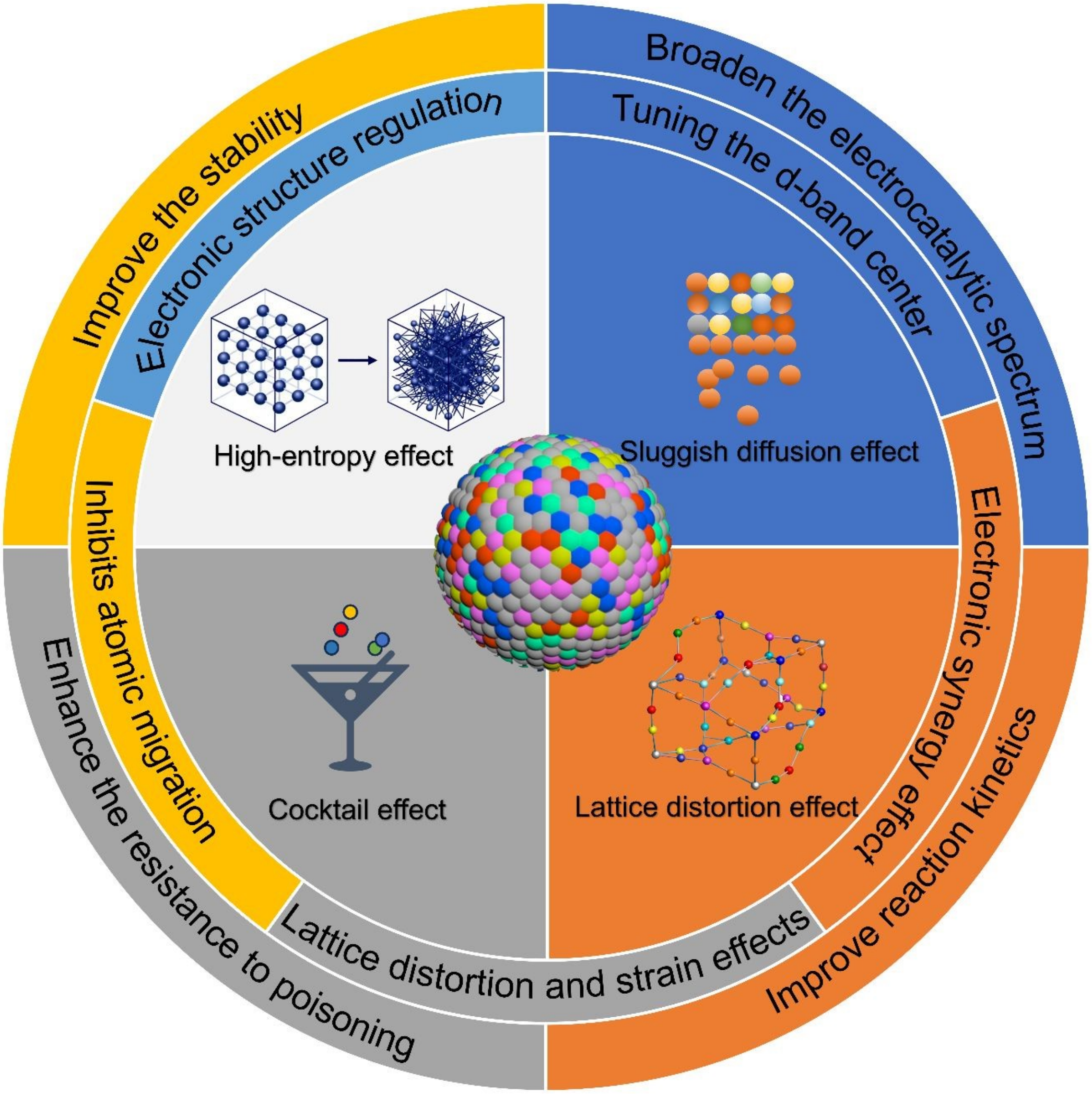

Fig. 1 Four "core effects" and performance enhancing mechanisms of HEAs.

The high configurational entropy effect arises from the near-equiatomic incorporation of multiple principal elements, which significantly lowers the Gibbs free energy of solid-solution phases and suppresses the formation of intermetallic compounds or phase segregation. This entropy-driven stabilization enables the formation of single-phase HEAs even among elements with large differences in atomic radius, electronegativity, and crystal structure, providing a robust structural

View Article Online
DOI: 10.1039/D6CC01653G

foundation for catalytic applications.[8] Meanwhile, the coexistence of multiple elements inevitably induces severe lattice distortion, leading to non-uniform local strain fields and heterogeneous coordination environments.[9] Such lattice distortion modifies the electronic structure of surface atoms, broadens the distribution of adsorption energies, and enables continuous tuning of the d-band center features that are particularly advantageous for optimizing the adsorption and desorption energies of key reaction intermediates in electrocatalysis.[10] In addition, the complex multi-elemental energy landscape gives rise to sluggish atomic diffusion, which increases diffusion barriers and suppresses long-range atomic migration. This kinetic effect effectively inhibits nanoparticle sintering, phase coarsening, and element dissolution under harsh electrochemical conditions, thereby significantly enhancing the long-term durability of HEA catalysts.[11,12] Beyond these thermodynamic and kinetic contributions, the cocktail effect describes the non-linear synergistic interactions among different constituent elements. Through electronic coupling, charge redistribution, and orbital hybridization, HEAs exhibit emergent properties that cannot be predicted from their individual components. For catalytic systems, this effect enables multi-active-site formation and cooperative reaction pathways, offering a powerful means to break conventional activity-stability trade-offs and scaling-relation limitations encountered in traditional low-entropy alloys.[13] These four core effects together constitute the theoretical foundation of the high-entropy paradigm and provide a unified framework for understanding the exceptional catalytic activity, durability, and tunability of HEAs.

The introduction of HEA concept into Pt-based catalytic systems further amplifies the inherent advantages of Pt. On the one hand, the dilute distribution of Pt atoms in HEAs can effectively reduce Pt dosage, while the local environment of Pt is regulated by surrounding multi-component

View Article Online
DOI: 10.1039/D6CC01653G

elements, thereby achieving effective adjustment of adsorption energy.[14] On the other hand, theoretical simulations and first-principles calculations have shown that Pt-based HEAs exhibit multi-active-site distribution and excellent energy barrier reduction effects in key reactions such as ORR,[15] hydrogen evolution reaction (HER),[16] and oxygen evolution reaction (OER).[17] This has made Pt-based HEAs gradually become a research hotspot in the field of electrocatalysis in recent years. Rather than representing a simple progression from precious-metal saving to high-entropy system construction, the development of Pt-based HEAs should be viewed as an expansion of Pt-based catalyst design strategies. Although reducing noble-metal usage remains an important motivation, the practical advantage of Pt-HEAs cannot be inferred solely from composition, because advanced low-Pt architectures such as Pt-skin structures, Pt monolayers on Pd-based cores, and Pt-transition-metal intermetallics can also achieve high Pt utilization and excellent activity. In this context, the distinctive value of Pt-based HEAs lies in their broad compositional flexibility, diverse local atomic environments, and the opportunity to couple electronic regulation with structural robustness within a single alloy framework. With the rapid development of atomic-level synthesis, in situ/operando characterization, and machine-learning-assisted calculations, Pt-based HEAs are expected to provide a broader platform for understanding structure–property relationships and for designing next-generation electrocatalysts

Since 2023, the research activity on Pt-based HEAs has grown rapidly, with an increasing number of publications reporting novel electrocatalysts and improved performance in alcohol oxidation and fuel cell applications. Recent reviews have further highlighted that high-entropy materials, especially nanostructured HEAs, are emerging as an important electrocatalyst platform, and their development is increasingly guided by rational design strategies rather than empirical composition

View Article Online
DOI: 10.1039/D6CC01653G

screening.[18,19] This surge is accompanied by a significant increase in high-impact publications, indicating that Pt-based HEAs have transitioned from a niche academic concept to a mainstream strategy for next-generation electrocatalysts.[20,21] Compared with conventional Pt-based alloys, many recently reported Pt-based HEAs have shown competitive or improved activity and durability in representative electrocatalytic reactions.[22,23] In practical membrane electrode assemblies (MEAs), Pt-based HEAs have demonstrated more than 90% performance retention after on the order of 100,000–200,000 durability cycles, in line with recent durability assessments reported for advanced electrocatalysts.[24]

Driven by the ultra-low platinum group metals (PGM) loading and long-term durability targets proposed by the U.S. DOE Hydrogen Shot and European hydrogen initiatives, high-entropy precious-metal-based catalysts have recently emerged as a promising materials platform to simultaneously enhance mass activity and structural stability in proton exchange membrane fuel cells (PEMFCs).[25] Recent studies indicate that Pt-based HEA anodes enable substantially improved power performance and durable operation in direct ethanol fuel cells (DEFCs), reflecting the rapid progress of HEA electrocatalysts in alcohol oxidation applications.[26,27] More strikingly, the ultra-high mixing entropy and severe lattice distortion unique to Pt-based HEAs enable simultaneous optimization of multiple reaction descriptors that were previously considered mutually exclusive, such as breaking ORR/OER scaling relations, approaching optimal hydrogen adsorption free energy (ΔG_{H^*}) for HER, and achieving intrinsic CO poisoning resistance.[28,29] Recent in situ/operando X-ray absorption spectroscopy (XAS) and identical-location transmission electron microscope (TEM) studies further reveal that the local coordination environment of Pt atoms in HEAs remains highly stable even under 1.5 V high potential or 1 A cm^{-2} high current

View Article Online
DOI: 10.1039/D6CC01653G

density, consistent with the robustness of multi-component Pt sites reported in advanced structural investigations.[30,31] Collectively, these advances suggest that Pt-based HEAs are emerging as a compelling materials platform for addressing the long-standing trade-offs among activity, stability, and cost that have constrained Pt-based electrocatalysis.

This review article will systematically review the research progress of Pt-based HEAs in the field of electrocatalysis. First, it will introduce the design concepts and typical synthesis methods. Subsequently, it will summarize their applications and performance in key reactions such as ORR, HER, and OER. Finally, it will reveal the origin of their activity and stability mechanisms by combining theoretical calculations and experimental studies.

2. Preparation of Pt-based HEAs

In recent years, the synthesis of Pt-based HEAs has evolved from traditional high-temperature smelting to atomic-level precise control.[32,33] Beyond conventional alloying, recent design-oriented reviews have emphasized the importance of composition regulation, morphology engineering, strain/defect control, and phase modulation in optimizing the electrocatalytic behavior of high-entropy materials.[34] However, current synthesis of Pt-based HEAs still faces critical challenges. Significant differences in atomic radii and chemical properties between Pt and other metals readily induce elemental segregation or formation of heterogeneous structures (e.g., intermetallic compounds), which disrupt the solid-solution characteristics of HEAs. Traditional high-temperature methods struggle to balance compositional uniformity and nanoscale structural control. Additionally, a trade-off exists between active site exposure and stability: ultrasmall nanoparticles (<3 nm) enhance specific surface area but are prone to sintering or dissolution during

View Article Online
DOI: 10.1039/D6CC01653G

catalysis.[35] Therefore, developing rational synthesis strategies that can simultaneously achieve compositional homogeneity, nanoscale structural control, and structural stability is highly desirable. In response to these challenges, a variety of synthetic approaches have been proposed in recent years to regulate the alloying process and structural evolution of Pt-based HEAs.

2.1 Electrodeposition method

Electrodeposition has emerged as an efficient and controllable method for preparing HEAs, and is particularly advantageous for designing functional materials with synergistic effects from multiple elements. This bottom-up synthetic strategy has garnered substantial attention due to its ability to afford precise control over the morphology and composition of nanostructures by modulating deposition parameters, such as potential, time, and template characteristics.

In this context, Fu et al.[36] employed a soft-template-assisted electrochemical deposition approach (Fig. 2a), in which polystyrene-b-poly(oxyethylene) (PS_{1800}-b-PEO_{7500}) served as the template to fabricate mesoporous HEA thin films (Fig. 2b) at a specific potential of −0.2 V (vs. Ag/AgCl). The as-prepared HEA films consisted of five constituent elements: Pt, Pd, Rh, Ru, and Cu. By tailoring the molecular weights of block copolymers, mesopores with distinct sizes were obtained. Controlling the deposition time enabled precise regulation of film thickness while maintaining the integrity of the mesoporous architecture. The surface of the resulting m-HEA thin films exhibited uniformly distributed mesopores with average pore sizes of 25.32 ± 3.01 nm and 25.26 ± 3.04 nm, respectively. The films featured abundant defects and a low work function, which facilitated the exposure of numerous active sites, promoted electron transfer kinetics, and enhanced catalytic activity. Notably, the mass activity of the m-HEA films toward the methanol oxidation reaction

View Article Online
DOI: 10.1039/D6CC01653G

(MOR) reached 4.2 A mg_{Pt}^{-1}, representing 7.2-fold and 35-fold enhancements compared to mesoporous Pt films and commercial Pt black, respectively.

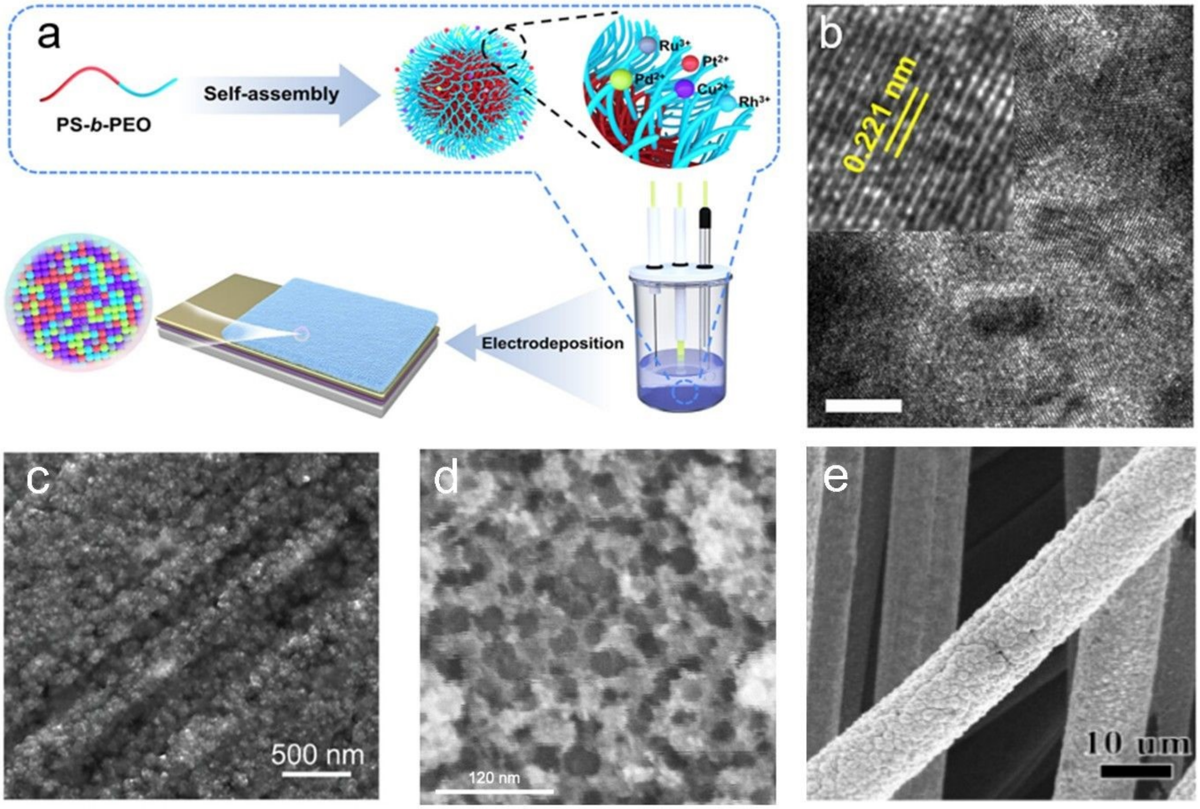

Fig. 2 (a) Schematic illustration of the electrodeposition of m-HEA film using block polymers. (b) High-resolution transmission electron microscopy (HRTEM) image of m-HEA film. Reproduced with permission.[36] Copyright 2024, American Chemical Society. (c) FESEM image showing the morphology of HEA with the solvent system D:A = 4:1. Reproduced with permission.[37] Copyright 2024, Wiley-VCH. (d) Top-view SEM image of the m-HEA film. Reproduced with permission.[38] Copyright 2025, Royal Society of Chemistry. (e) SEM images of HEA $Pt_1Bi_2Co_1Cu_1Ni_1$/CC. Reproduced with permission.[39] Copyright 2024, American Chemical Society.

View Article Online
DOI: 10.1039/D6CC01653G

Through theoretical calculation, Chandran et al.[37] predicted that the optimal elemental composition of the electrocatalyst comprised Pt, Pd, Ni, Co, and Mn. And they synthesized the HEA via electrodeposition in a mixed organic solvent system of N, N-dimethylformamide (DMF) and acetonitrile. Following systematic optimization of the electrolyte composition and deposition potential, the optimal conditions were established as a 4:1 DMF/acetonitrile mixture and a deposition potential of 1.5 V. The catalyst prepared under these conditions exhibited superior performance, achieving an overpotential of 22.6 mV at 10 mA cm^{-2} toward HER, which outperformed commercial Pt/C. Moreover, the HEA catalyst demonstrated excellent activity and stability in both simulated and real seawater environments. Thermodynamic analysis based on average free energy further revealed that its adsorption behavior toward reaction intermediates was more favorable than that of pure Pt, underscoring the synergistic advantages of the multi-elemental composition (Fig. 2c). Saso et al.[38] reported a polymer micelle-templated electrochemical deposition strategy for synthesizing m-HEA films containing eight elements (Pt, Pd, Rh, Ru, Cu, Au, Se, and Mo). By precisely tuning the deposition potential, the configurational entropy of the mixed system was maximized (>1.95R) (Fig. 2d). Zheng et al.[39] developed an innovative electrochemical deposition approach to fabricating Pt-based HEA nanocomposites ($Pt_1Bi_2Co_1Cu_1Ni_1$/CC). By monitoring the reaction process, they elucidated the growth mechanism of the material. Notably, the introduction of Bi as a morphology-directing agent enabled precise control over the nanosheet structure by adjusting the concentration of the Bi precursor (Fig. 2e).

2.2 Laser-based method

HEAs fabricated by traditional methods such as vacuum arc melting and powder metallurgy are prone to grain coarsening, compositional segregation, or phase separation due to low cooling rates

View Article Online
DOI: 10.1039/D6CC01653G

or process limitations.[40] Laser synthesis of HEAs, as an emerging preparation technology, has shown significant advantages in material performance control, structural design, and production efficiency. At present, most of the laser synthesis methods need to prepare complex alloy targets in inert gas or vacuum.[41,42]

For example, Guo et al.[43] developed a strategy called FLASH for preparing multi-component alloy nanoparticles (Fig. 3a). This strategy consists of two steps: preparation of microreactor substrates and reduction of metal precursors by laser etching technology. The microreactor substrate prepared by laser etching polyimide film has an internal structure composed of three-dimensional porous graphene. This method realizes the synthesis of high-entropy alloy nanoparticles (HEA-NPs) in air. The HEA prepared by this method has uniform composition. It was found that the five element alloy nanoparticles, whether composed of noble metals or non-noble metals, could form stable single-phase solid solutions. Through experiments and theoretical calculations, it is revealed that the porous graphene microreactor can effectively prevent the combination of oxygen and transition metals, so as to realize the synthesis of non-oxidized nanoparticles.

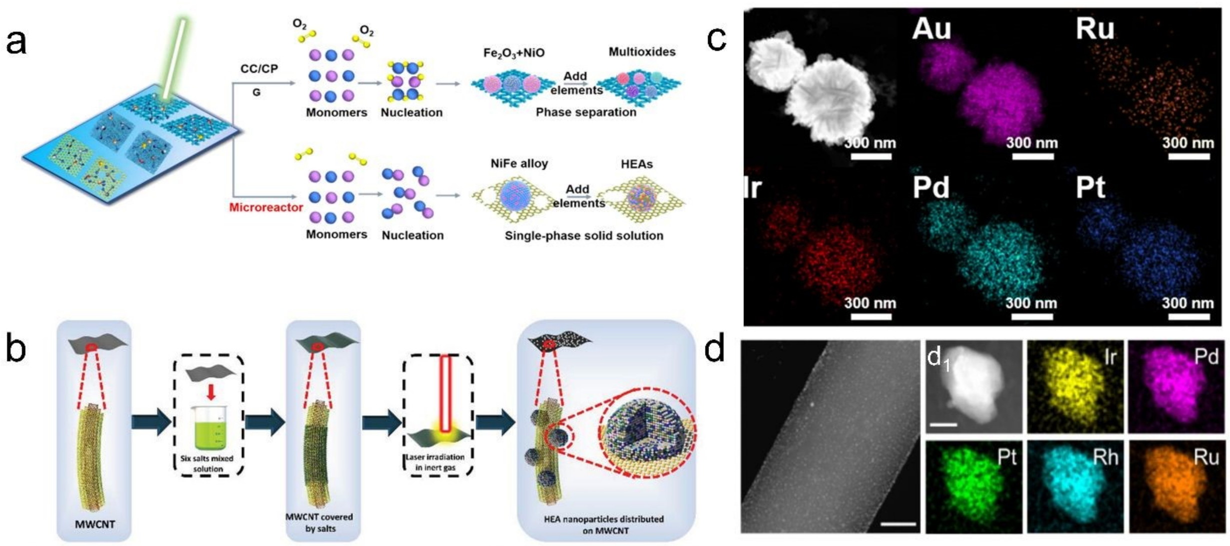

View Article Online
DOI: 10.1039/D6CC01653G

Fig. 3 (a) Schematic diagram for the synthesis of single-phase HEA solid solution NPs and phase-separated oxides on different hosts via the FLASH strategy. Reproduced with permission.[43] Copyright 2024, American Chemical Society. (b) Laser irradiation synthesis of HEA on MWCNTs. Reproduced with permission.[44] Copyright 2022, Wiley-VCH. (c) HAADF-STEM element mapping images of the flowers in HEA-60 synthesized via the CW CO_2 laser. Reproduced with permission.[45] Copyright 2024, Royal Society of Chemistry. (d) HAADF STEM image of IrPdPtRhRu HEA-NPs/CFs, scale bar of 100 nm. (d_1) HAADF STEM image and EDS elemental mappings of IrPdPtRhRu HEA-NPs, scale bar of 10 nm. Reproduced with permission.[46] Copyright 2025, Elsevier.

Similarly, ultrafast laser-induced thermal processes have also been exploited to enable rapid synthesis of HEA nanoparticles on carbon supports. Lu et al.[44] prepared a precursor solution by dissolving equimolar amounts of Fe, Co, Ni, Cu, Pt, and Ir metal precursors in ethanol. Multi-walled carbon nanotube (MWCNT) paper was subsequently immersed in this solution and dried at room temperature, resulting in a uniform coating of metal precursors on the MWCNT surface to form a precursor-support composite (Fig. 3b). This composite was then subjected to ultrafast pulsed laser irradiation. Benefiting from the rapid thermal effect induced by the interaction between the laser and the carbon substrate, the metal precursors were completely decomposed, and the decomposed metal atoms recombined to form HEA nanoparticles uniformly anchored on the MWCNT surface, yielding the HEA@MWCNT composite catalyst. The entire laser irradiation process was completed within less than one millisecond, which drastically shortened the synthesis time compared with conventional time-consuming HEA fabrication techniques such as arc melting and solvothermal methods, demonstrating great potential for scalable production. Moreover, the

View Article Online
DOI: 10.1039/D6CC01653G

pulsed laser's non-continuous irradiation mode effectively suppressed grain growth, leading to uniformly dispersed HEA nanoparticles with an average diameter below 10 nm and without noticeable aggregation, thereby providing abundant exposed active sites for catalytic reactions.

In addition, laser-based approaches have been further explored for the rapid synthesis of diverse HEA systems. Myong Yong Choi et al.[45] employed continuous-wave CO_2 laser irradiation (90 s) to rapidly synthesize AuRuIrPdPt HEA. Among the samples, the HEA-60 prepared at 60% laser power exhibited optimal morphology, the most abundant active sites, and the lowest charge-transfer resistance (Fig. 3c). Yu et al.[46] developed a laser thermal reduction strategy for the rapid and large-area synthesis of multicomponent HEA-NPs with controllable size and composition and broad substrate compatibility. The as-prepared IrPdPtRhRu HEA-NPs exhibited outstanding HER activity and durability across a wide pH range, featuring low overpotential and excellent cycling stability, offering a promising pathway for the rational design of highly efficient electrocatalysts (Fig. 3d).

2.3 Carbon thermal shock technology

Carbon thermal shock (CTS) technology is a synthesis method to reduce metal precursors and form HEAs through rapid temperature rise and fall. Its core is to use the high conductivity and thermal stability of carbon-based materials (such as carbon nanofibers,[47] and graphene[48] to achieve rapid reduction and alloying of metal salts combined with instantaneous high temperature (usually higher than 1000 °C). CTS is considered to have great potential for preparing HEAs. However, the difference of reduction kinetics of various metals may lead to uneven distribution of elements,

View Article Online
DOI: 10.1039/D6CC01653G

especially in the system of complex components, which is prone to local segregation or incomplete alloying. In addition, there may also be a problem of excessive grain size.

The development of CTS synthesis by Yao et al.[49] marked a conceptual breakthrough in constructing high-entropy nanocatalysts, particularly those incorporating Pt as key active components. In their pioneering work, Yao and co-workers demonstrated that applying an ultrafast Joule heating pulse to mixed metal salts supported on conductive carbon leads to rapid formation of single-phase solid-solution HEA nanoparticles composed of up to eight mutually immiscible elements. This nonequilibrium process bypasses the thermodynamic constraints that typically limit multimetallic alloying in wet-chemical or furnace-based syntheses, allowing simultaneous liquid-state mixing and quenching-induced kinetic trapping, thereby preventing phase segregation even among elements with disparate reduction potentials, atomic radii, and crystal structures. Moreover, Yao's work uncovered the critical role of catalytic fission-fusion behavior of transient liquid metal droplets, driven by both high temperature and substrate-mediated dispersion, which results in nanoscale HEAs featuring narrow size distributions and maximized configurational entropy. These findings not only expanded the synthesis window for Pt-based HEAs but also provided the first mechanistic foundation for ultrafast entropy-driven alloying at the nanoscale.

Following this milestone, Huang and colleagues advanced CTS from a purely alloying technique to a platform enabling rational control over nanoparticle dispersion and loading by engineering carbon substrates.[50] They used different solvents (water, ethanol, and their mixtures) and carbon carriers treated differently (unoxidized, oxidized) to prepare precursors. The average particle size of the W/U-PtFeCoNiMn/C catalyst prepared using water as the solvent is 5.98 nm. After replacing

View Article Online
DOI: 10.1039/D6CC01653G

water with ethanol, the average particle size of E/U-PtFeCoNiMn/C catalyst decreased to about 3.51 nm, with a reduction of about 41% and a more uniform particle size. Using mixed solvents of water and ethanol in different ratios, as the ethanol ratio increases, the average particle size of the synthesized HEA catalyst decreases. In detail, for V_{water}:$V_{ethanol}$ = 4:1, it is 4.17 nm; for 1:1, it is 3.86 nm, and for 1:4, it is 3.52 nm (Fig. 4a–f). The interaction between the original carbon carrier and nanoparticles is weak. After moderate oxidation treatment of the carbon carrier, the E/O-PtFeCoNiMn/C catalyst prepared using ethanol and oxidized carbon simultaneously has a HEA-NPs size precisely controlled at about 2.68 nm. Low concentration of polarity solvents (such as ethanol) can weaken the interactions between metal ions and form small ion clusters. Carbon carriers rich in dangling bonds can enhance the interaction between ion clusters and carbon surfaces, limiting the growth of nanoparticles. Finally, the size of E/O-PtFeCoNiMn HEA nanoparticles was controlled at approximately 2.68 nm, and the catalyst exhibited higher activity than Pt/C. Through tuning conductivity, defect density, and surface oxygen species, they demonstrated that CTS is substrate-coupled: the carbon matrix does not merely serve as mechanical support but actively governs nucleation kinetics, dispersion uniformity, and alloy homogeneity during the sub-millisecond heating stage. In contrast to Yao's primarily composition-centered demonstration, Huang's work[50] introduced design principles related to substrate chemistry and pulse-modulated growth dynamics, enabling higher spatial density of Pt-based HEA nucleation and scalable formation to substrate-directed engineering. It highlights an emerging direction in CTS synthesis: leveraging nonequilibrium thermodynamics not only to access metastable Pt-based HEAs, but also to structurally and spatially optimize them for catalytic deployment.

View Article Online
DOI: 10.1039/D6CC01653G

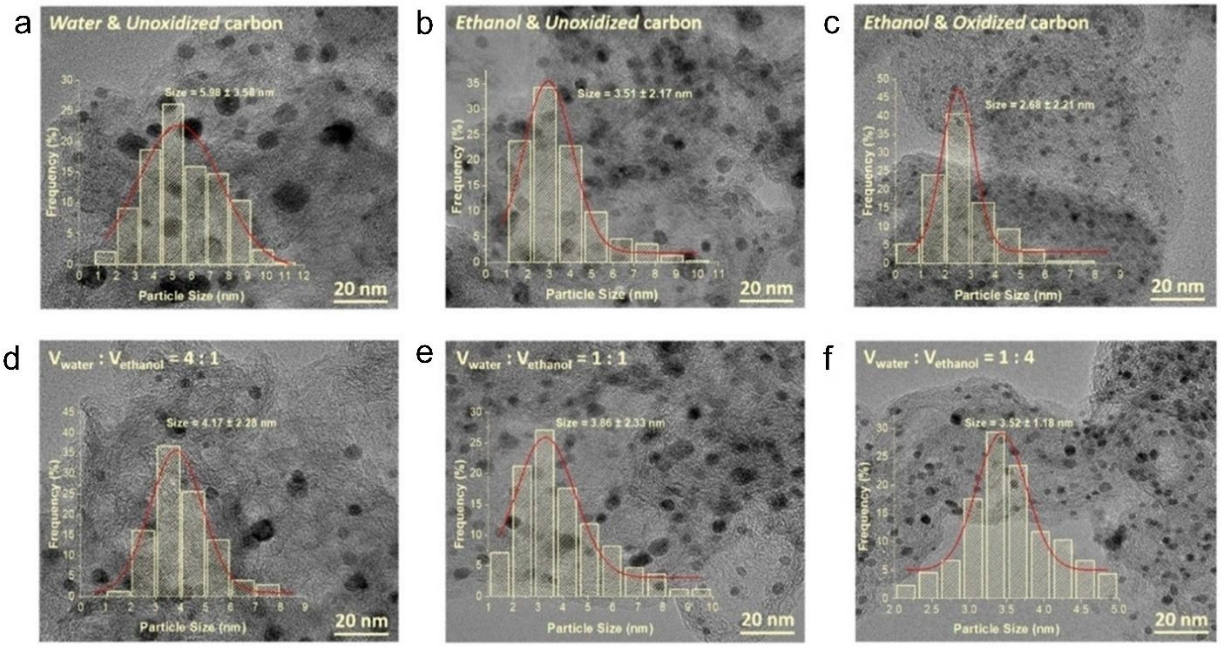

Fig. 4 (a) TEM image and size distribution of the W/U-PtFeCoNiMn/C catalyst derived using water as the solvent and unoxidized carbon as the support. (b) TEM image and size distribution of the E/U PtFeCoNiMn/C catalyst derived using ethanol as the solvent and unoxidized carbon as the support. (c) TEM image and size distribution of the E/ O-PtFeCoNiMn/C catalyst derived using ethanol as the solvent and oxidized carbon as the support. (d) TEM image and size distribution of the W:E (4:1)/O-PtFeCoNiMn/C catalyst derived using hydroalcoholic solution (V_{water}:$V_{ethanol}$ = 4:1) as the solvent and oxidized carbon as the support. (e) TEM image and size distribution of the W:E (1:1)/O-PtFeCoNiMn/C catalyst. (f) TEM image and size distribution of the W:E (1:4)/O-PtFeCoNiMn/C catalyst. Reproduced with permission.[50] Copyright 2024, Elsevier.

2.4 Spray drying-thermal decomposition reduction

In the realm of HEA synthesis, numerous methods have been developed to suppress elemental diffusion and phase separation via ultra-rapid heating and quenching processes occurring on millisecond-to-second timescales, thereby leading to the formation of single-phase solid solutions

View Article Online
DOI: 10.1039/D6CC01653G

or metastable architectures. Typical methods encompass the carbothermal shock approach,[49] microwave-assisted heating technique,[51] and moving-bed pyrolysis strategy.[52] Nevertheless, these approaches inherently entail the requirement for extremely rapid thermal ramping rates, sophisticated heating apparatuses, and specific substrate/carrier systems, thus posing substantial challenges for the realization of straightforward, cost-effective, and scalable synthesis protocols.

The spray drying method is a technique for preparing micro-to-nano-scale powder particles by atomizing a homogeneous solution or suspension into tiny droplets, which undergo rapid solvent evaporation (typically water or organic solvents) in a hot gas stream. Zhao et al.[53] synthesized Pt-based HEA nanoparticles using a spray drying-thermal decomposition reduction (SD-TDR) method (Fig. 5g). This approach involves dissolving precursor metal salts in deionized water and mixing them with graphene oxide (GO) to form a stable precursor solution (SSP). The SSP is then spray-dried at 165 °C to deposit well-dispersed multi-metal precursor nanoparticles (MPNPs) onto the GO surface. Finally, the spray-dried precursor supported on GO is reduced under a H_2 atmosphere with a moderate heating rate (3 °C/min), thermal decomposition temperatures ranging from 300 to 850 °C, a holding time of 30 min, and a cooling rate of 5-10 °C/min.

Atomized droplets achieve ultra-high velocity ($V > 58$ m/s) within a transport distance of less than 0.01 m, coupled with a heating rate exceeding 10^4 °C/s, ensuring the entire drying process is completed within 0.6 s. This rapid kinetics guarantees fast and uniform precipitation of elements, avoiding segregation or local aggregation. The abundant oxygen-containing functional groups on the GO surface enhance substrate hydrophilicity, enabling homogeneous anchoring of the precursor solution onto GO via hydrogen bonding. No obvious nanoparticle agglomeration or

View Article Online
DOI: 10.1039/D6CC01653G

elemental clustering/segregation is observed in the final GO-supported precursor materials. By tuning the thermal decomposition temperature (TDT) within the range of 150–850 °C, the average size of HEA-NPs can be precisely regulated from approximately 2 nm to 13 nm (Fig. 5a–f). The as-synthesized PtCoCuRuFeNi nanoparticles exhibit superior electrocatalytic performance toward MOR compared to commercial Pt/C. In their study, Zhao et al. demonstrated that Pt-containing HEA-NPs can be synthesized at a low thermal decomposition temperature of 300 °C. In contrast, Pt-free multimetallic nanoparticles (MMNPs) exhibit phase separation, elemental segregation, uncontrollable micro-morphology, and a significantly higher decomposition temperature (>400 °C). Among monometallic nanoparticles, Pt develops an initial face centered cubic (FCC) crystal structure at 150 °C, while other metal precursors remain unreduced at 300 °C. Upon the addition of Pt, Pt-based binary alloy nanoparticles form an FCC crystal structure free of precursor salt phases or other metallic phases at 300 °C.

In a separate work, Zhao et al.[54] employed the same method to synthesize HEA three-dimensional nanoframes (HEA-3DNFs) with quinary to octonary compositions, including Pt-based, Ir-based, Ru-based, and PtRu-based HEAs. Precious metal elements such as Pt, Ru, and Ir can be reduced by H_2 at relatively low temperatures (300 °C), whereas non-precious metal elements (Ni, Co, Cu, Fe) remain unreduced under the same conditions when present in isolation (Fig. 5h and i). The introduction of Pt lowers the reduction temperatures of Ni, Co, Cu, and Fe, facilitating the formation of single-phase solid-solution alloys. Concurrently, the study reveals that adjusting the Pt/Ru ratio and treatment temperature enables precise control over phase composition. When the Ru ratio exceeds that of Pt, characteristic peaks of the hexagonal-close-packed (HCP) structure emerge. However, increasing Ru content alone is insufficient to induce a complete phase transition

View Article Online
DOI: 10.1039/D6CC01653G

from FCC to HCP. Reheating the PtNiCoCuRu sample to elevated temperatures activates atomic mobility within the FCC lattice. These activated atoms overcome energy barriers, ultimately forming a more thermodynamically stable Ru-rich HCP structure.

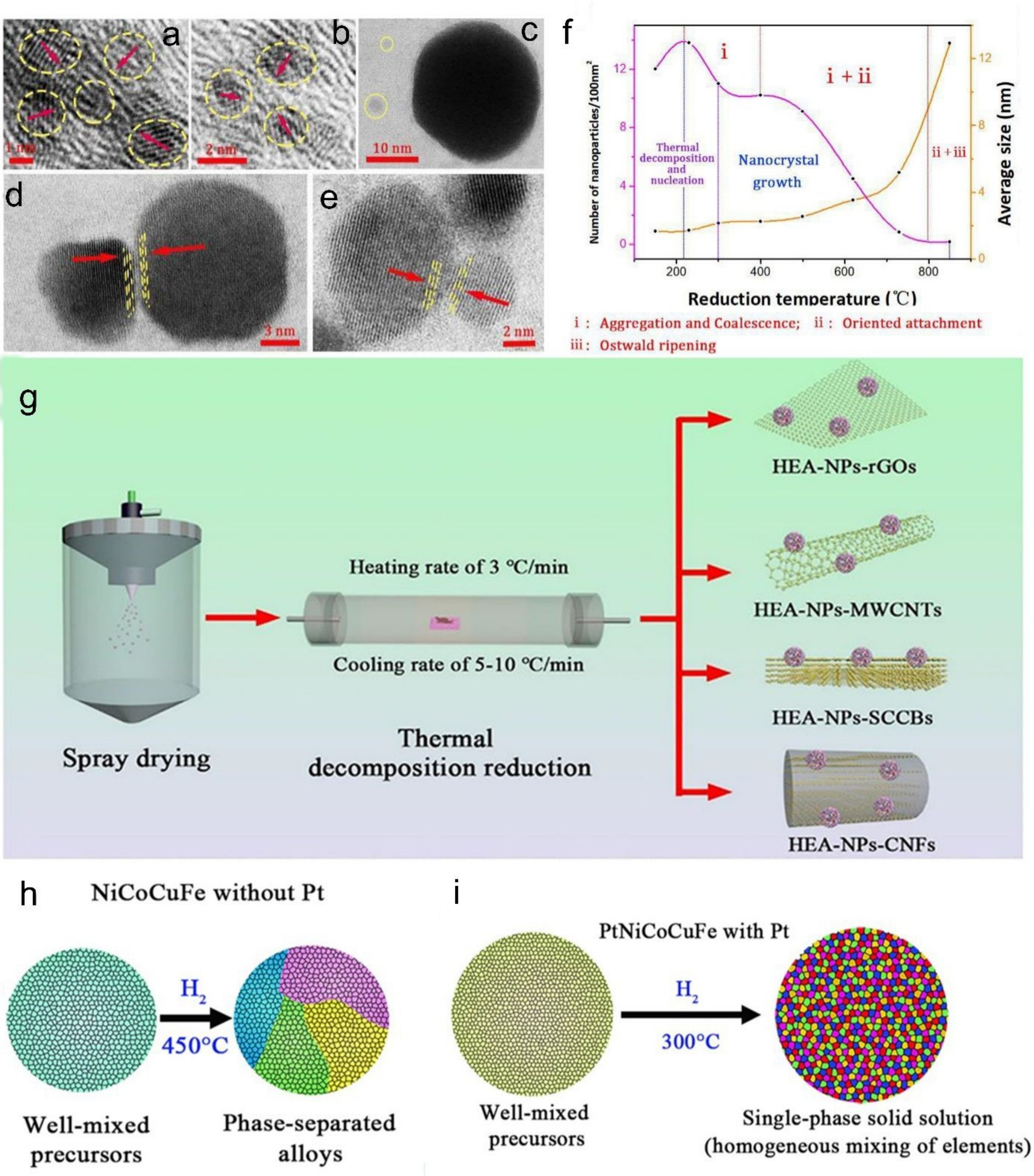

View Article Online
DOI: 10.1039/D6CC01653G

Fig. 5 (a–e) TEM and ABF-STEM images of Pt-based HEA-NPs synthesized at different reduction temperatures: (a) 400 °C, (b) 500 °C, (c) 850 °C, (d) 620 °C, and (e) 730 °C. (f) The trend of number of nanoparticles per 100 nm^2 and average size with increasing reduction temperature. (g) Schematic diagram of SD-TDR method. Reproduced with permission.[53] Copyright 2022, American Chemical Society. (h) Formation diagram of phase-separated alloy in the absence of Pt. (i) Formation diagram of single-phase solid solution HEA in the presence of Pt. Reproduced with permission.[54] Copyright 2022, The American Association for the Advancement of Science.

2.5 Joule heating technique

Joule heating technique represents a preeminent ultra-rapid method widely employed in nanomaterials synthesis. By applying direct current or pulsed current to preformed compacts, electrical energy is converted into thermal energy via contact resistance among powder particles and bulk resistance of the material, enabling rapid heating of the compact to the sintering temperature. Under the synergistic action of elevated temperature and external pressure, diffusion, fusion, and densification occur among powder particles, culminating in the fabrication of bulk HEAs.[55]

In this context, Zhang et al.[56] exploited the Joule heating protocol to mix transition metal chloride salts with carbon black, followed by lyophilization, and subsequent ultra-rapid pyrolysis at 1500 °C under nitrogen atmosphere (Fig. 6a). The entire process was completed within 0.35 seconds, achieving atomic-level homogeneous dispersion and integration of Pt, Fe, Co, Ni, and Ir elements. TEM characterization revealed that PtFeCoNiIr/C nanocomposites exhibited an average particle size of 2 ± 0.5 nm (Fig. 6b). Systematic investigations on varying pyrolysis temperatures

View Article Online
DOI: 10.1039/D6CC01653G

and durations indicated that particle size exhibited a significant positive correlation with both parameters, while showing negligible dependence on metal loading. HRTEM characterization revealed a lattice spacing of 0.225 nm, which corresponds well to the characteristic (111) crystallographic plane (Fig. 6c). X-ray diffraction (XRD) analysis exhibited characteristic diffraction patterns of FCC crystal structure, consistent with pure Pt or Ir reference standards, with no observable diffraction peaks from pure Co, Ni, Fe phases or their compounds, confirming the formation of homogeneous solid solutions. The PtFeCoNiIr/C catalyst demonstrated exceptional electrocatalytic performance, featuring low onset potential, high peak current density, and robust anti-ammonia poisoning capability in ammonia oxidation reaction (AOR). Besides, it also showed superior half-wave potential and durability in ORR, as well as low overpotential, high turnover frequency, and stability in HER.

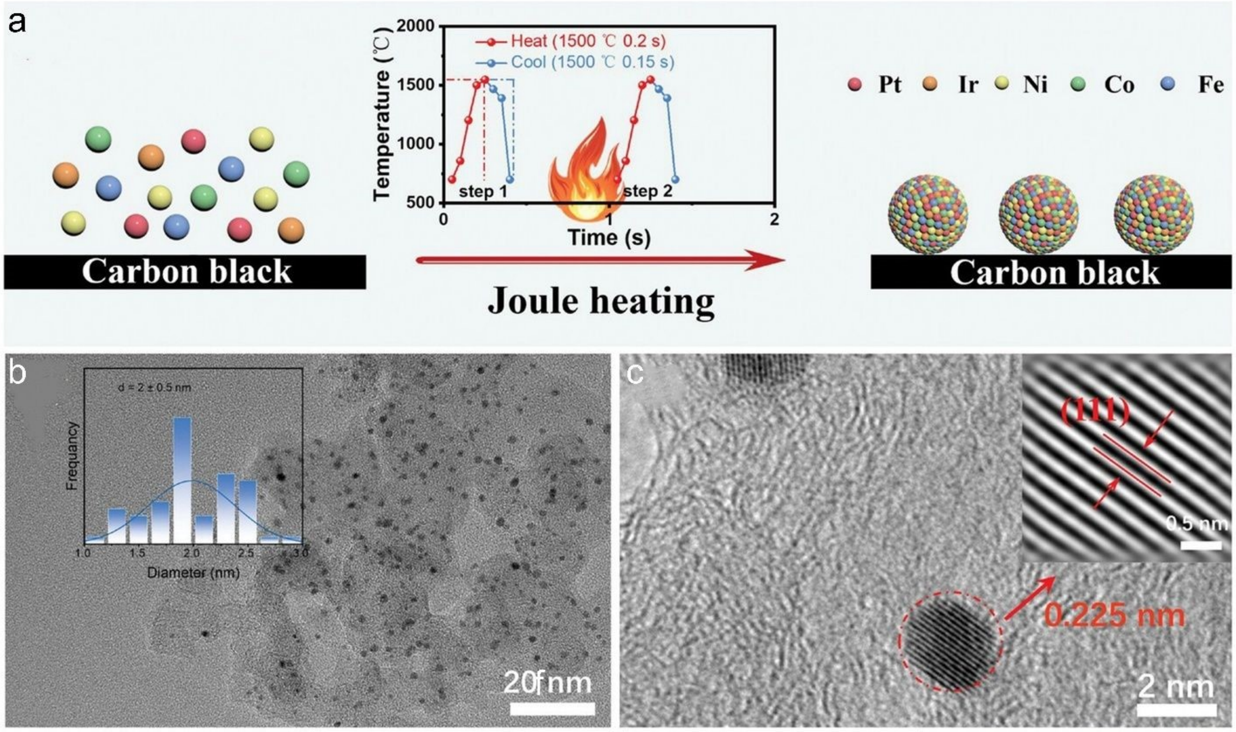

View Article Online
DOI: 10.1039/D6CC01653G

Fig. 6 Synthesis principles and morphologies analysis. (a) Schematic diagram of the preparation process of PtFeCoNiIr/C. (b) TEM image (inset: size distribution), (c) HRTEM image. Reproduced with permission.[56] Copyright 2024, Wiley-VCH.

The strategy of ultrafast synthesis of HEAs under extreme conditions has been extensively studied, but the preparation of small-scale ultrafine HEA nanoparticles using ultrafast synthesis strategy remains a challenge. On the contrary, the reaction process of liquid-phase method is more convenient and easier to control. However, traditional liquid-phase methods have slow heating and cooling rates, and long reaction time. Cui et al.[57] used high-temperature liquid shock (HTLS) technology to prepare HEA-NPs (Fig. 7a), hoping to solve the shortcomings of traditional joule heating methods and obtain nano-catalysts with adjustable elemental composition, ultrafine particle size, controllable crystal phase and lattice strain. Using metal acetylacetonate as precursor, carbon black as substrate, oleylamine and oleic acid as surfactant and solvent. After ultrasonic and magnetic stirring, the precursor was decomposed into metal cations and adsorbed on the surface of carbon black. HTLS was carried out in a high-temperature reactor at 750 K argon atmosphere. The heating and cooling rates were 1200 and 840 K min^{-1}, respectively, which was much higher than the traditional method. HTLS could rapidly freeze atoms, promote the formation of multi-element single-phase HEA, and retain the high entropy structure. The PtCoNiRuIr HEA-NPs synthesized by HTLS method have an average diameter of 3.24 nm and are uniformly and densely anchored on carbon black (Fig. 7b). The synergistic effect of oil amine and oleic acid makes the nanoparticle size uniform and well dispersed. Compared with other rapid synthesis methods, the HEA prepared by HTLS method has smaller particle size and faster synthesis speed. HTLS method combines joule heating and liquid environment, with fast heating and cooling rate, high reaction

View Article Online
DOI: 10.1039/D6CC01653G

temperature and long duration, and can regulate the morphology, size, dimension and crystal phase of HEA-NPs, overcoming the limitations of traditional methods. The prepared PtCoNiRuIr HEA-NPs showed ultra-low overpotential and high stability for HER, which was superior to the commercial Pt/C catalyst.

Beyond compositional control, recent studies have shown that Joule heating can be coupled with support and interface engineering to construct structurally stabilized HEA catalysts. Wang et al.[58] synthesized self-encapsulated quinary HEA-NPs (PtNiCoFeCu@ACW) within activated carbonized wood (ACW) through Joule heating followed by rapid quenching. Driven by defect-engineered surface modulation, the HEA nanoparticles nucleate in situ at defect sites of ACW and become encapsulated by a carbon shell. This structure significantly enhances the interfacial stability between the catalyst and the support (Fig. 7c). Zou et al.[59] fabricated noble-metal high-entropy alloy (NM-HEA) thin films with a subsurface amorphous structure on glassy carbon electrodes by combining atomic layer deposition (ALD) with electro-Joule heating. The resulting HEA films exhibit outstanding HER activity in acidic, neutral, and alkaline electrolytes (Fig. 7d). Ahn et al.[60] developed an oxide-assisted rapid Joule heating strategy to prepare oxide-encapsulated HEA nanoparticles. The oxide overlayer promotes precursor adsorption, suppresses particle growth, and strengthens metal-support interactions, thereby achieving high activity and exceptional stability in CO_2 conversion reactions (Fig. 7e and f).

View Article Online
DOI: 10.1039/D6CC01653G

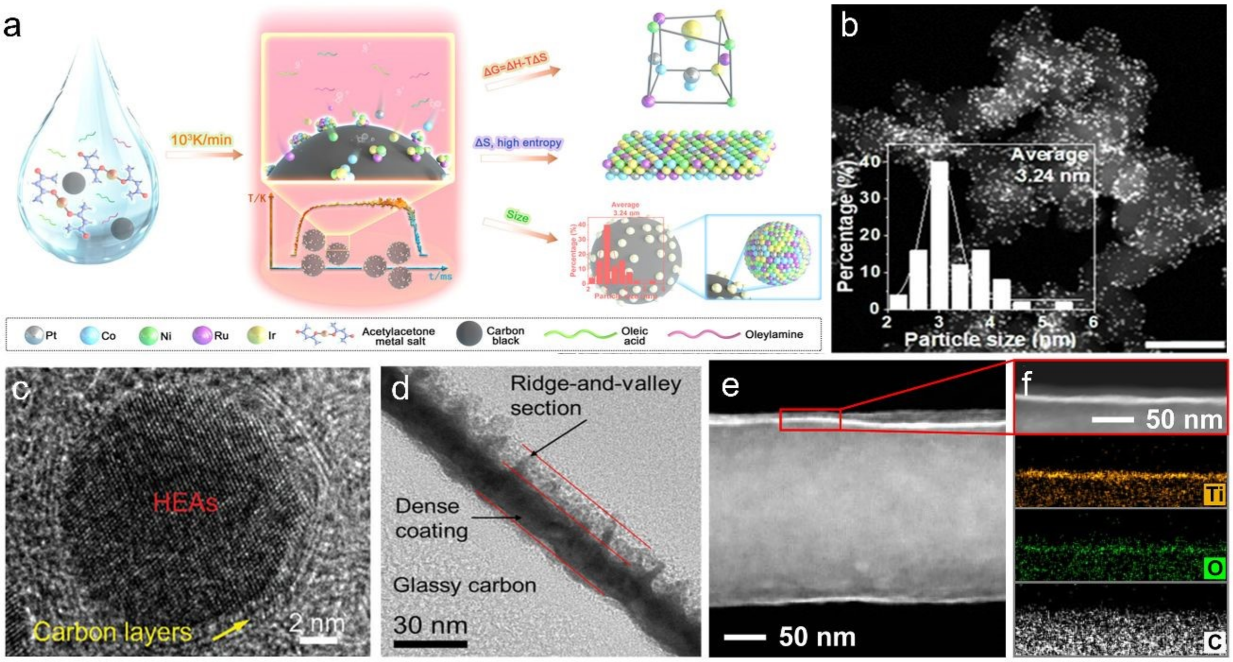

Fig. 7 (a) Schematic illustration for the synthetic process of PtCoNiRuIr/C via a high-temperature liquid shock method. (b) Low-magnification TEM image of PtCoNiRuIr/C. Inset: statistical particle size distribution of PtCoNiRuIr HEA-NPs. Reproduced with permission.[57] Copyright 2024, American Chemical Society. (c) HRTEM images of HEAs@ACW present the HEAs encapsulated by the carbon layers. Reproduced with permission.[58] Copyright 2024, Wiley-VCH. (d) Cross-sectional HR-TEM image of HEA/GC. Reproduced with permission.[59] Copyright 2024, Royal Society of Chemistry. (e) Reference STEM image of the surface of a single CNF@TiO_2 fiber and (f) the corresponding EDS chemical mapping images for Ti, O, and C. Reproduced with permission.[60] Copyright 2023, American Chemical Society.

2.6 Microwave-assisted synthesis

Microwave-assisted synthesis has recently emerged as an attractive strategy for fabricating Pt-based HEA, offering rapid energy delivery, uniform heating, and efficient promotion of multi-

View Article Online
DOI: 10.1039/D6CC01653G

metal atom mixing.[61] In this method, electromagnetic radiation interacts directly with dielectric or conductive substrates, typically reduced graphene oxide, carbon fibers, or other carbonaceous materials, creating highly localized and instantaneous thermal fields that facilitate precursor decomposition and alloy nucleation. The general procedure involves dispersing equimolar metal salts onto a microwave-responsive support, drying or pre-activating the composite, and subjecting it to either continuous or pulsed microwave irradiation. Within seconds, the system reaches temperatures sufficient to induce simultaneous reduction and transient melting, followed by rapid quenching that favors the formation of homogeneous solid-solution nanoparticles.[62] This process minimizes the diffusion barriers faced in traditional thermal routes and effectively suppresses phase segregation, allowing multi-metal elements to mix at the atomic level.

A representative example is the protocol developed by Qiao et al.[51] (Fig. 8a), in which GO films were partially reduced at 570 K under Ar to obtain rGO-570 with optimized dielectric loss. Equimolar Fe, Co, Ni, Pd, and Pt precursors (0.1 mmol each) were sonicated and drop-cast onto the rGO-570 film, dried, sealed under Ar, and irradiated in a 1200 W microwave for approximately 10 s. The rGO substrate reached approximately 1850 K within milliseconds and cooled at approximately 6×10^4 $K\cdot s^{-1}$, enabling precursor decomposition, transient metal melting, and ultrafast quenching to yield uniform approximately 12 nm PtPdFeCoNi HEA nanoparticles with a single FCC phase and homogeneous elemental distribution (Fig. 8b and c). Key parameters include the defect density of rGO, which governs microwave absorption, and precursor concentration, which strongly affects particle size. Notably, the resulting nanoparticles exhibited a higher Pt atomic ratio due to Pt's significantly lower vapor pressure versus Fe, Co, Ni, and Pd, leading to

View Article Online
DOI: 10.1039/D6CC01653G

less evaporation; this temperature-vapor pressure relationship provides a guideline for tuning compositions by adjusting precursor ratios (Fig. 8d).

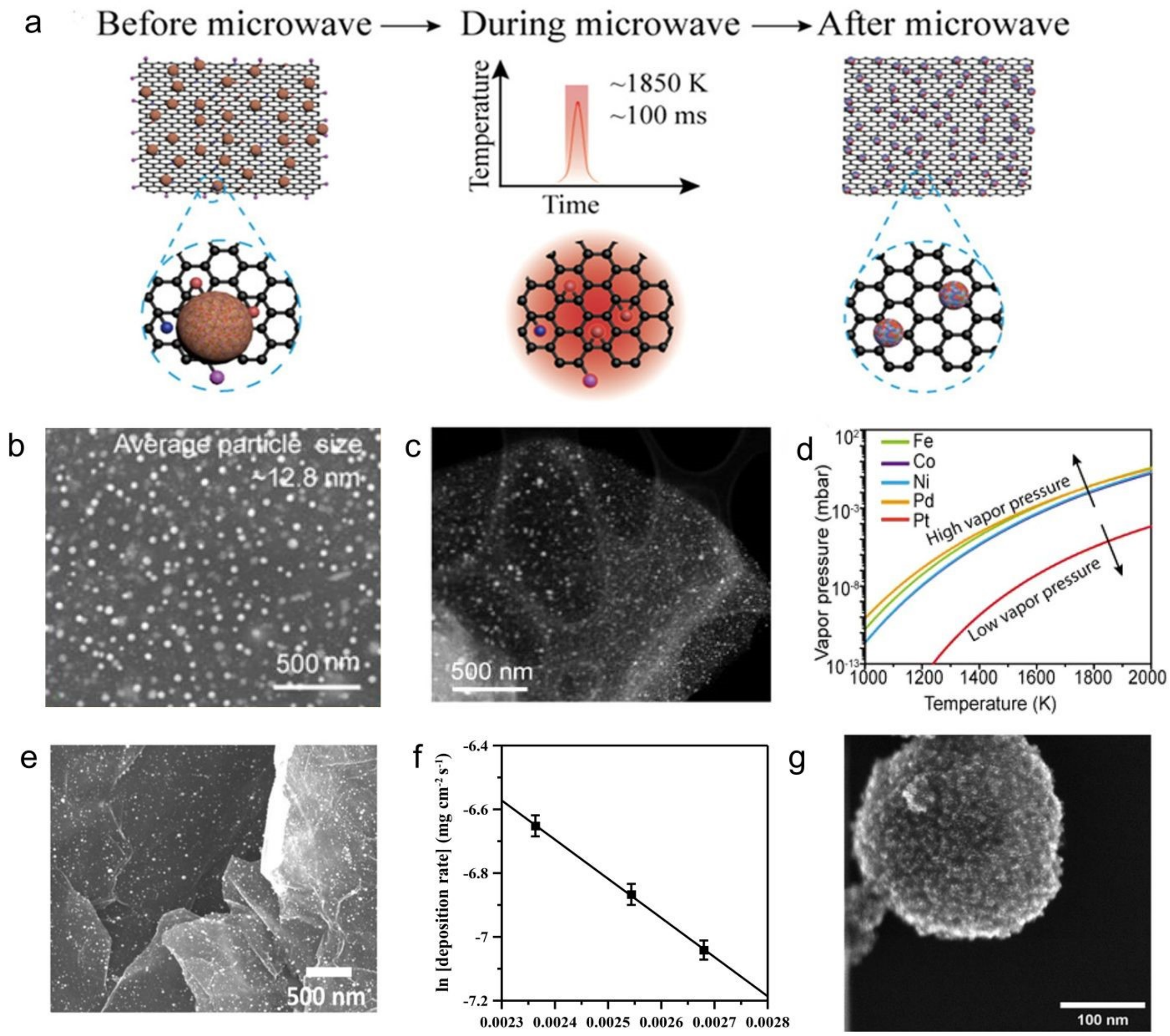

Fig. 8 (a) Schematic illustration of the formation of HEA-NPs on rGO by microwave heating. (b) SEM of the HEA-NPs/rGO film. (c) TEM image of the PtPdFeCoNi HEA-NPs on rGO substrates. (d) Relationship of temperature and vapor pressure for each element in the PtPdFeCoNi HEA-NPs. Reproduced with permission.[51] Copyright 2021, American Chemical Society. (e) Top-view FE-SEM images of Cu-HEA-GO catalysts. Reproduced with permission.[63] Copyright 2024,

View Article Online
DOI: 10.1039/D6CC01653G

Elsevier. (f) Arrhenius linear plot of ln [deposition rate] versus inverse temperature, ranged from 100 to 150 °C. Reproduced with permission.[64] Copyright 2025, Elsevier. (g) SE-STEM image of mesoporous Au HEA-NPs. Reproduced with permission.[65] Copyright 2025, Royal Society of Chemistry.

Complementary studies highlight the versatility of microwave chemistry. Khan et al.[63] demonstrated that low-temperature pulsed microwave irradiation (t_{on}:t_{off} = 3:2 s) enables the formation of small (4–10 nm), well-dispersed Pt-based HEA nanoparticles directly on graphene oxide by effectively separating nucleation and growth (Fig. 8e). Panda et al.[64] showed that modest temperature differences (100–150 °C) in liquid-phase pulsed microwave synthesis on carbon supports significantly affect crystallinity, growth kinetics, and electrochemically active surface area (ECSA) (Fig. 8f). Ni et al.[65] further expanded the methodology by integrating microwave heating with soft-templating, producing mesoporous RhAgCuPdPt HEA nanoparticles within only one minute at 130 °C, illustrating the compatibility of microwave activation with hierarchical structure formation (Fig. 8g). Together, these results highlight the advantages of microwave heating, including ultrafast reaction kinetics, inhibited phase segregation, and compatibility with scalable platforms, while also underscoring challenges associated with thermal uniformity, compositional reproducibility, and controlling high-temperature element mobility.

Overall, microwave-assisted synthesis offers several advantages, including ultrafast reaction kinetics, reduced energy consumption, minimized diffusion-driven segregation, and strong compatibility with scalable reactor designs. However, challenges still remain, such as controlling spatial thermal gradients, maintaining compositional reproducibility across multi-element systems,

View Article Online
DOI: 10.1039/D6CC01653G

and preventing element redistribution or volatilization under the extremely high transient temperatures. Nevertheless, the method provides a uniquely efficient route to generating homogeneous Pt-based HEAs and continues to gain prominence as a versatile tool for next-generation electrocatalyst development.

2.7 Comparison of methods

This section compares various preparation methods for Pt-based HEAs, including electrodeposition, laser scribing, carbothermal shock, high-temperature liquid shock, spray drying followed by thermal decomposition, and the Joule heating method. Overall, these methods each have their own advantages and disadvantages in terms of achieving uniform component mixing, controlling nanostructures, and implementing defect engineering: rapid thermal processes (such as CTS, HTLS, and Joule heating) can achieve uniform alloying of multiple components within a sub-second timescale, while mild methods (such as electrodeposition and spray drying) have greater advantages in morphological controllability and large-scale fabrication. However, due to the significant differences in atomic radius and chemical properties among the components, challenges such as elemental segregation, phase separation, and uncontrollable particle size still exist. Therefore, further in-depth exploration is required in process innovation and multi-component ratio design in the future to realize HEA catalysts with high stability and high uniformity.

Table 1 Summary of the characteristics of preparation methods of HEA catalysts.

Synthesis method	Timescale	Typical particle/film size	Elemental mixing level	Morphology & structural control

View Article Online
DOI: 10.1039/D6CC01653G

Electrodeposition	10 min–2 h	5–50 nm films/3–20 nm NPs	Good	Mesoporous, nanosheets, 3D
Laser-based method	1 ms–90 s	3–12 nm	Good	Spherical, anchored on CNT
Carbothermal shock	55 ms–2 s	2.0–5.5 nm	Good	Spherical, size tunable by solvent/substrate
Spray-drying thermal decomposition reduction	0.6 s (drying) + 30 min (reduction)	2–13 nm	Good	Nanoframes, size control by TDT
Rapid Joule heating	0.3–10 s	2–8 nm	Good	Ultrafine, dense on carbon encapsulated, wood-derived
Microwave-assisted method	10 s–3 min	4–15 nm	Good	Mesoporous, core-shell

Beyond activity-oriented synthesis, the practical value of Pt-based HEA preparation methods must also be judged by scalability, reproducibility, and industrial viability. In this respect, wet-chemical routes and electrodeposition offer relatively good compositional tunability and morphology control, but their batch-to-batch reproducibility may be affected by precursor chemistry, reduction kinetics, and local mass-transfer conditions, especially in multicomponent systems. Ultrafast methods such as carbothermal shock, Joule heating, laser-based synthesis, and microwave-assisted routes are highly effective for accessing metastable single-phase HEAs and suppressing phase segregation, yet they often rely on extreme transient temperature fields, specialized equipment, and narrow process windows, which may complicate scale-up and process consistency. By contrast, spray-drying-assisted routes seem more compatible with continuous powder production and thus are among the most promising methods for large-scale fabrication, although phase purity,

View Article Online
DOI: 10.1039/D6CC01653G

compositional homogeneity, and support integration still require careful control during downstream thermal reduction. Overall, no current method simultaneously satisfies atomic-level compositional homogeneity, precise nanostructure control, high reproducibility, and clear industrial scalability. Future progress should therefore move beyond proof-of-concept synthesis and focus on manufacturing-oriented optimization, including process standardization, batch consistency, energy efficiency, and compatibility with practical catalyst-layer fabrication.

3. Electrocatalytic applications of Pt-based HEA alloys

Electrocatalysis plays a central role in renewable energy conversion and storage systems, facilitating key reactions such as HER and ORR through the use of catalytic materials that lower activation energies and enhance reaction rates. The performance of these catalysts is critically determined by their ability to optimize adsorption energies of reaction intermediates, maximize active site availability, and maintain structural stability under operating conditions. Pt-based HEAs address these challenges via multi-component synergy and entropy stabilization. These characteristics not only enhance catalytic activity and durability but also introduce versatility across a wide pH range and diverse catalytic environments.

Table 2 Comparison of representative Pt-HEAs and Pt catalysts.

Reaction	Catalyst	Electrolyte	Activity	Stability	Ref
HER	HEA-QDs/C (PtRuMoFeCoNi)	0.5 M H_2SO_4	11 mV @10 mA/cm^2	~1000 h	66
	EE.300s (FeCoNiCrPt)	1.0 M KOH	18 mV @10 mA/cm^2	~500 h	67
	Ru-PtFeNiCuW/CNTs	0.5 M H_2SO_4 & 1.0 M KOH	9/16 mV @10 mA cm^{-2}	~1200 h	68
	IrCuNiPdPt/C HEA	0.5 M H_2SO_4	25.5 mV @10 mA cm^{-2}	~300 h	69
	(FeCoNiPt)$_2$Nb HEA	0.5 M H_2SO_4	11 mV @10 mA cm^{-2}	~2200 h	70
	Pt-HEA-cluster/CeO$_2$/C	1.0 M KOH	12.3 mV @10 mA cm^{-2}	~500 h	71

View Article Online
DOI: 10.1039/D6CC01653G

	(PtMnNiCoMo)				
	PtRhNiFeCu/C	1.0 M KOH	13 mV @10 mA cm^{-2}	~100 h	72
	PtPdIrRhAuAgCu-rEGO	1 M KOH	11.3 mV @10 mA cm^{-2}	~25 h	73
	AL-Pt/Pd_3Pb	0.5 M H_2SO_4	13.8 mV @10 mA cm^{-2}	~25 h	74
	Pt-Ru/RuO_2	1 M KOH	18 mV @10 mA cm^{-2}	~100 h	75
OER	Co-Fe-Ni-Pt-Ta-vxc72	1.0 M KOH	290 mV @10 mA cm^{-2}	~20 h	76
	N/Pt/HEA NPs-C (PtFeNiCoMn)	1.0 M KOH	376 mV @10 mA cm^{-2}	~135 h	77
	FeCoNiCuPtIr HEA	1.0 M KOH	255 mV @10 mA cm^{-2}	~20 h	44
	$Pt_{26}Ir_7Fe_{13}Co_{22}Ni_{32}$ NFs	1.0 M KOH	197 mV @10 mA cm^{-2}	negligible degradation after 40000 s	78
	HEA@Pt (PtRuFeCoNi)	0.1 M KOH	370 mV @10 mA cm^{-2}	7 mV degradation after 5000 cycles	79
HOR	HEA-SNWs/C (PtRuNiCoFeMo)	0.1 M KOH	6.75 A mg_{Pt+Ru}^{-1} @50 mV	6.2% degradation after 2000 cycles	80
	HEA10 (PtPdRuMoNi)	1.0 M KOH	151 A g_{Pt}^{-1} @30 mV	negligible degradation after 10000 cycles	81
	PtRuRhPdIr HEAAs/C	0.1 M KOH	5.75 A mg_{PGM}^{-1} @50 mV	5.9 % degradation after 6 h	82
	PtIrFeCoNiMo HEA NDs/C	0.1 M KOH	3.53 A mg_{PGM}^{-1} @50 mV	15.77 % degradation after 20000 s	83
	5-PtRuMoIrCo HEA NWs/C	0.1 M KOH	5.8 A mg $_{Pt+Ru}^{-1}$ @50 mV	18.9 % degradation after 2000 s	84
	s-$Ru_1Pt@W_1$/N	0.1 M KOH	7.54 A mg_{Pt+Ru}^{-1} @50 mV	6.2 % degradation after 20 h	85
ORR	PtRhNiFeCu/C	0.1 M $HClO_4$	1.23 A mg_{Pt}^{-1} (0.9 V vs. RHE)	10 mV negative shift after 10000 cycles	72
	N-Pt/HEA/C (PtCoFeNiCu)	0.1 M $HClO_4$	1.34 A mg_{Pt}^{-1} (0.9 V vs. RHE)	20.9% degradation after 30000 cycles	86
	PtPdFeCoNi HEA/C	0.1 M KOH	1.23 A mg_{Pt}^{-1} (0.9 V vs. RHE)	6 mV negative shift after 50000 cycles	87
	MHEI-PtPdFeCoNi	0.1 M KOH	0.63 A mg_{Pt+Pd}^{-1} (0.9 V vs. RHE)	12.7% degradation 50000 cycles	88
	PtCuGaFeCo NPs	0.1 M $HClO_4$	3.11 A mg_{Pt}^{-1} (0.9 V vs. RHE)	13 mV negative shift after 1000 cycles	89
	PtFeCoNiMn/OMC	0.1 M $HClO_4$	1.12 A $mg^{-1}{}_{Pt}$ (0.88 V vs RHE)	32.4% ECSA loss after 30000 cycles	15
	Pt_3Ni (Pt-skin)/Pd/C	0.1 M $HClO_4$	14.2 A mg_{Pt}^{-1} (0.9 V vs. RHE)	2 mV negative shift after 20000 cycles	90
	Pt@Pt-skin Pt_3Ni	0.1 M $HClO_4$	6.69 A mg_{Pt}^{-1} (0.9 V vs. RHE)	4 mV negative shift after 50000 cycles	91

To more rigorously distinguish the catalytic merits of Pt-HEAs, it is necessary to benchmark them against state-of-the-art low-entropy Pt catalysts, including Pt-skin structures, Pt-based core-shell

View Article Online
DOI: 10.1039/D6CC01653G

catalysts, and binary or ternary Pt alloys. As summarized in Table 2, Pt-HEAs do not always exhibit the highest activity in every individual reaction, and in some cases the optimized low-entropy Pt catalysts can deliver even lower overpotentials or higher mass activities because of their highly tailored surface structures and maximized Pt utilization. Nevertheless, the overall catalytic performance of Pt-HEAs remains highly competitive, especially when evaluated across multiple reactions and under more practically relevant operating conditions. More importantly, Pt-HEAs generally show superior durability, including smaller activity decay, higher resistance to element dissolution, reduced structural coarsening, and stronger tolerance to harsh electrochemical environments. Therefore, the key advantage of Pt-HEAs does not simply lie in achieving the highest activity, but in offering a more balanced combination of activity, structural robustness, and long-term operational stability compared to some low-entropy Pt catalysts.

3.1 HER

HER as the cathodic half-reaction in water electrolysis for hydrogen production, directly influences the energy consumption and cost of hydrogen generation. As a zero-carbon energy carrier, hydrogen plays a pivotal role in the hydrogen economy, making the development of efficient HER catalysts critical for achieving low-energy-consumption water electrolysis, particularly of strategic significance for the storage and conversion of renewable energy. The kinetics of HER are constrained by the adsorption of hydrogen ions/water and the desorption efficiency of hydrogen, requiring an additional "overpotential" to drive the reaction even under ideal conditions, which leads to energy loss. Platinum exhibits ΔG_{H*} close to zero (ca. 0.09 eV), ideally balancing the thermodynamic requirements for H^+ adsorption and H_2 desorption, thus avoiding active site blockage from strong adsorption or kinetic sluggishness from weak

View Article Online
DOI: 10.1039/D6CC01653G

adsorption.[92] However, Pt's high cost and limited reserves pose significant challenges. Pt-HEAs reduce Pt usage while boosting stability and kinetics.

For example, Zhao et al.[66] synthesized PtRuMoFeCoNi high-entropy alloy quantum dots (HEA-QDs) via rapid microwave radiation. The HEA-QDs catalyst was supported on Vulcan XC-72R carbon to fabricate HEA-QDs/C (Fig. 9a). In N_2-saturated 0.5 M H_2SO_4, HEA-QDs/C exhibited overpotentials of 11 mV/102 mV to reach 10/100 mA cm^{-2} (Fig. 9b), outperforming Pt/C, Ru/C, and PtRu/C. The Tafel slope of 28.7 mV decade^{-1} indicated the Volmer-Tafel mechanism, with the Tafel step as the rate-determining step. The exchange current density is approximately 3.899 mA cm^{-2} (Fig. 9c), higher than that of Pt/C and Ru/C. Both mass activity and specific activity surpassed those of the reference catalysts. After 10,000 cycles and 20 h of continuous electrolysis, HEA-QDs/C showed negligible performance decay, outperforming Pt/C (Fig. 9d). Inductively coupled plasma mass spectrometry (ICP-MS) revealed partial leaching of transition metals at the initial test stage and stabilization after 15 h. XRD, TEM, and X-ray photoelectron spectroscopy (XPS) analyses confirmed structural stability, while valence state changes of partial elements were identified as the main cause of performance decay. Electrochemical impedance spectroscopy (EIS) showed that HEA-QDs/C has the smallest charge transfer resistance and the fastest electron transfer rate. The more negative H_{upd} oxidation peak potential indicated weaker M-H bond energy. Arrhenius and Eyring model analyses demonstrated lower activation energy and Gibbs activation free energy, confirming superior reaction kinetics (Fig. 9e and f). Tafel kinetics of HEA-QDs/C with different loadings remained stable. The activity of HEA-QDs/C exceeded that of Pt-HEA/C and Ru-HEA/C, indicating a synergistic effect between Pt and Ru. The introduction of Ru reduced the chemical state of Pt, promoting proton desorption. Density functional theory (DFT)

View Article Online
DOI: 10.1039/D6CC01653G

calculations showed strong cross-boundary electron transfer from Fe, Co, Ni, and Mo to Pt and Ru, increasing the electron density at Pt and Ru sites and weakening the adsorption strength of hydrogen. The absolute values of ΔG_{H^*} at Pt, Ru, and PtRu sites in HEA-QDs were lower than those in pure metals and alloys (Fig. 9g), indicating optimal hydrogen adsorption strength. The Tafel reaction activation energy was lower, and Tafel kinetics at Pt and Ru sites were faster, primarily attributed to increased electron density and weakened M-H bonds.

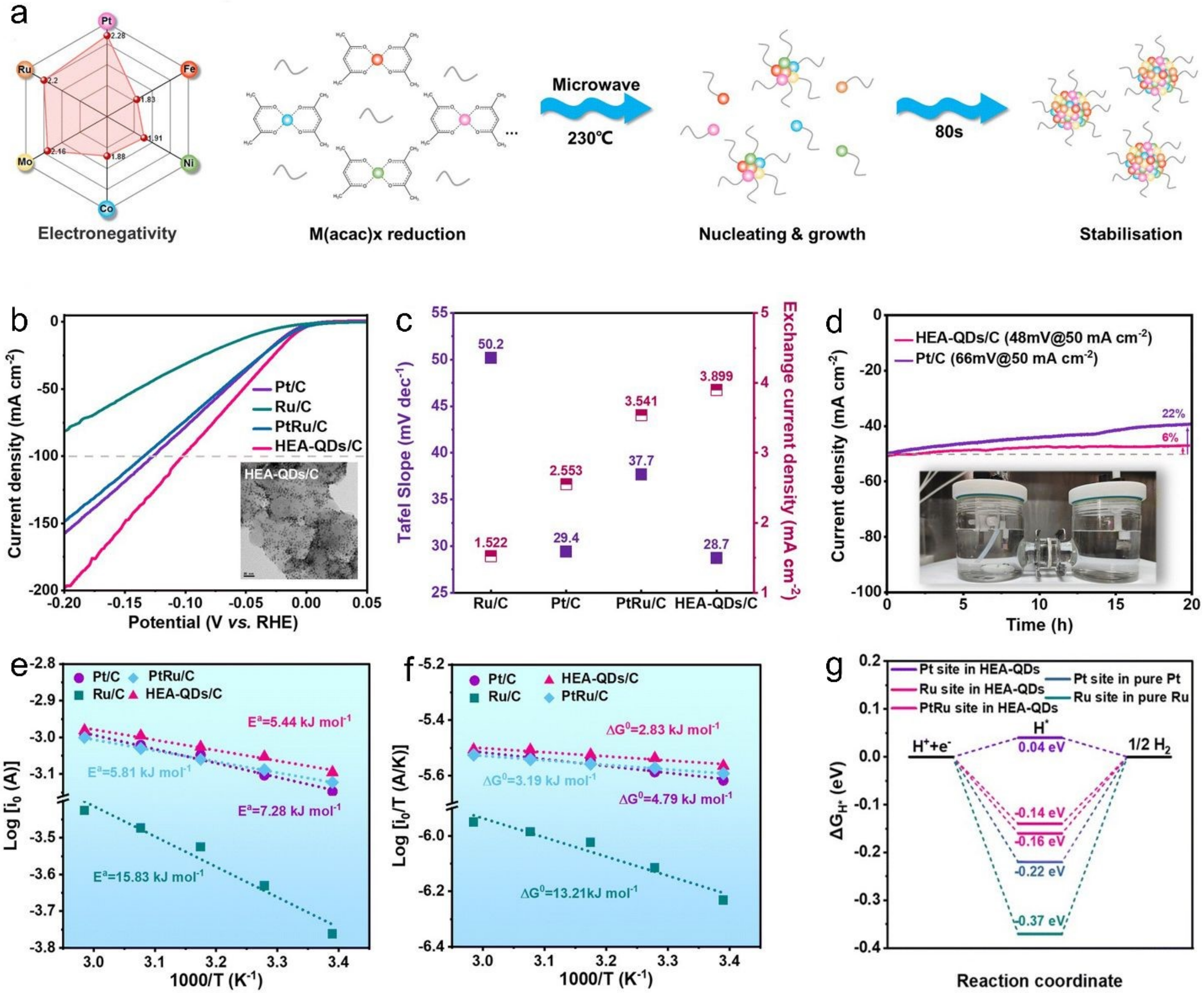

Fig. 9 (a) The preparation procedure of HEA-QDs. (b) Polarization curves (insert is the TEM image of HEA-QDs/C). (c) Tafel slope and corresponding j_0. (d) current-time chronoamperometry

View Article Online
DOI: 10.1039/D6CC01653G

response. (e) Arrhenius plots and (f) Eyring plots at the equilibrium potential in the temperature range of 295–335 K. (g) Calculated ΔG_{H*} profiles for Pt/Ru sites on HEA-QDs, pure Pt and pure Ru. Reproduced with permission.[66] Copyright 2024, Royal Society of Chemistry.

While compositional optimization significantly improved HER performance, understanding the underlying catalytic origin required insights into local atomic environments and reaction intermediates under working conditions. Yang et al.[67] prepared equiatomic FeCoNiCrPt HEA films via pulsed laser deposition (PLD) (Fig. 10a), exhibiting a homogeneous FCC structure in the as-deposited state. Electrochemical etching in 0.5 M H_2SO_4 induced a rough surface morphology with the FCC phase retained. The sample etched for 300 s (EE.300s) featured abundant surface vacancies, leading to significant lattice micro-strain fluctuations with normal strain ranging from −15% to +19%, far exceeding other samples. In 1.0 M KOH, EE.300s achieved an overpotential of only 18 mV at 10 mA cm^{-2}, outperforming other samples and Pt/C nanoparticles. It also exhibited remarkably lower overpotentials in acidic and neutral media compared to most reported electrocatalysts. The smallest Tafel slope and EIS results confirmed its fast reaction kinetics. The mass activity of EE.300s is about 11 times of that of Pt/C nanoparticles, while its large ECSA (indicated by double-layer capacitance, C_{dl}) and high turnover frequency (TOF) revealed excellent intrinsic activity. DFT calculations showed that EE.300s shows significantly enhanced H_2O adsorption at all active sites, primarily due to strengthened interactions between H_2O molecules and Co, Ni, and Cr sites (Fig. 10b). The etching process effectively reduced the H_2O dissociation energy barrier, accelerating proton supply for HER. In the EE.300s model, Pt-Fe-Co, Pt-Fe-Cr, Pt-Co-Cr sites, and single-atom Pt sites exhibited ΔG_H* values closer to zero, demonstrating that strain engineering optimized HER performance. The FeCoNiCrPt HEA films showed outstanding

View Article Online
DOI: 10.1039/D6CC01653G

HER activity and stability across all pH values (Fig. 10c–f). Strain modulation optimized charge distribution, adjusted bond lengths and d-band center positions, and optimized intermediate binding energies and, while maintaining catalyst durability. Under alkaline and acidic conditions, the films required overpotentials of 104 and 106 mV at 1 A cm^{-2}, respectively, and sustained operation for approximately 500 h in an anion exchange membrane (AEM) electrolyzer, achieving a lifespan nearly 40 times longer than that of commercial Pt/C||IrO_2 systems (Fig. 10g).

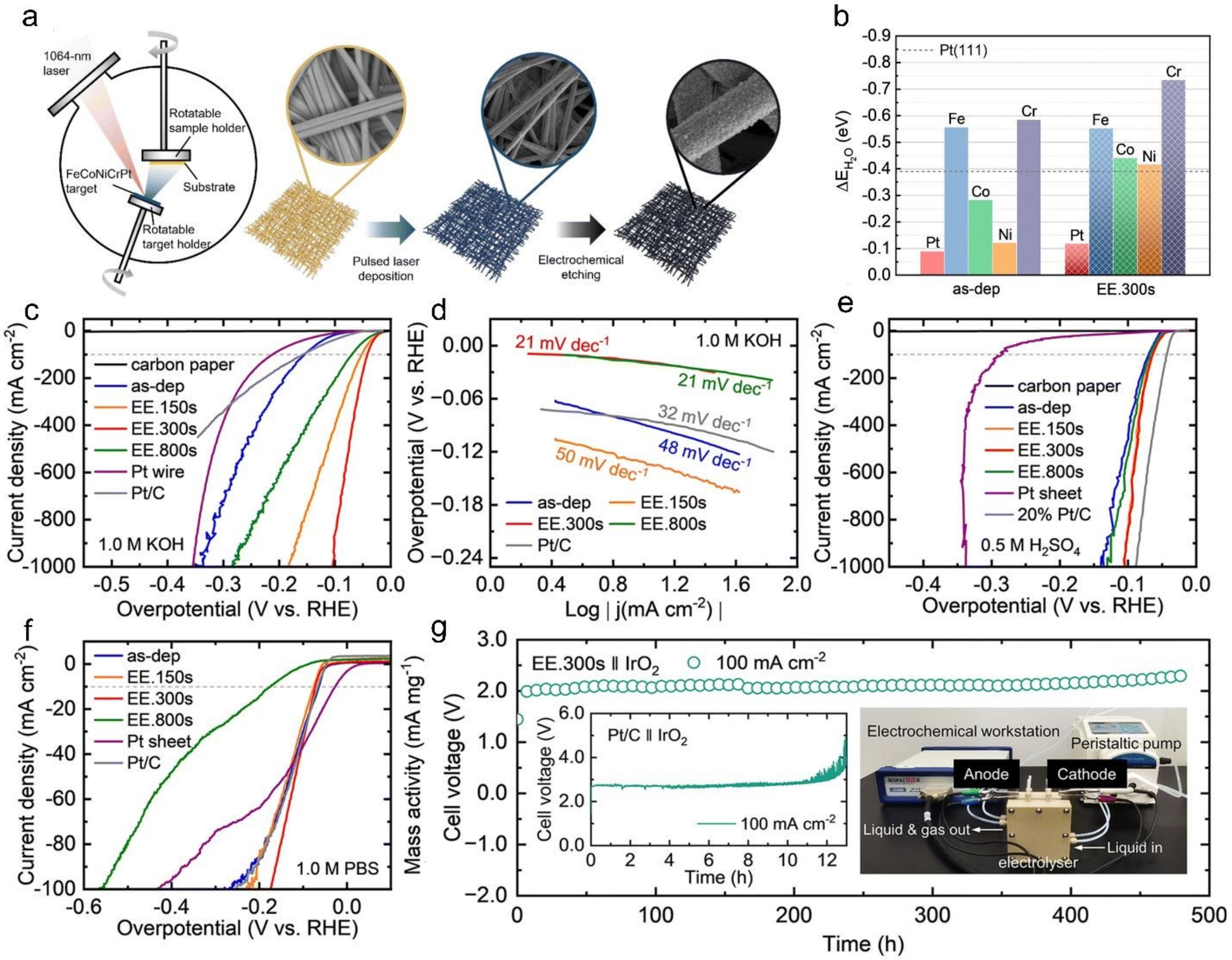

Fig. 10 (a) Schematic diagrams of the PLD and electrochemical etching processes of the HEA film on a carbon paper substrate. (b) Adsorption energy of H_2O molecules on Pt, Fe, Co, Ni, and Cr sites of the as-dep and EE.300s models. (c) HER polarization curves and (d) Tafel plots of the

View Article Online
DOI: 10.1039/D6CC01653G

HEA films in 1.0 M KOH solution. HER polarization curves in (e) 0.5 M H_2SO_4 and (f) 1.0 M PBS solutions. (g) AEM performance using EE.300s HEA film as the cathodic HER catalyst and commercial IrO_2 as the anodic OER catalyst at room temperature, insets show the photograph of the AEM water electrolyzer (right) and the performance of Pt/C||IrO_2 AEM electrolyzer (left) for comparison. Reproduced with permission.[67] Copyright 2024, Royal Society of Chemistry.

An advantage of HEA catalysts lies in its high stability arising from the lattice distortion effect, which favors the design and preparation of highly stable electrocatalysts in wide pH ranges especially in acidic media. For example, Wang et al.[68] synthesized Ru-PtFeNiCuW/CNTs HEA octahedral nanocrystals via a one-pot co-reduction method (Fig. 11a and b). The Ru-PtFeNiCuW/CNTs catalyst demonstrates exceptional HER performance in both acidic and alkaline electrolytes. At 10 mA cm^{-2}, the overpotentials are 9 mV in acidic (Fig. 11d–f) and 16 mV in alkaline (Fig. 11g–i) conditions, with corresponding Tafel slopes of 19.2 mV dec^{-1} and 27.9 mV dec^{-1}, respectively. In two-electrode overall water splitting tests, the catalyst maintains stability for 1500 hours in acidic media and 1200 hours in alkaline media. Ru doping and $W(CO)_6$ regulation of reduction kinetics enable uniform growth of octahedral nanocrystals, ensuring high-density exposure and uniform distribution of active sites, which fundamentally guarantees consistent performance across broad pH ranges. XPS analysis reveals that W exists exclusively in W^{5+}/W^{6+} oxidation states (Fig. 11c). The high oxidation state of W indicates that its surface preferentially acts as an active center for H_2O dissociation, while the low oxidation states of Pt/Cu facilitate H* adsorption-desorption. In alkaline/neutral conditions, W sites exhibit a H_2O adsorption free energy (ΔG_{H_2O}=−0.45 eV) and hydrolysis energy barrier (0.67 eV) significantly lower than other metals (e.g., Fe, Ni), serving as key sites in the rate-determining step to accelerate

View Article Online
DOI: 10.1039/D6CC01653G

H_2O activation into H intermediates. The hydrogen adsorption free energy at Cu-Cu-Cu and Cu-Cu-Pt hollow sites approaches the ideal value, enabling rapid H desorption across all pH ranges, which particularly dominates the Volmer-Tafel mechanism in acidic conditions. Multicomponent regulation shifts the d-band center of Cu to −2.22 eV (close to Pt's −2.25 eV), optimizing *H adsorption energy, while W's d-band center shifts downward (−0.44 eV) to weaken excessive adsorption, synergistically ensuring reaction kinetics across different pHs. The electronically structured multicomponent synergy, dual-active-site mechanism, and stable octahedral crystal plane structure endow the Ru-PtFeNiCuW/CNTs electrocatalyst with outstanding HER performance in broad pH ranges.

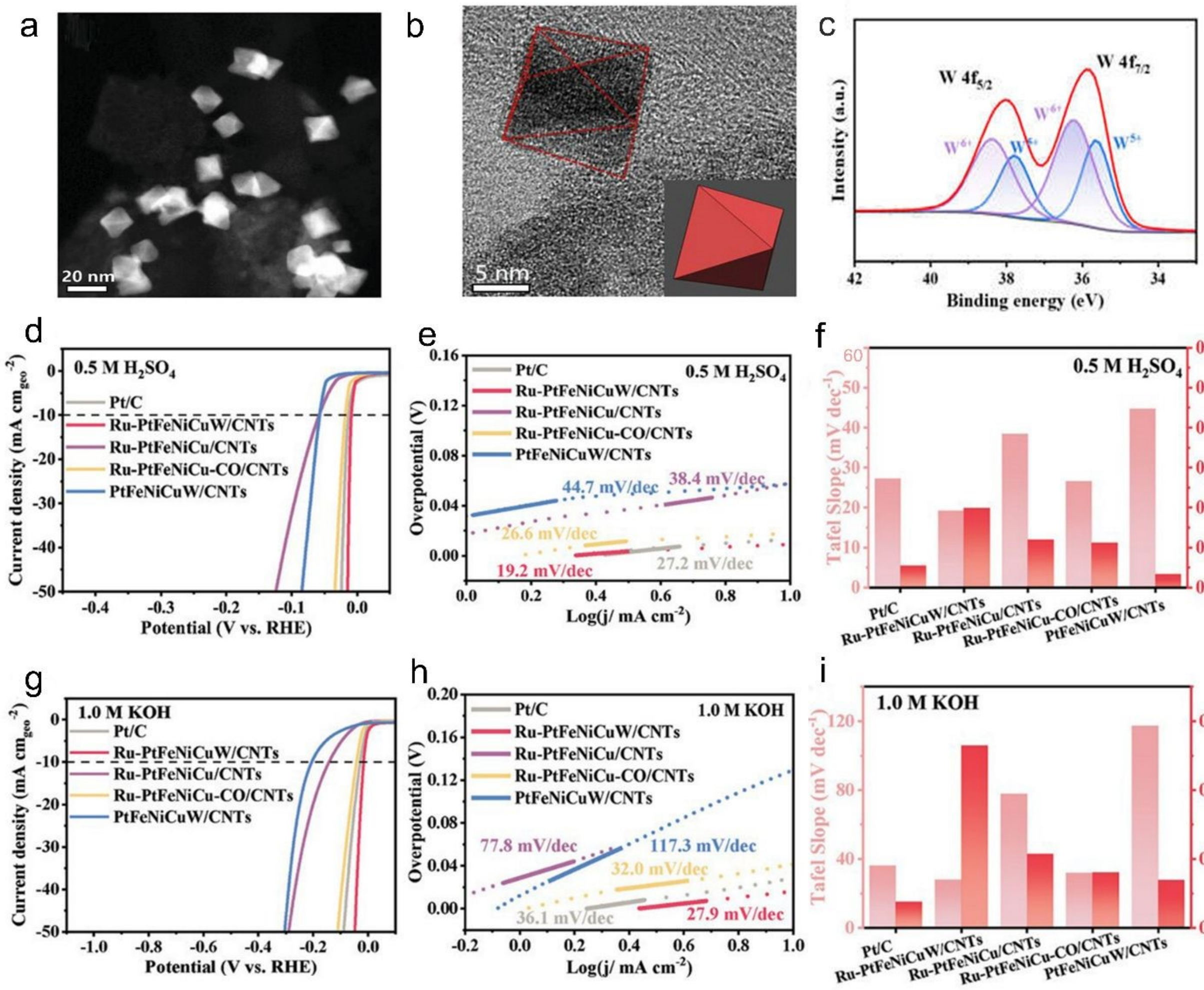

View Article Online
DOI: 10.1039/D6CC01653G

Fig. 11 (a) HAADF-STEM image of Ru-PtFeNiCuW/CNTs. (b) TEM image of a Ru-PtFeNiCuW octahedron and the corresponding projected octahedron model (inset in [b]). (c) XPS spectra for W 4f. (d) HER polarization curves (normalized by geometric area of electrode), (e) Tafel plots, (f) the histogram for Tafel slopes and exchange current densities of commercial Pt/C, Ru-PtFeNiCuW/CNTs, Ru-PtFeNiCu/CNTs, Ru-PtFeNiCu-CO/CNTs, and PtFeNiCuW/CNTs in 0.5 M H_2SO_4 electrolyte. (g) HER polarization curves (normalized by geometric area), (h) Tafel slopes, and (i) the histogram for Tafel slopes and exchange current densities of commercial Pt/C, Ru-PtFeNiCuW/CNTs, Ru-PtFeNiCu/CNTs, Ru-PtFeNiCu-CO/CNTs, and PtFeNiCuW/CNTs in 1.0 M KOH electrolyte. Reproduced with permission.[68] Copyright 2024, Wiley-VCH.

Besides the above demonstration, there are also other reports of Pt-based HEA catalysts. For instance, Fu et al.[69] proposed an artificial intelligence-assisted high-throughput screening strategy and identified the optimal IrCuNiPdPt/C catalyst, which was synthesized via a rapid thermal method. This catalyst exhibited superior HER activity compared to commercial Pt/C and demonstrated remarkable stability over 300 hours. Li et al.[70] constructed a dynamic dissolution-redeposition equilibrium mechanism and developed a FeCoNiNbPt HEA catalyst. The amorphous NbO_x buffer layer effectively suppressed metal dissolution, while Pt_3(FeCoNi) nanocrystals enhanced the HER activity. Wang et al.[71] designed a Pt-based HEA cluster coupled with a superhydrophilic CeO_2-supported porous carbon catalyst (Pt-HEA-cluster/CeO_2/C). The Ce-Pt dual-site synergy accelerated water dissociation kinetics, and the combination of metallic bonding within the HEA and interfacial Pt-O-Ce interactions optimized the Pt electronic structure, achieving outstanding HER performance. Hu et al.[72] synthesized ultrasmall PtRhNiFeCu HEA nanoparticles via a one-pot method. The catalyst's high activity was attributed to multicomponent

View Article Online
DOI: 10.1039/D6CC01653G

synergistic effects that modulated the electronic structure, optimized hydrogen adsorption, and activated non-Pt active sites. Li et al.[73] further reported a UV-induced radical-assisted wet-chemical approach for synthesizing HEA nanoparticles under ambient conditions. Leveraging the strong reducing ability of isopropanol radicals, HEA nanoparticles containing 5–7 metal elements were successfully fabricated and supported on reduced electrochemical graphene oxide (rEGO). Among them, the PtPdIrRhAuAgCu-rEGO catalyst exhibited excellent HER activity across the entire pH range.

Overall, an effective HER-oriented Pt-HEA should not simply maximize compositional complexity, but should deliberately construct neighboring Pt-rich and oxophilic sites with different catalytic functions. Pt or Pt-like surface sites should provide near-optimal hydrogen adsorption, whereas adjacent Ru, Mo, W, or early-transition-metal-containing motifs should accelerate water dissociation and interfacial proton supply, particularly in alkaline media. Structurally, nanoscale morphologies that expose bridge or hollow Pt–M ensembles, together with moderate lattice strain and strong support interaction, are preferred to simultaneously enhance intrinsic kinetics and long-term stability. Therefore, the key design principle for HER-active Pt-HEAs is to engineer bifunctional Pt–M interfacial motifs rather than relying on compositional complexity alone.

3.2 OER

The OER is a core anodic process in clean energy technologies such as water electrolysis for hydrogen production, metal-air batteries, and artificial photosynthesis. Fundamentally, it involves the oxidation of water molecules (H_2O or OH^-) to molecular oxygen, encompassing complex four-electron transfer and O–O bond formation.[93] This reaction suffers from intrinsically sluggish

View Article Online
DOI: 10.1039/D6CC01653G

kinetics and high energy barriers, representing a critical efficiency bottleneck in related technologies. Conventional high-performance catalysts based on precious metals (e.g., IrO_2, RuO_2) face significant challenges including prohibitively high costs and susceptibility to dissolution under acidic conditions. Non-noble metal alternatives, such as Ni/Co-based materials, exhibit inadequate stability in acidic media. While catalysts leveraging the lattice oxygen mechanism (LOM) offer the potential to circumvent scaling relation limitations, they are often compromised by structural instability and collapse risks.[94] HEAs present a transformative approach to addressing these limitations. Their multi-principal element compositions enable substantial reduction in the required loading of precious metals like Ru or Ir. Concurrently, synergistic interactions among the constituent metallic elements facilitate modulation of the d-band center. This electronic structure optimization weakens the adsorption energy of key intermediates (e.g., OOH), thereby lowering the energy barrier of the rate-determining step ($O \rightarrow OOH^*$).[95] The emergence of HEA catalysts in the OER field provides a novel pathway to overcome the persistent bottlenecks associated with traditional electrocatalysts, namely the activity-stability trade-off, precious metal dependency, and the theoretical overpotential limit. Compared with single-functional catalyst systems, HER/OER bifunctional catalysts exhibit revolutionary advantages in terms of system integration, energy efficiency, stability, and cost control.[96] Pt possesses nearly irreplaceable superiority in the HER. However, conventional perspectives hold that Pt is not the most ideal catalyst for the OER.[97] HEAs can effectively ameliorate the inherent drawbacks of Pt in OER through the synergistic effects of multi-metallic components, lattice distortion, and regulation of electronic structures, thereby enabling the development and application of HER/OER bifunctional catalysts.

View Article Online
DOI: 10.1039/D6CC01653G

For instance, Chen et al.[76] synthesized HEA nanoparticles with low Pt content, such as Co-Fe-Ni-Pt-Ta-vxc72, at room temperature via a shear-assisted liquid metal reduction method (Fig. 12a). The composition of the synthesized sub-2 nm Pt-based HEA-NPs form a single-phase FCC solid solution (Fig. 12d). The Co-Fe-Ni-Pt-Ta-vxc72 catalyst demonstrates excellent performance in the OER (Fig. 12f–h). In a 1.0 M KOH electrolyte, the overpotential is merely 290 mV when the current density reaches 10 mA cm^{-2}, which is superior to that of commercial IrO_2 and other comparative alloy catalysts. The Tafel slope is 35 mV dec^{-1}, significantly lower than the 59 mV dec^{-1} of IrO_2. Calculation results of the C_{dl} indicate that the C_{dl} value of Co-Fe-Ni-Pt-Ta-vxc72 is twice of that of IrO_2, suggesting a larger ECSA that can provide more active sites for the reaction. XPS analysis reveals significant electronic interactions among various elements in the alloy. Ta primarily exists in the Ta^{5+} valence state (Fig. 12e), which tends to lose electrons and can act as an "electronic modulator" to donate electrons to Co, Fe, and Ni, increasing the electron density of these elements, optimizing the adsorption energy of key OER intermediates (e.g., OH*, O*, OOH*), and thus accelerating the reaction process. The average size of the synthesized Co-Fe-Ni-Pt-Ta nanoparticles is approximately 1.8 nm (Fig. 12b and c). This ultra-small size endows them with an extremely high specific surface area, which can expose more catalytic active sites and provide sufficient reaction interfaces for the OER.

View Article Online
DOI: 10.1039/D6CC01653G

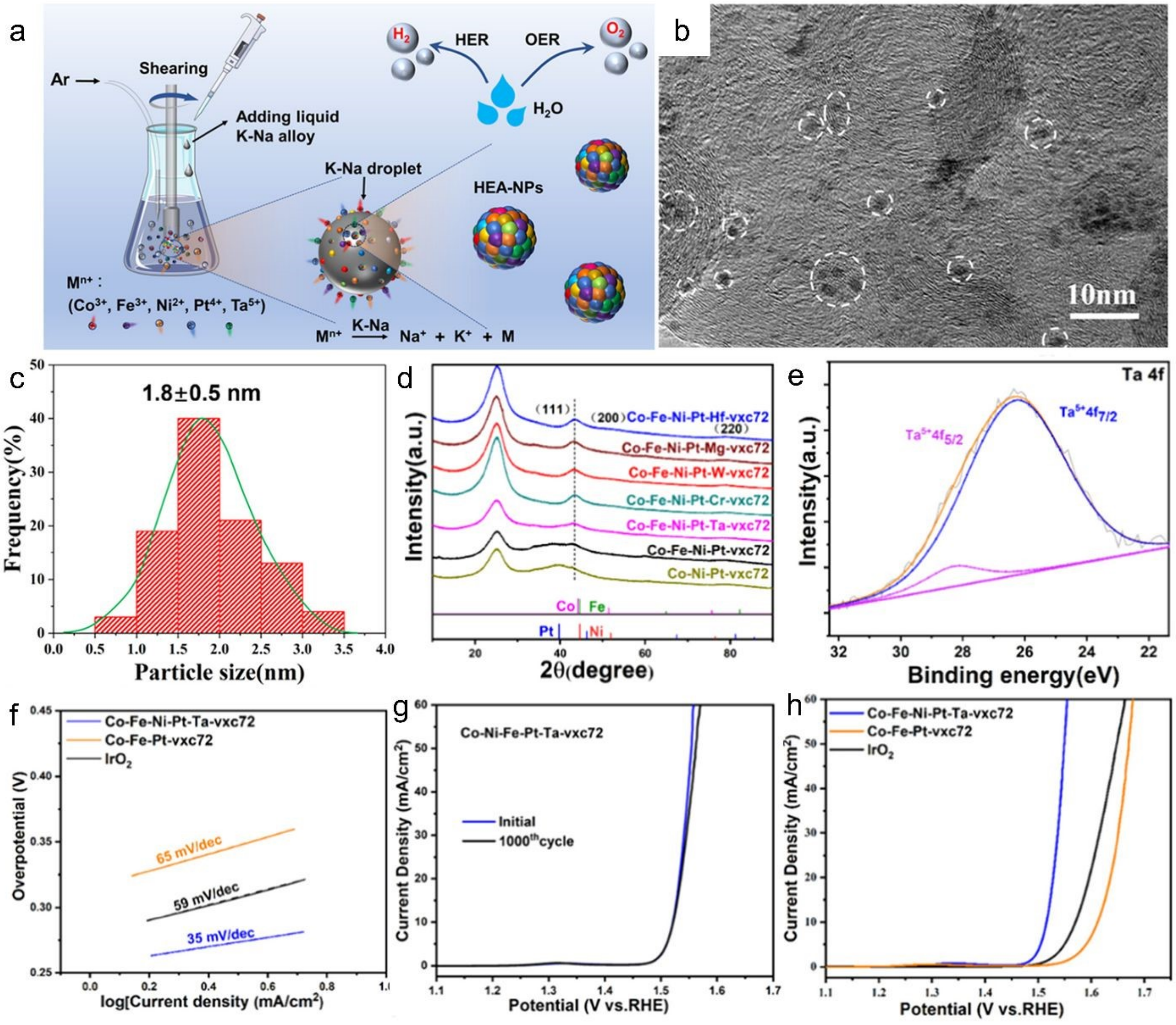

Fig. 12 (a) Schematic illustration of the synthesis method for HEA-NPs via the shearing-assisted liquid K-Na droplet surface reduction process. (b) TEM image and (c) average particle size statistics for Co-Fe-Ni-Pt-Ta-vxc72 NPs. (d) XRD spectrum of the Co-Fe-Ni-Pt-X-vxc72 (X: Hf, Mg, W, Cr, Ta) NPs, (e) XPS spectrum of Ta 4f. (f) LSV curves of Co-Fe-Ni-Pt-Ta-vxc72, Co-Fe-Pt-vxc72 and IrO_2. (g) Tafel plot of the samples. (h) Capacitance of Co-Fe-Ni-Pt-Ta-vxc72 and IrO_2 measured at 1.25 V as a function of the scan rate. Reproduced with permission.[76] Copyright 2022, American Chemical Society.

View Article Online
DOI: 10.1039/D6CC01653G

Although elemental selection plays a dominant role in regulating OER activity, recent studies suggest that additional electronic modulation strategies, for example, heteroatom incorporation, can further refine adsorption energetics and reaction pathways. Niu et al.[77] synthesized nitrogen-doped quinary PtFeNiCoMn nanoalloys (N/Pt/HEA NPs-C) via the rapid Joule heating method (Fig. 13b). XRD patterns reveal that both the nitrogen-doped and undoped samples maintain a uniform single-phase FCC solid solution. The subtle peak broadening or minor shifts induced by N doping indicate localized lattice strain without disrupting the overall FCC framework (Fig. 13a). High-resolution N 1s XPS spectrum of N/Pt/HEA NPs-C reveals the presence of multiple nitrogen species, primarily including pyridinic-N, pyrrolic-N, graphitic-N, and metal-N coordinated bonds. These diverse N configurations confirm effective nitrogen incorporation into the alloy lattice and/or surface sites, contributing to electronic modulation and enhanced long-term stability in oxygen electrocatalysis (Fig. 13c). In 1.0 M KOH electrolyte, the OER performance of N/Pt/HEA NPs-C is significantly superior to that of the non-nitrogen-doped Pt/HEA NPs-C and the commercial catalyst RuO_2. At a current density of 10 mA cm^{-2}, the overpotential of N/Pt/HEA NPs-C is as low as 376 mV, which is lower than that of Pt/HEA NPs-C (411 mV) and RuO_2 (383 mV) (Fig. 13d). Computational results reveal that nitrogen doping (N) induces a more negative shift in the d-band center of the Pt 5d-d_{z^2} orbital through the formation of strong N-metal bonds (the d-band center of N/Pt/HEA is −2.693 eV, lower than that of Pt/HEA at −2.571 eV) (Fig. 13f). This change weakens the adsorption energy of Pt towards reaction intermediates (such as O* and OH*), reduces the energy barrier of the OER reaction, and particularly accelerates the rate-determining step (O*→OOH), thereby enhancing the activity. Theoretical simulations indicate that the adsorption energy of N/Pt/HEA towards O (ΔE_{O*}) is weaker than that of Pt/HEA (ΔE_{O*} of N/Pt/HEA is −1.456 eV, while that of Pt/HEA is −1.544 eV) (Fig. 13e). The weaker adsorption

View Article Online
DOI: 10.1039/D6CC01653G

energy of intermediates avoids the excessive binding of reaction intermediates on the catalyst surface and promotes the rapid conversion of intermediates during the OER process, further improving the activity. Besides, Lu et al.[44] employed a pulsed laser irradiation method in an inert atmosphere to rapidly synthesize FeCoNiCuPtIr HEA nanocatalysts. The resulting catalyst exhibits a low overpotential, a small Tafel slope, and excellent stability for the OER under alkaline conditions. DFT calculations reveal that Ir donates electrons to hollow sites, thereby weakening the coupling strength between adsorbates and the alloy surface. Ma et al.[78] successfully synthesized $Pt_{26}Ir_7Fe_{13}Co_{22}Ni_{32}$ HEA NFs with a FCC structure. The $Pt_{26}Ir_7Fe_{13}Co_{22}Ni_{32}$ NFs deliver an overpotential of 197 mV at a current density of 10 mA cm^{-2} for OER, along with a Tafel slope of 37.7 mV dec^{-1}. TOF is 57.52 times higher than that of commercial IrO_2. Zhang et al.[79] designed a HEA@Pt spatial heterostructure catalyst, in which interfacial electronic redistribution modulates the d-band center of metal atoms, optimizes the adsorption energy of oxygen species, reduces the reaction energy barrier for OER, and accelerates the overall reaction kinetics.

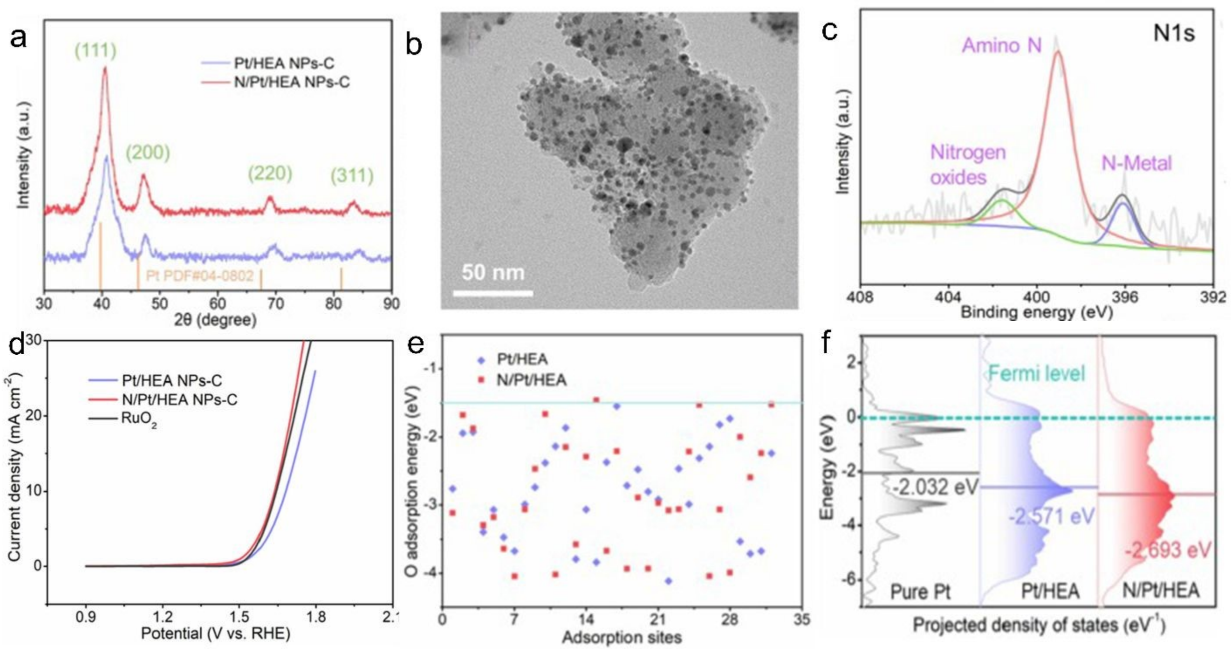

View Article Online
DOI: 10.1039/D6CC01653G

Fig. 13 (a) XRD spectrum of Pt/HEA NPs-C and N/Pt/HEA NPs-C. (b) TEM images of N/Pt/HEA NPs-C. (c) XPS spectrum of N 1 s of N/Pt/HEA NPs-C. (d) OER polarization curves of N/Pt/HEA NPs-C, Pt/HEA NPs-C, and RuO_2 in O_2-saturated 1.0 M KOH electrode. (e) ΔE_{O*} values of Pt/HEA and N/Pt/HEA at various hollow sites. (f) The calculated projected density of states of Pt-5d-dz^2 electrons of pure Pt slab, Pt/HEA, and N/Pt/HEA. The gray, blue, and red lines stand for the d-band centers of pure Pt slab, Pt/HEA, and N/Pt/HEA, respectively. Reproduced with permission.[77] Copyright 2025, Elsevier.

For OER, Pt-based HEAs should be designed such that Pt primarily serves as an electronic regulator and corrosion-resistant noble-metal component, while the surface preferentially exposes oxophilic sites derived from Ru, Ir, Fe, Co, Ni, Ta, or related elements. The most desirable surface motifs are those that can moderate the adsorption strength of OH*, O*, and OOH* without inducing excessive dissolution or irreversible amorphization. In practice, this means favoring Pt-containing multimetallic surfaces that either form stable oxyhydroxide-like active layers under operation or maintain electronically tuned metal–oxygen interfacial sites, rather than maximizing Pt exposure itself. Thus, the most effective OER design principle is to place Pt in a stabilizing and electronic-modulating role while enriching the working surface with oxygen-affinitive neighboring motifs.

3.3 HOR

Hydrogen oxidation reaction (HOR) is the core electrochemical reaction occurring at the anode of hydrogen fuel cells, which efficiently converts the chemical energy of hydrogen directly into electrical energy. It involves the rapid oxidation of hydrogen at the anode to release electrons (e^-)

View Article Online
DOI: 10.1039/D6CC01653G

and protons (H^+), where electrons form an electric current to drive external devices. The kinetic rate of HOR directly affects the power density and startup performance of fuel cells, while its catalytic efficiency, particularly the anti-poisoning ability and stability, is a key determinant of battery cost and lifespan, serving as the fundamental guarantee for realizing efficient and zero-emission hydrogen energy applications.[97] HOR requires high-performance catalysts to facilitate the adsorption and dissociation of hydrogen molecules as well as the electrochemical desorption of hydrogen atoms. As a new type of catalyst, Pt-based HEAs optimize the adsorption energy of reaction intermediates through multi-element synergistic effects, significantly enhancing reaction activity. Meanwhile, they possess advantages of stronger resistance to carbon monoxide poisoning and structural stability, thus representing an important direction for improving fuel cell performance and durability.

In this context, Zhan et al.[80] synthesized PtRuNiCoFeMo high-entropy alloy sub-nanowires (HEA-SNWs/C) via glucose reduction, using metal acetylacetonates as precursors and Stearyltrimethylammonium bromide (STAB) as the structure-directing agent (Fig. 14e). The HEA SNWs has a diameter of 1.8 ± 0.3 nm and possesses FCC crystal structure (Fig. 14a and b). This catalyst demonstrates outstanding HOR performance (Fig. 14c and d). At 50 mV vs. RHE, it achieves a mass activity of 6.75 A mg_{Pt+Ru}^{-1} and a specific activity of 8.96 mA cm^{-2}, which are 2.8/4.1/19.8 times and 2.6/2.4/18.7 times higher than those of HEA-NPs/C, commercial PtRu/C, and Pt/C, respectively. The exchange current density (1.26 mA) is also enhanced by 1.5/2.4/4.5 times compared with the three reference catalysts. Even after 2000 accelerated durability cycles, the catalyst retains excellent stability, with only a 6.2% decrease in mass activity and a 22.3% loss in electrochemical surface area, while maintaining its morphology and composition and

View Article Online
DOI: 10.1039/D6CC01653G

significantly outperforming all benchmarks. In a 1000 ppm CO environment, the limiting current density drops by 5.4%, and activity decreases by 26.4% after 2000 s, indicating significantly stronger CO tolerance than HEA-NPs/C and commercial Pt-based catalysts. The authors attribute its excellent HOR performance to strong multi-metal electronic interactions and precise regulation of reaction intermediate adsorption energies. DFT calculations show significant d-orbital overlap among metals (Fig. 14f), forming a strong coupling effect to promote inter-site electron transfer. In detail, Co/Ni maintain stable valences via the "pinning effect" of adjacent Fe/Mo, while Pt/Ru optimize electroactivity through flexible electronic modulation. For CO tolerance, XPS confirms electron transfer from Pt/Ni/Co/Fe/Mo to Ru (positive shifts of Pt^0 4f and Ni/Co/Fe/Mo oxidation-state peaks, negative shift of Ru^0 3p), which optimizes surface electronic states and weakens CO adsorption. Its d-band center (−3.835 eV) is lower than those of references, reducing CO adsorption energy and active site occupation. DFT further reveals Ru enhances OH^- adsorption, that is, OH^- competes with CO for sites occupation via the "bifunctional mechanism" to accelerate CO oxidative desorption. CO stripping experiments confirm a positive shift in CO desorption potential vs. Pt/C, facilitating adsorbed CO removal and improving anti-toxicity.

View Article Online
DOI: 10.1039/D6CC01653G

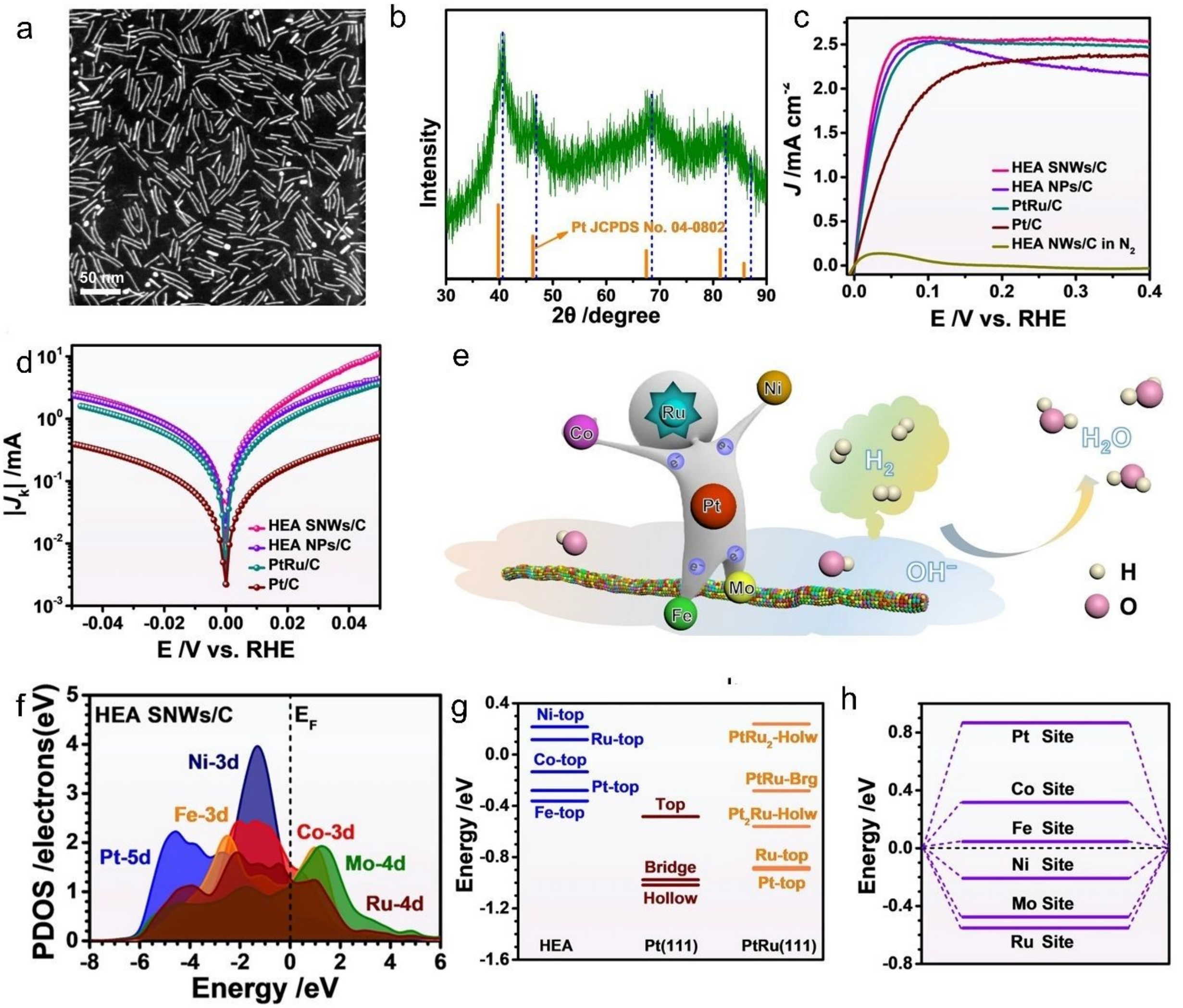

Fig. 14 (a) HAADF-STEM image and (b) XRD pattern of HEA SNWs. (c) Polarization curves in H_2-saturated 0.1 M KOH. (d) Tafel plots. (e) Schematic illustration of HOR over HEA SNWs/C. (f) The PDOSs. Site-dependent PDOSs of Pt-5d, Ni-3d, Co-3d, Fe-3d and Mo-4d. (g) The HBE comparison between HEA SNWs/C, Pt (111) and PtRu (111). Holw= Hollow sites. Brg = Bridge sites. (h) The OH binding energy on HEA SNWs/C. Reproduced with permission.[80] Copyright 2021, Springer Nature.

View Article Online
DOI: 10.1039/D6CC01653G

Building on these insights into nanoscale and electronic effects, subsequent studies explored how HEA architectures could be further optimized through structural design. Nandan et al.[81] synthesized PtPdRuMoNi mesoporous HEA nanospheres via a low-temperature triblock copolymer-assisted wet-chemical reaction. In an alkaline medium, the PtPdRuMoNi mesoporous HEA nanospheres (HEA10) exhibit excellent HOR performance. The mass activity at an overpotential of 30 mV reaches 151 A $g^{-1}{}_{Pt}$, which is much higher than that of the commercial Pt/C electrocatalyst (48 A $g^{-1}{}_{Pt}$). The HEA characteristics bring about a cocktail effect through multi-element synergy, providing a continuous range of adsorption energies, and lattice distortion optimizes the adsorption/desorption of intermediates. The mesoporous structure increases the specific surface area, exposes more active sites, and promotes mass transfer. Mott-Schottky analysis shows that HEA10, as an n-type semiconductor, has a significantly higher carrier (electron) density than Pt/C, and its flat-band potential is more positive (−0.223 V compared to −0.246 V for Pt/C). This reduces the charge transfer barrier, enhances the electric field in the space charge layer at the electrode-electrolyte interface, and accelerates electron transfer. Furthermore, XPS reveals that the Pt 4f peak shifts to the lower energy end by approximately 0.5 eV, indicating an increase in Pt electron density and a downward shift of the d-band center, which weakens the excessive adsorption of H, enhances the adsorption of OH, and facilitates the binding reaction between H and OH. DFT calculations also confirm that the activation energy of its rate-determining step is lower, and multiple factors collectively enhance the reaction kinetics.

Furthermore, studies have shown that HEA electrocatalysts can achieve remarkable HOR performance through multi-metal synergy, high-entropy effects, and tailored nanoscale structures. Li et al.[82] synthesized highly distorted PtRuRhPdIr high-entropy alloy aerogels (HEAAs) as

View Article Online
DOI: 10.1039/D6CC01653G

efficient electrocatalysts for the alkaline HOR, and achieved controllable construction of PtRu-based metal aerogels (MAs) from binary to septenary compositions. The PtRuRhPdIr HEAAs/C exhibited outstanding HOR performance, delivering a PGM-mass-normalized activity of 5.75 A mg_{PGM}^{-1} at 50 mV, 16.9 times of that of commercial Pt/C, as well as an ECSA-normalized exchange current density of 0.69 mA cm^{-2}, which is 4.1 times higher than that of Pt/C. Mechanistic analysis revealed that the highly distorted lattice provides abundant unsaturated surface sites, while the synergistic interactions among multiple active metals effectively balance the adsorption of H and OH intermediates, thereby enhancing HOR kinetics. Ma et al.[83] developed PtIrFeCoNiMo high-entropy alloy nano-dendrites (HEA NDs) via a wet-chemical approach to further improve HOR performance under alkaline conditions. The HEA NDs delivered a mass activity of 3.53 mA g_{PGM}^{-1}, which is 14 times higher than that of commercial Pt/C, and exhibited excellent durability and CO tolerance. Combined with DFT calculations, the superior activity was attributed to the multi-metal synergistic modulation of hydrogen binding energy (HBE) and hydroxyl binding energy (OHBE), namely, a moderate weakening of HBE and enhancement of OHBE, which jointly accelerate the reaction kinetics. This finding offers a new design strategy for high-performance HOR electrocatalysts. Geng et al.[98] constructed Pt_3Ni@PtNiCuCoIn HEA nanowires as highly efficient bifunctional catalysts for proton exchange PEMFCs. The catalyst exhibited the highest limiting diffusion current density in HOR tests. Under pure H_2, the current decreased by only 8.8% after 12 h of chronoamperometry test. Even in 1000 ppm CO/H_2, its current decay remained significantly lower than that of benchmark catalysts, demonstrating exceptional stability and CO tolerance. The enhanced performance resulted from weakened Pt-CO binding, rapid CO removal, and more favorable CO adsorption configurations. Sun et al.[84] proposed a low-temperature reduction-diffusion strategy to fabricate atomically thin Pt-based HEA nanowires containing up to

View Article Online
DOI: 10.1039/D6CC01653G

ten elements. The resulting $Pt_{30}Rh_{27}Mo_{17}Ir_{16}Ru_{10}$ HEA NWs exhibited exceptional HOR performance, delivering an exchange current density of 0.7 A mg_{Pt+Ru}^{-1}, surpassing ternary alloys and commercial catalysts. Moreover, the mass-normalized kinetic current density reached 5.8 A $mg^{-1}{}_{Pt+Ru}$ at 50 mV of overpotential, indicating highly accelerated kinetics. The catalyst also showed excellent CO tolerance and stability with minimal performance decay under harsh testing conditions. These remarkable properties originate from the pronounced lattice distortion in HEAs, which induces compressive strain and optimizes the adsorption behavior of reaction intermediates.

For HOR, the most effective Pt-HEA design is to create surface environments in which Pt-based sites retain rapid H_2 dissociation capability, while adjacent Ru, Mo, Ni, or other OH-affinitive motifs facilitate hydroxyl adsorption and interfacial charge transfer. In addition, alloying elements that electronically downshift the Pt d-band should be selected to weaken Pt–CO binding strength and accelerate poison removal under practical fuel-cell conditions. Therefore, HOR-active Pt-HEAs should be designed around adjacent Pt–M motifs that simultaneously optimize HBE, OHBE, and CO tolerance, instead of focusing only on increasing the number of constituent elements.

3.4 ORR

ORR is an electrochemical process in which O_2 molecules are reduced to H_2O or OH^- through accepting electrons and combining with protons (in acidic media) or water molecules (in alkaline media).[99] As the sole reaction occurring at the cathode of PEMFCs, direct methanol fuel cells (DMFCs), and other related devices, the efficiency of ORR directly determines the energy conversion efficiency of the cells. Ideally, ORR follows a four-electron ($4e^-$) transfer pathway

View Article Online
DOI: 10.1039/D6CC01653G

($O_2 \rightarrow H_2O$ or $O_2 \rightarrow OH^-$). However, this process often competes with a two-electron ($2e^-$) transfer pathway, which generates hydrogen peroxide (H_2O_2) as an intermediate.[100] This side reaction pathway not only reduces the Faraday efficiency but also produces H_2O_2 with strong oxidizing properties, which can cause chemical degradation of key battery components such as membranes and catalysts, thereby severely impairing the durability of the system. The cleavage of the O–O bond requires a high activation energy, and the kinetics is particularly sluggish in acidic media, leading to a high overpotential. The core challenge in ORR catalysis lies in the difficulty of simultaneously achieving high activity, high stability, and low cost, as these three characteristics are often mutually restrictive. To address these limitations, HEAs have emerged as promising electrocatalysts due to their unique multi-element synergy, lattice distortion effects, and tunable electronic structures. By carefully designing the composition and structure of HEAs, it is possible to simultaneously enhance ORR kinetics, improve durability, and optimize active site utilization.

Building on these principles, Zhao et al.[86] designed a nitrogen-doped HEA electrocatalyst supported on a carbon carrier (N-Pt/HEA/C), whose structural feature is the synergistic construction of a nitrogen-doped PtCoFeNiCu HEA core and a Pt-enriched surface shell (Fig. 15a). XRD pattern confirms the formation of a uniform single-phase FCC solid solution in the N-Pt/HEA/C (Fig. 15b). This catalyst shows remarkable ORR activity (Fig. 15c–h). Rotating disk electrode (RDE) measurements reveal a mass activity of 1.34 A mg_{Pt}^{-1} and a specific activity of 1.93 mA cm^{-2} at 0.9 V, which are 7.4 and 6.2 times higher than those of commercial Pt/C, respectively. The half-wave potential reaches 924 mV, outperforming N-HEA/C, Pt/HEA/C, and commercial Pt/C catalysts. After 30,000 accelerated durability cycles, the mass activity decreases by only 20.9%, indicating exceptional stability well above the commercial benchmark. Moreover,

View Article Online
DOI: 10.1039/D6CC01653G

MEA tests confirm its strong practical potential, delivering a current density of 1437 mA cm^{-2} at 0.7 V and showing only an 18 mV half-wave potential shift after 30,000 cycles, demonstrating its application prospect in heavy-duty vehicle (HDV) fuel cells. The authors believe that the synergistic effect of N-doping and HEA jointly enhances the ORR performance of N-Pt/HEA/C. Nitrogen doping optimizes the position of the d-band center of Pt, weakens the adsorption energy barrier of O*/OH* intermediates, and significantly accelerates the ORR kinetic process. The lattice distortion effect of the HEA core further regulates the electronic structure and provides diverse adsorption sites. In terms of stability, the stable M-N bonds formed by N and metals such as Co and Ni inhibit the dissolution of transition metals through the "pinning effect", while the inherent high-entropy effect and sluggish diffusion characteristics of HEAs synergistically inhibit atomic migration and particle agglomeration, collectively improving the durability of the catalyst.

View Article Online
DOI: 10.1039/D6CC01653G

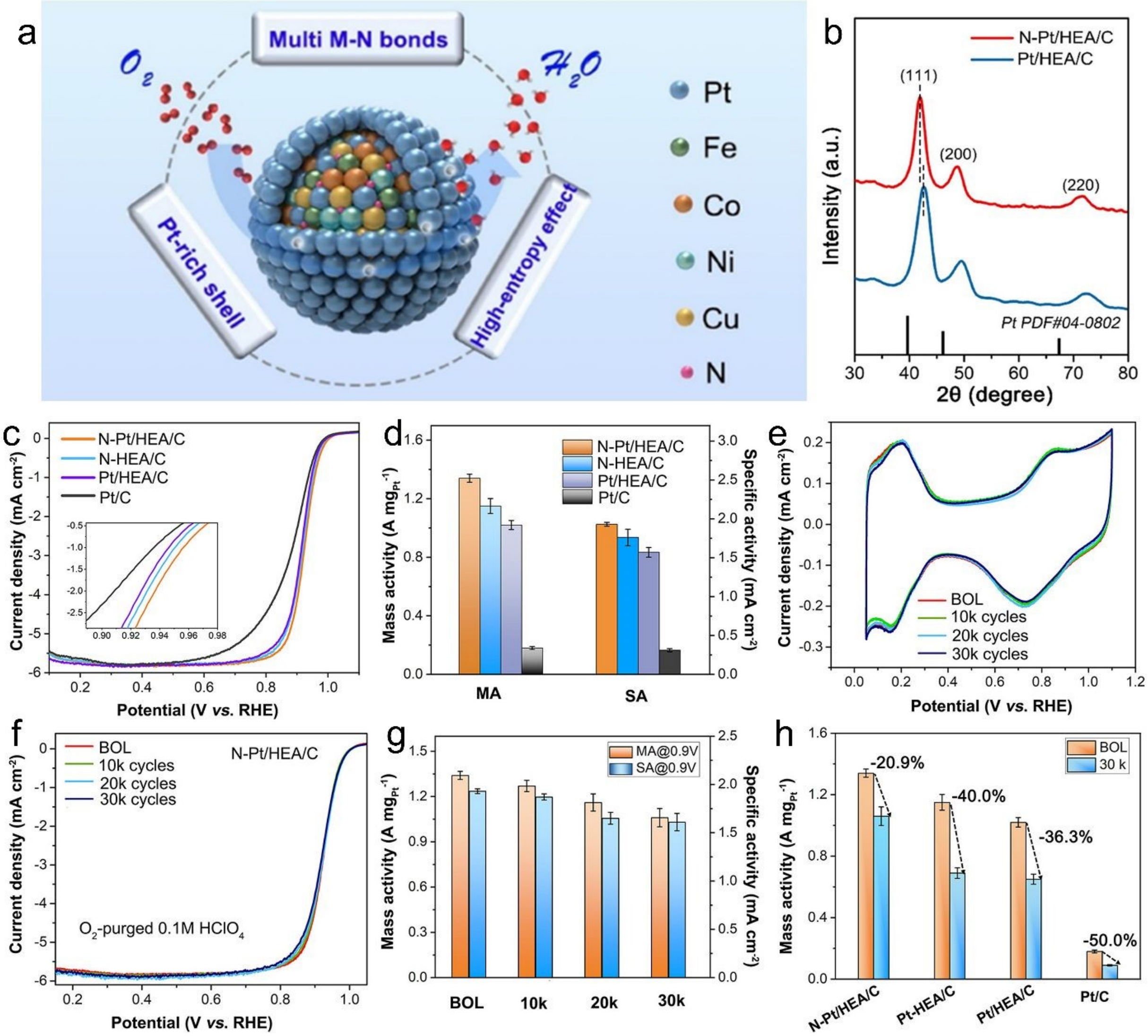

Fig. 15 (a) Pt-rich shell/HEA core architecture for highly active and durable electrocatalysis. (b) XRD patterns of N-Pt/HEA/C and Pt/HEA/C (Cu Kα=1.5406 Å). The standard line of Pt (PDF#04-0802) is included for comparison. (c) ORR polarization curves of N-Pt/HEA/C, N-HEA/C, Pt/HEA/C, and commercial Pt/C in an O_2-saturated 0.1 mol L^{-1} $HClO_4$ (sweep rate=10 mV s^{-1}). (d) Specific activity and mass activity of N-Pt/HEA/C, N-HEA/C, Pt/HEA/C, and commercial Pt/C at 0.9 V. CV curves (e) and ORR polarization curves (f) of the N-Pt/HEA/C catalyst tested at the beginning-of-life (BOL) and after various potential cycles between 0.6 and 0.95 V in 0.1 mol

View Article Online
DOI: 10.1039/D6CC01653G

L^{-1} $HClO_4$ solution. (g) Specific activity and mass activity of the N-Pt/HEA/C catalyst at BOL and different potential cycles. (h) Variations of MA for N-Pt/HEA/C, N-HEA/C, Pt/HEA/C, and Pt/C after 30,000 potential cycles. Reproduced with permission.[86] Copyright 2024, American Chemical Society.

In a similar vein, other HEA designs have also demonstrated excellent ORR activity and durability. For example, Hu et al.[72] synthesized PtRhNiFeCu HEA nanocatalysts via a one-pot method, which exhibit a uniform particle size of approximately 3.53 nm (Fig. 16a and b), FCC structure (Fig. 16c), and homogeneous distribution of the five elements. The PtRhNiFeCu/C catalyst shows excellent catalytic performance. RDE tests reveal that its half-wave potential reaches 0.9 V vs. RHE, which is significantly higher than that of PtRhNi/C (0.875 V vs. RHE) and commercial Pt/C (0.844 V vs. RHE) (Fig. 16d). At 0.9 V vs. RHE, the mass activity of this catalyst is 1.23 A mg^{-1} (Fig. 16e), which is 3.24 times and 6.5 times of that of PtRhNi/C (0.38 A mg^{-1}) and commercial Pt/C (0.19 A mg^{-1}), respectively. The specific activity reaches 2.67 mA cm^{-2}, 2.3 times and 9.9 times of that of PtRhNi/C and commercial Pt/C (Fig. 16f), respectively. In terms of stability, after 10,000 ADT, the half-wave potential of the PtRhNiFeCu/C catalyst only shifts by 10 mV (Fig. 16g), which is much better than that of commercial Pt/C (27 mV) and PtRhNi/C (17 mV). Its mass activity decay rate is 24.2%, which is also lower than that of the contrast catalysts. Moreover, no significant changes in the morphology and elemental ratio of the catalyst are observed after cycling, indicating good durability. DFT calculations demonstrate that the non-platinum sites (e.g., Ni, Cu) on the catalyst surface have thermodynamic limiting potentials close to that of Pt (111) (Fig. 16h and i). These sites can effectively participate in the four-electron transfer process of ORR and possess moderate hydroxyl binding energy, which avoids the deviation of the reaction path caused

View Article Online
DOI: 10.1039/D6CC01653G

by excessively strong or weak binding, thereby facilitating the preferential occurrence of the four-electron reaction generating H_2O.

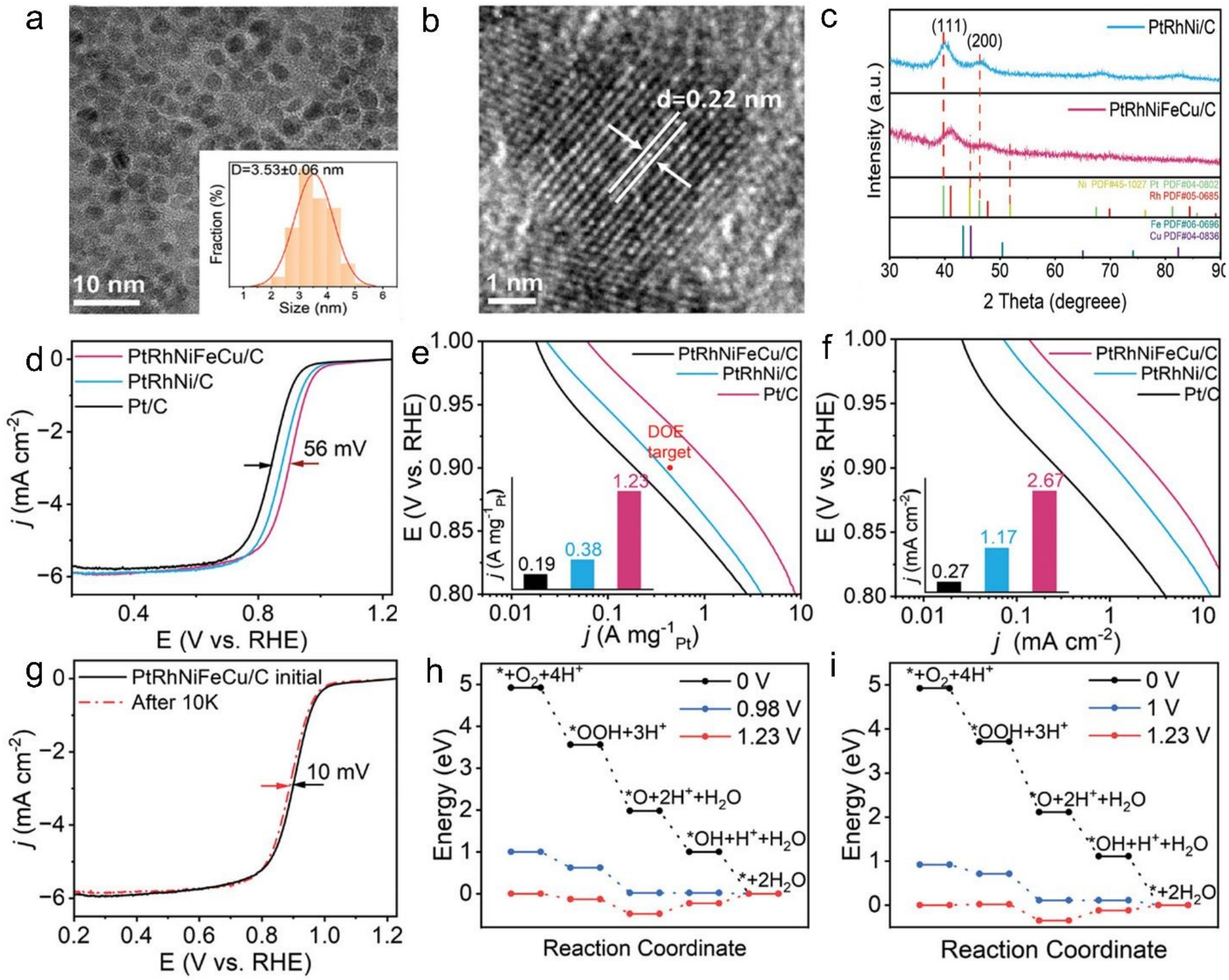

Fig. 16 (a) TEM image, (b) HRTEM image of the surface atomic arrangement on one PtRhNiFeCu nanoparticle. (c) XRD patterns of PtRhNiFeCu/C and PtRhNi/C. (d) LSV curves recorded in O_2-saturated 0.1 M $HClO_4$ solutions at a rotation rate of 1600 rpm. Tafel plots of (e) specific activity and (f) mass activity. (g) LSV curves of PtRhNiFeCu/C catalyst before and after 10 k potential cycles. (h) Gibbs free energy variation diagram of ORR catalytic reaction at Ni and (i) Cu sites. Reproduced with permission.[72] Copyright 2024, Wiley-VCH.

View Article Online
DOI: 10.1039/D6CC01653G

HEAs have emerged as versatile electrocatalysts for ORR, offering a combination of multi-metal synergy, lattice distortion, and electronic structure tuning to enhance activity and stability. Yu et al.[87] synthesized PtPdFeCoNi HEA nanoparticles via a high-temperature injection method and evaluated their electrocatalytic performance toward ORR. Benefiting from the high-entropy effect, lattice distortion, and sluggish diffusion, the HEA catalyst exhibited markedly enhanced activity and durability. Its mass and specific activities are 6.2 and 4.9 times higher than those of commercial Pt/C, respectively. After 50,000 accelerated durability test cycles, the half-wave potential showed only a minor negative shift of 6 mV, demonstrating excellent structural robustness. Zhang et al.[79] proposed a strategy for constructing spatial heterostructured HEA@Pt catalysts by in situ growing Pt dendrites on PtRuFeCoNi HEA cores, forming a core-satellite architecture. The heterointerface-induced electronic redistribution effectively modulates the d-band center of surface metal atoms, optimizing the adsorption of oxygenated intermediates and accelerating ORR kinetics. In O_2-saturated 0.1 M KOH, HEA@Pt delivers a half-wave potential of 0.85 V, significantly higher than that of pure Pt (0.74 V). Further structural innovations have been explored to maximize ORR performance. Wang et al.[88] reported a general approach for synthesizing mesoporous high-entropy intermetallics (MHEIs) featuring ordered polyhedral morphology, bicontinuous gyroid-like mesostructure, and long-range $L1_0$ ordering. The MHEI-PtPdFeCoNi catalyst exhibited ORR mass and specific activities of 0.63 A mg^{-1} and 1.01 mA cm^{-2}, respectively, 1.85 and 1.87 times of those of MHEAs, and 5.25 and 7.21 times of those of Pt/C. DFT calculations revealed that the $L1_0$ ordered phase optimizes OH* adsorption and lowers the energy barrier of the rate-determining step (1.54 eV), thereby accelerating ORR kinetics. Kuang et al.[89] synthesized highly dispersed, ultrasmall (~2 nm) PtCuGaFeCo HEA nanoparticles via a one-pot solution method at 160 °C under ambient pressure. The resulting catalyst achieved a half-

View Article Online
DOI: 10.1039/D6CC01653G

wave potential of 0.88 V (vs. RHE), with mass and specific activities of 6 and 4 times higher than those of Pt/C. Its ECSA reached 143 m^2 $g^{-1}{}_{Pt}$, surpassing that of Pt/C (102 m^2 $g^{-1}{}_{Pt}$). XPS and XAS analyses indicated that the enhanced activity originates from surface strain, optimized coordination environments, and ultrasmall particle-size effects. Wang et al.[15] further developed thermodynamically stable PtFeCoNiMn HEA nanoparticles that also achieved a half-wave potential of 0.88 V (vs. RHE) and a mass activity of 1.12 A $mg_{Pt}{}^{-1}$. After durability testing, the ECSA loss is 32.4%, significantly lower than the 42.1% observed for Pt/C, and overall ORR performance remained superior to Pt/C. Mechanistic analysis suggests that the broadened distribution of surface d-band centers promotes selective adsorption of reaction intermediates, while electronic interactions enable non-noble metal atoms to serve as active sites, collectively enhancing catalytic activity and stability.

For ORR, the most desirable Pt-HEA architecture is not a uniformly exposed multimetal surface, but a Pt-enriched near-surface region that remains electronically modulated by a multimetallic subsurface. Such a structure can preserve high Pt utilization for oxygen reduction while tuning the adsorption of O*, OH*, and OOH* through subsurface strain and ligand effects. Accordingly, ORR-active Pt-HEAs should prioritize controlled surface Pt enrichment, subsurface incorporation of electronically complementary transition metals, and nanostructures that resist leaching, coarsening, and excessive reconstruction during high-potential cycling. In this sense, the design principle is to combine the surface chemistry of a Pt-rich catalyst with the subsurface complexity of a high-entropy framework.

3.5 Formic acid oxidation

View Article Online
DOI: 10.1039/D6CC01653G

The formic acid oxidation reaction (FAOR) serves as the core anodic reaction in direct formic acid fuel cells (DFAFCs). Conventional catalysts tend to follow the less active indirect pathway (dehydration pathway, generating CO*)[101] rather than the more efficient and cleaner direct pathway (dehydrogenation pathway, generating CO_2).[102] Moreover, they are highly susceptible to poisoning by strongly adsorptive intermediates (such as CO) produced during formic acid dehydrogenation, leading to rapid decline in catalytic activity.[103] In addition, traditional catalysts are prone to dissolution, agglomeration, or surface reconstruction under harsh electrochemical environments.

To address these challenges, HEA catalysts offer unique opportunities to steer reaction pathways and improve selectivity in FAOR. The inherent diversity of surface sites in HEAs allows preferential activation of the direct dehydrogenation pathway while suppressing the undesired CO-generating indirect pathway. Zhan et al.[104] developed a novel PtBiPbNiCo high-entropy alloy hexagonal nanoplates (HEA HPs) catalyst with a unique core-shell structure (Fig. 17a and b), consisting of a PtBiPb medium-entropy core and a PtBiNiCo high-entropy shell. The catalyst exhibits excellent catalytic activity and stability toward FAOR, with a mass activity and specific activity of 7.1 A mg^{-1} and 27.2 mA cm^{-2} (Fig. 17d), respectively, which are 56 times and 133 times higher than those of commercial Pt/C (Fig. 17e). Furthermore, the power density of the membrane MEA based on HEA HPs reaches up to 321.2 mW cm^{-2} in DFAFCs. HRTEM (Fig. 17f) and XAS analyses revealed that the lattice distortion and electronic structure regulation in the core-shell structure significantly promote the direct dehydrogenation pathway of formic acid molecules (generating CO_2) while inhibiting the indirect pathway (generating CO*). Fourier transform infrared spectroscopy (FTIR) and DFT calculations further confirmed that the optimized

View Article Online
DOI: 10.1039/D6CC01653G

d-band center on the surface of HEA HPs and the multi-element synergistic effect reduce the reaction energy barrier, thereby greatly improving the catalytic efficiency (Fig. 17g–i).

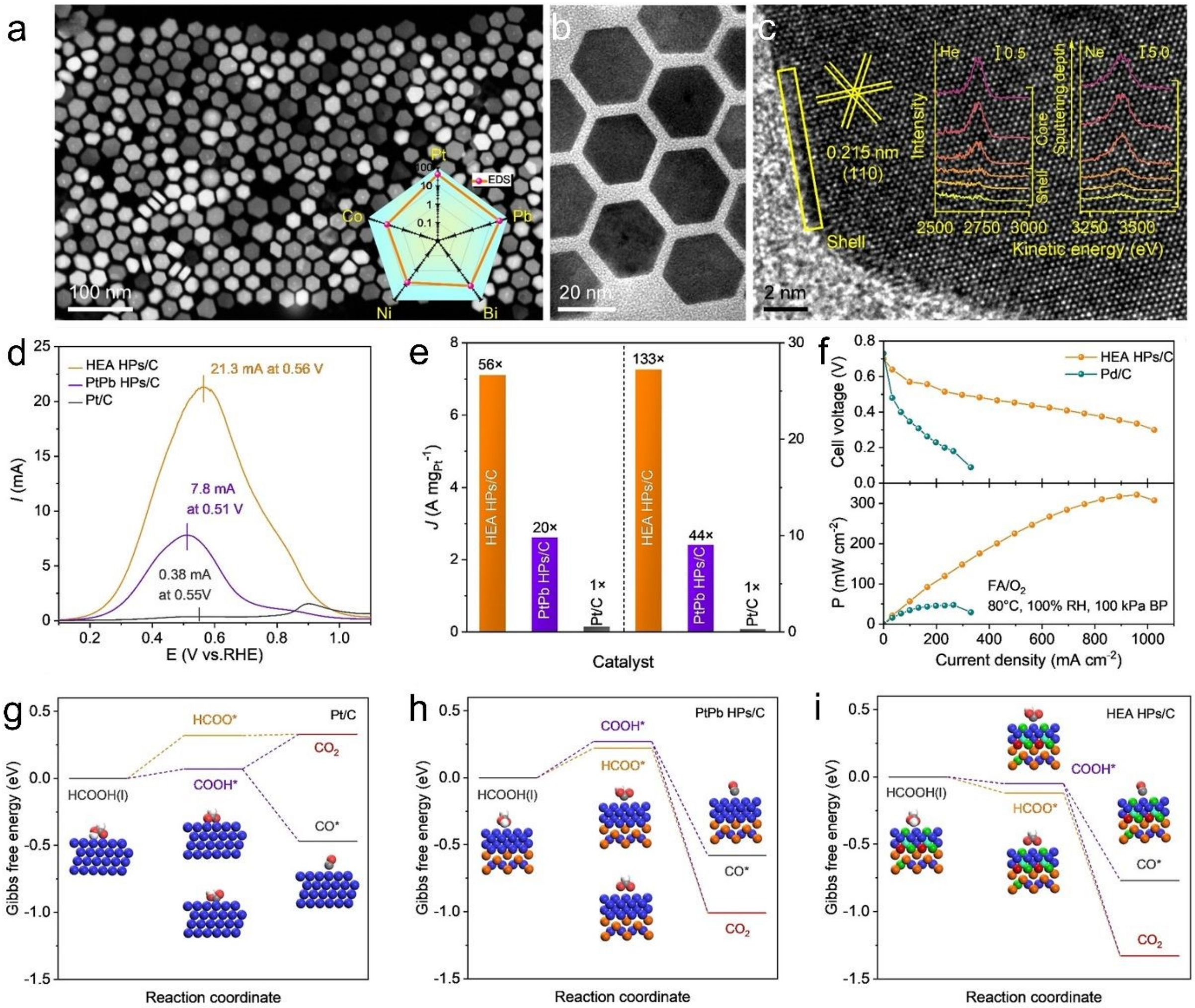

Fig. 17 (a) HAADF-STEM image. Insets of the HAADF-STEM-EDS of an individual HEA HP. (b) TEM image. (c) HRTEM image. Insets of the ISS with He and Ne polishing treatments for 120 s each time, respectively (1–2 nm thick after three polishing). (d) Forward-scan CV curves of different catalysts in 0.5 M H_2SO_4 + 0.5 M HCOOH. (e) Mass and specific activities of different catalysts. (f) Steady-state polarization and power density curves for MEA under 9 M HCOOH.

View Article Online
DOI: 10.1039/D6CC01653G

The Gibbs free energy diagram of (g) Pt/C, (h) PtPb HPs/C, and (i) HEA HPs/C for FAOR. Reproduced with permission.[104] Copyright 2022, Wiley-VCH.

Along similar lines, other HEA architectures have also demonstrated outstanding FAOR performance and anti-CO poisoning ability. Si et al.[105] synthesized PtRhNiCoFeGaW HEA nanoflowers (HEA NFs) with a three-dimensional nanoflower structure via a wet-chemical method (Fig. 18a). For FAOR, its mass activity is 0.52 A mg^{-1}, which is 3.25 times of that of Pt/C (Fig. 18b). The HEA NFs is capable of maintaining a high current density over a long-term operation period of 3600 hours (Fig. 18c). Stability tests showed that after 1000 cycles, the HEA NFs can still retain 84.7% of the initial activity (Fig. 18d). CO stripping experiments (Fig. 18e–g) and in situ diffuse reflectance infrared fourier transform spectroscopy (DRIFTS) analyses indicated that there is almost no CO adsorption peak on the surface of HEA NFs, demonstrating their excellent anti-CO poisoning ability. The authors suggested that under multi-element synergy, elements such as Co and Fe promote the dissociation of water at low potentials to generate OH* which oxidizes CO* to CO_2. Rh and Ni transfer electrons to Pt, reducing the CO adsorption energy. Furthermore, the lattice distortion results in a moderate d-band center position, weakening the interaction with CO* thus enhancing the anti-poisoning performance of the catalyst.

View Article Online
DOI: 10.1039/D6CC01653G

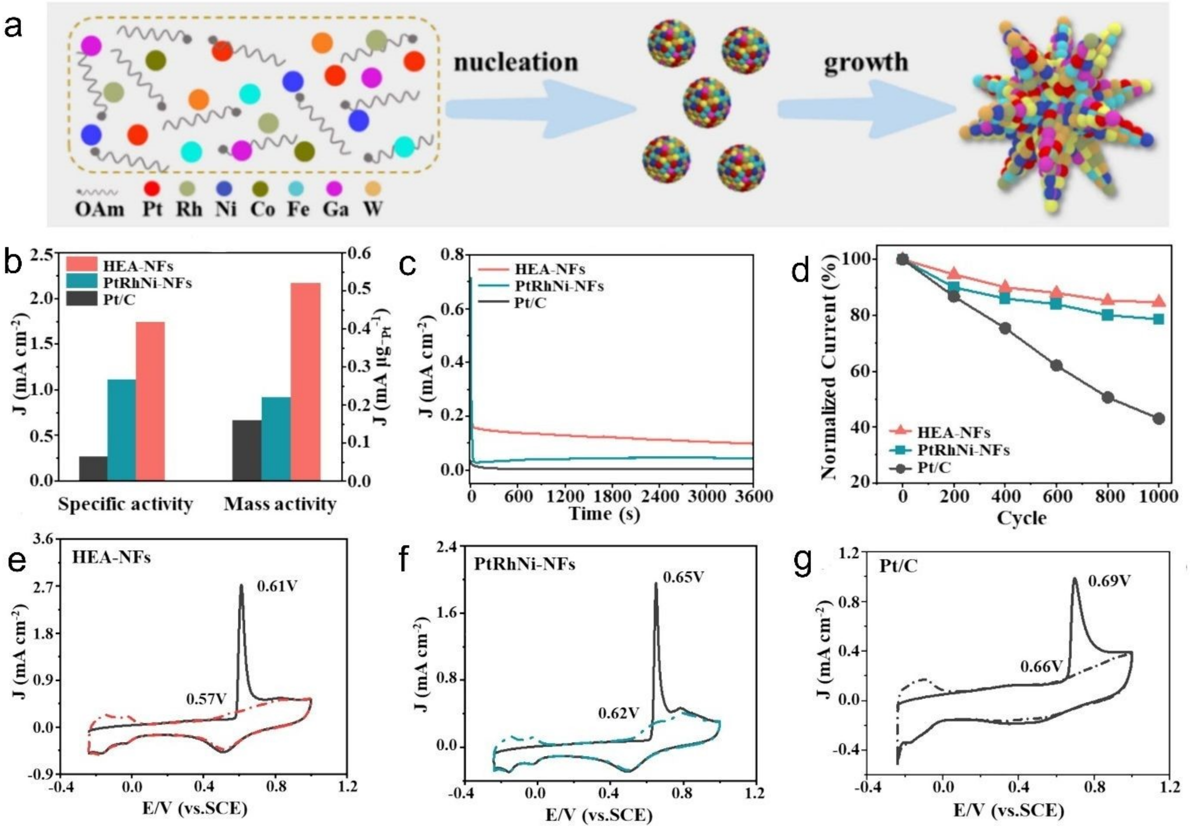

Fig. 18 (a) Synthetic schematic of HEA NFs. (b) Mass and specific activities across the catalysts for FAOR, (c) current-time (i–t) profiles at a potential of 0.06 V within the same electrolytic medium, again at a 50 mV s^{-1} scan rate, (d) the activity retention following various cycles. CO-stripping voltammograms of (a) HEA NFs, (b) PtRhNi NFs, and (c) commercial Pt/C in 0.5 M H_2SO_4 at a scan rate of 50 mV s^{-1}. Reproduced with permission.[105] Copyright 2024, Elsevier.

This diversity of HEA designs for FAOR illustrates how structural and compositional variations can be leveraged to enhance activity, CO-tolerance, and stability, motivating the exploration of different architectures and compositional strategies. Cheng et al.[106] synthesized PtCuNiCoMn HEA nanoparticles on reduced graphene oxide by a solvothermal co-reduction strategy, achieving significantly improved FAOR activity and long-term stability compared with binary/ternary Pt

View Article Online
DOI: 10.1039/D6CC01653G

alloys and commercial Pt/C. The performance enhancement originates from the high-entropy effect, severe lattice distortion, and sluggish diffusion that suppress dealloying of non-noble constituents and modulate the electronic structure of Pt active sites. Beyond random solid-solution HEAs, Shen et al.[107] engineered ultrasmall high-entropy intermetallic i-$(PtPdIrRu)_2FeCu$, which integrate the structural ordering of intermetallics with the atomic-level site dilution characteristic of HEAs. The resulted isolated Pt-group metal ensembles exhibit weakened CO* binding and impeded CO* diffusion, thereby enabling a direct FAOR pathway and delivering over one order of magnitude higher intrinsic activity than pure Pt while retaining superior durability under potential cycling. Complementarily, Zuo et al.[108] reported hollow PdCuMoNiCo HEA spheres supported on graphene/CNT hybrids, whose high-entropy composition together with the hollow architecture substantially increases electrochemically accessible surface area, optimizes intermediate adsorption, and stabilizes the catalyst against corrosion. These HEAs exhibit exceptional FAOR mass activity surpassing commercial Pt/C and outperforming solid Pd-based alloys, highlighting the synergistic advantages of structural voids and multi-element entropy stabilization.

For FAOR, the most important design principle is to suppress contiguous Pt ensembles that favor the indirect CO-producing pathway, while preserving Pt-based motifs that can efficiently activate formic acid through the direct dehydrogenation route. This can be achieved by diluting Pt with electronically complementary elements such as Bi, Pb, Co, or Ni, and by introducing neighboring sites that facilitate OH-assisted oxidation of poisoning intermediates. Structurally, surface-segregated or core–shell architectures with entropy-stabilized outer layers are especially attractive because they allow simultaneous control over Pt ensemble size, adsorption energetics, and resistance to deactivation. Therefore, the design principle for FAOR-active Pt-HEAs is to tailor the local Pt neighborhood so that direct-pathway selectivity and anti-poisoning behavior are simultaneously improved .

3.6 Alcohol oxidation

The alcohol oxidation reaction in fuel cells is the core anodic process of direct alcohol fuel cells, which converts liquid alcohols into carbon dioxide through electrocatalytic oxidation while releasing electrons and protons to drive the external circuit to generate current. Liquid alcohol fuels have high energy density, with an electrical energy conversion efficiency of 40–60%, far exceeding the 30% conversion efficiency of traditional internal combustion engines. In addition, the fuel storage and transportation are convenient and safe. Meanwhile, they possess significant green sustainability: alcohols prepared from biomass can achieve a carbon closed-loop cycle, and the reaction process is nearly zero-pollution-free. They play an important role in realizing efficient and green energy conversion. Research on electrocatalysts for alcohol oxidation reactions mainly focuses on two key alcohols: methanol and ethanol. Pt-based catalysts are considered as the most active electrocatalysts in acidic electrolytes. Methanol, which lacks C–C bonds, can be relatively efficiently and completely oxidized to CO_2 (with $6e^-$ transfer),[109] but toxic intermediate CO* is easily generated during the dehydrogenation process, leading to poisoning of traditional Pt catalysts.[110] Ethanol, due to its C–C bonds, has an extremely high C–C bond cleavage energy barrier, resulting in the actual reaction being dominated by incomplete oxidation (producing acetaldehyde/acetic acid, releasing only $4e^-$), which reduces the energy conversion efficiency.[111]

View Article Online
DOI: 10.1039/D6CC01653G

Given the challenges of incomplete oxidation, CO poisoning, and limited energy conversion efficiency in conventional alcohol oxidation reactions, designing advanced catalysts that can both enhance activity and mitigate poisoning is critical. HEAs offer a promising strategy in this regard, as their multi-element composition allows fine-tuning of the electronic structure at active sites to improve both activity and durability. Lv et al.[112] proposed a HEA dual-site catalyst design strategy based on electronegativity modulation to address the challenges of low activity and susceptibility to CO poisoning faced by catalysts for MOR. By incorporating elements with low electronegativity (Ga, Ni) and high electronegativity (W) into the PtRhGaNiW HEA, bidirectional regulation of the d-band center of Pt-Rh dual sites is achieved. This regulatory mechanism can drive the redistribution of electron clouds of Pt-Rh dual sites over a wide orbital range, optimizing their electronic structure. PtRhGaNiW HEA nanowires exhibit excellent performance (Fig. 19d), with a MOR current density of up to 5.61 mA cm^{-2}, which is 3.38 times and 9.75 times of that of PtRh alloy and commercial Pt/C, respectively (Fig. 19e). They also show significantly improved stability and CO poisoning resistance. DFT calculations indicate that low electronegativity Ga/Ni donate electrons to Pt-Rh, while high electronegativity W withdraws electrons from Pt-Rh, synergistically inducing electron cloud redistribution within a wide orbital window (Fig. 19a). This shifts the d-band center of Pt from −2.24 eV in PtRh to −2.40 eV (Fig. 19d), moving away from the Fermi level, weakening CO adsorption (Fig. 19b and c), and promoting the direct oxidation of OH, thereby optimizing catalytic activity.

Building on the strategy of electronic structure tuning in HEAs, researchers have further explored core-shell architectures and site-specific element placement to enhance alcohol oxidation activity and durability. Lao et al.[113] prepared Pd-enriched core/Pt-enriched shell high-entropy alloy

View Article Online
DOI: 10.1039/D6CC01653G

nanoparticles (PdAgSn/PtBi HEA-NPs) via a facile synthesis method under low-temperature and atmospheric pressure (Fig. 19f). PdAgSn/PtBi HEA-NPs exhibit excellent electrocatalytic activity and durability in both MOR and ethanol oxidation reaction (EOR) (Fig. 19g and h). Their specific activity and mass activity for MOR reach 4.7 mA m^{-2} and 2874 mA mg_{Pd+Pt}^{-1}, which are 1.7 times and 5.9 times of that of commercial Pd/C catalyst, and 1.5 times and 4.8 times of that of commercial Pt/C catalyst, respectively. The mass activity for EOR reaches 3386 mA mg_{Pd+Pt}^{-1}, which is 5.4 times and 4.9 times of that of commercial Pd/C and Pt/C, respectively (Fig. 19i). Meanwhile, the lattice distortion and tensile strain caused by differences in atomic radii increase the number of surface-active sites, optimize the adsorption energy of reaction species, and provide abundant active centers for catalytic reactions. Ligand effect and tensile strain cause the upshift of Pt's d-band center, enhancing the binding ability to reaction species such as OH*. Differences in d-band centers across different sites enable efficient execution of elementary steps in multi-step reactions at suitable sites. Synergistic effects between Pt and Pd sites in the core-shell structure facilitate multi-step reaction processes such as ethanol oxidation. Oxygen-philic element Sn, by adsorbing OH*, accelerates the oxidation of intermediates to final products, enhancing overall reaction efficiency.

View Article Online
DOI: 10.1039/D6CC01653G

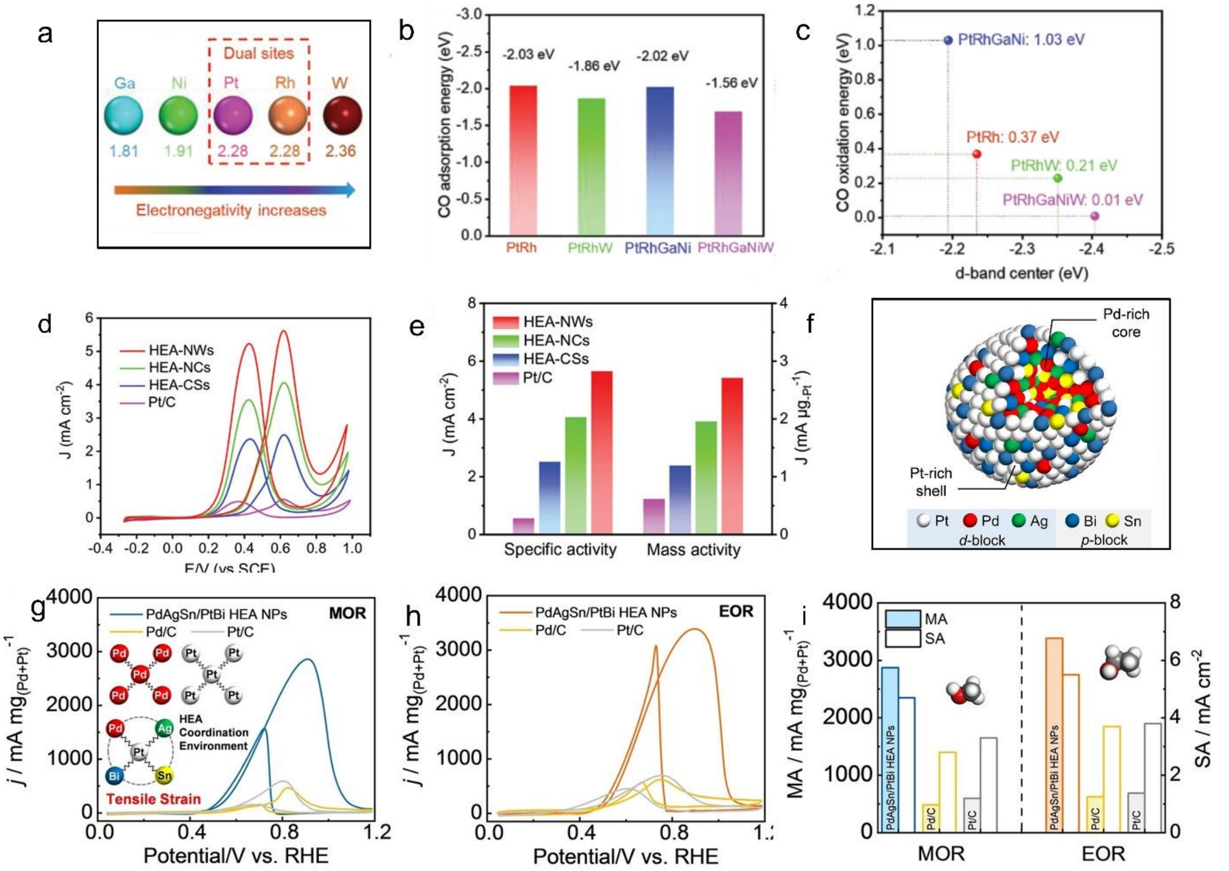

Fig. 19 (a) The electronegativity order for Ga, Ni, Pt, Rh, and W elements. (b) CO adsorption energy barriers. (c) CO oxidation energy barriers assisted by OH* (d) Cyclic-voltammogram curves of HEA-NWs, HEA-NCs, HEA-CSs, and Pt/C in 0.5 M H_2SO_4 + 2 M CH_3OH. (e) The comparison of catalytic performances. Reproduced with permission.[112] Copyright 2024, Wiley-VCH. (f) Structure diagram of PdAgSn/PtBi HEA-NPs. MOR and EOR performance and kinetic analysis of PdAgSn/PtBi HEA-NPs. (g) MOR curves, (h) EOR curves, (i) MA and SA values. Reproduced with permission.[113] Copyright 2023, Wiley-VCH.

Beyond electronic structure tuning and core-shell designs, further advances in alcohol oxidation catalysis have focused on morphology engineering, heterostructure formation, and atomic-level site control to maximize activity, CO tolerance, and long-term stability. Hu et al.[114] synthesized single-phase PdPtPbSnNi HEA nanowires through a mild solvothermal route, revealing that Pb-assisted nucleation and sequential reduction govern the formation of ordered nanowire networks. The synthesized HEA NWs deliver high activity toward both methanol and ethanol oxidation due to abundant active sites and optimized adsorption energetics. Beyond morphology-engineered HEAs, nanoscale structural reconstruction also plays a critical catalytic role. Wang et al.[115] developed septenary PtIrRhCoFeNiCu HEA nanodendrites exhibiting high-index facets and substantial lattice distortion that enhance ethanol adsorption, promote C–C bond cleavage, and improve resistance to CO poisoning, enabling mass activities far surpassing that of commercial Pt/C. Heterostructure engineering further expands HEA functionality in alcohol catalysis. For example, Yang et al.[116] reported a mesoporous PtPd-high-entropy oxide (HEO) heterostructure derived from HEA precursors, where interfacial electronic modulation between the PtPd alloy and HEO promotes OH generation, suppresses CO adsorption, and stabilizes active sites during methanol oxidation. The catalyst exhibits a mass activity for the MOR that is an order of magnitude higher than that of Pt/C, along with superior durability under DMFC operation. At the atomic scale, the introduction of high-entropy coordination environments to isolate Pt atoms provides an effective strategy to mitigate CO poisoning. Liu et al.[117] demonstrated that single-atom Pt embedded in a multi-element HEA matrix (Pt_1-NiCoMgBiSn) retains high MOR activity while avoiding Pt-Pt ensembles that generate CO*, achieving excellent mass activity and extraordinary stability over 180,000 s due to weakened CO* binding and facilitated intermediate oxidation. In ethanol fuel cell systems, tuning HEA composition provides a route to simultaneously enhance C-C bond cleavage and long-term device performance. Chang et al.[118] designed a septenary PtPdFeCoNiSnMn HEA with a PtPd-rich surface, where Pd accelerates C-C bond scission, Sn and Ni modulate OH adsorption, and Fe/Co/Mn facilitate water activation. This multi-element synergy

View Article Online
DOI: 10.1039/D6CC01653G

enables complete 12-electron ethanol oxidation, delivering a record power density of 0.72 W cm^{-2} and stable operation for over 1,200 h in DEFCs.

For methanol and ethanol oxidation, Pt-based HEAs should be designed to spatially couple at least three catalytic functions: alcohol adsorption/dehydrogenation on Pt-like sites, OH* generation on oxophilic neighboring sites such as Sn, W, or Ni containing motifs, and poison/intermediate removal on electronically tuned multimetal interfaces. For ethanol oxidation, additional attention should be paid to constructing surface environments that facilitate C–C bond cleavage rather than merely promoting partial oxidation to acetaldehyde or acetate. Morphologies such as nanowires, nanodendrites, mesoporous frameworks, or core–shell structures are particularly valuable because they expose multifunctional neighboring sites while maintaining mass transport and durability. Thus, the design principle is not simply to weaken CO adsorption, but to deliberately distribute different catalytic tasks across chemically distinct surface motifs.

3.7 Electrochemical synthesis

Electrochemical synthesis, as a green and sustainable chemical manufacturing strategy, utilizes electrical energy to drive target reactions, enabling the efficient and highly selective synthesis of high-value-added chemicals under mild conditions. However, the development of high-performance, stable, and low-cost catalysts for electrochemical synthesis remains a significant challenge. Many crucial electrochemical synthesis reactions, such as the carbon dioxide reduction reaction (CO_2RR),[119] nitrogen reduction reaction (NRR) for ammonia synthesis,[120] electro-oxidation/electro-reduction of organic molecules,[121] and electrocatalytic hydrogenation or dehydrogenation,[122] often depend on noble metal catalysts to ensure adequate activity and

View Article Online
DOI: 10.1039/D6CC01653G

selectivity. Nevertheless, their exorbitant cost, limited reserves, and the challenges of activity-selectivity trade-offs or stability issues in complex reaction networks severely restrict their large-scale practical applications. In this context, HEAs exhibit tremendous potential in advancing electrocatalytic synthesis.

To illustrate this potential, Luo et al.[123] proposed a progressive construction strategy (Fig. 20a) and successfully fabricated FCC phase Pt-based HEA catalyst PtCuSnAuPd/SiO_2 with an average particle size of 2.8 nm (Fig. 20d and f). In this study, elements including Cu (for dilution), Sn (for encapsulation), Au (for surface segregation), and Pd (for inducing heterogeneity) were introduced to achieve precise regulation of Pt active sites. This design not only ensures a high Pt exposure degree but also effectively suppresses side reactions and deactivation processes. In the propane dehydrogenation (PDH) reaction, the catalyst exhibits excellent performance. The propylene selectivity exceeds 97% (Fig. 20b), with formation rates of 256 and 390 $\mathrm{mol_{C_3H_6}\ g_{Pt}^{-1}\ h^{-1}}$ at 550 °C and 600 °C (Fig. 20c), respectively. Furthermore, it maintains high activity over 220 hours of continuous operation (Fig. 20e), demonstrating exceptional durability under harsh reaction conditions. This achievement not only sets a new performance record for multi-metallic alloys in small-molecule activation but also provides an important paradigm for the application of HEAs in complex reaction systems. This work demonstrates that the "gradual coupling of alloying effects" plays a crucial role in performance enhancement, where the electronic structure and spatial distribution of active sites are optimized through the synergistic regulation of different elements.

View Article Online
DOI: 10.1039/D6CC01653G

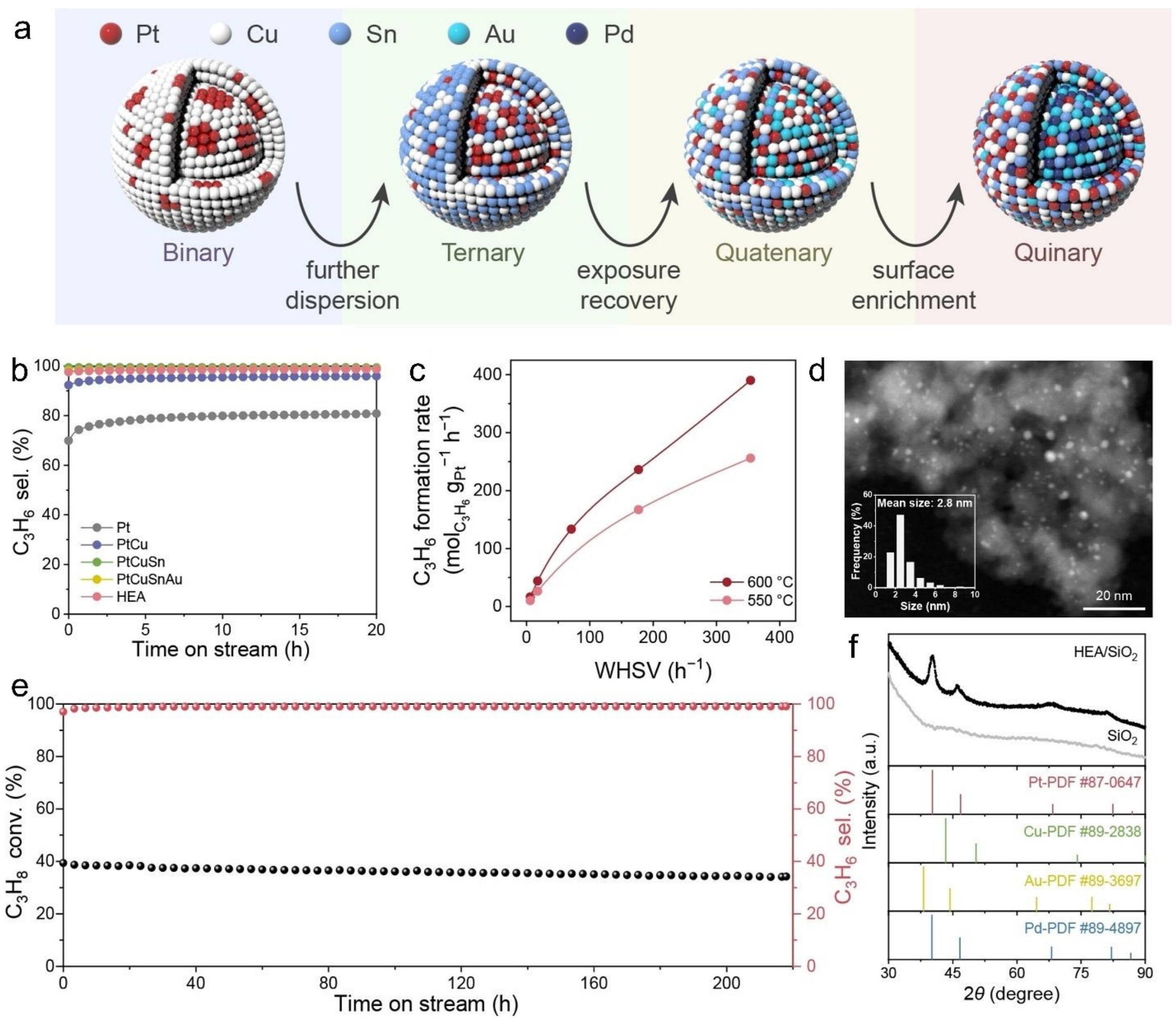

Fig. 20 (a) Schematic progressive design of the HEA catalyst with abundant isolated Pt sites on the surface by introducing Cu, Sn, Au, and Pd. (b) C_3H_6 selectivity of Pt/SiO_2, PtCu/SiO_2, PtCuSn/SiO_2, PtCuSnAu/SiO_2, and HEA/SiO_2 (c) Initial C_3H_6 formation rate as a function of WHSV for HEA/SiO_2 at 550 and 600 °C. (d) HAADF-STEM image and corresponding size distribution of HEA/SiO_2. (e) Long-term stability test of HEA/SiO_2. Catalytic conditions of (a–d): 550 °C, atmospheric pressure, C_3H_8:H_2:Ar=1:1:8, weight hourly space velocity (WHSV) of 5.9 h^{-1}. (f) XRD patterns of HEA/SiO_2 and pure SiO_2. Reproduced with permission.[123] Copyright 2024, Wiley-VCH.

View Article Online
DOI: 10.1039/D6CC01653G

Building on the importance of multi-metallic alloys, Zhang et al.[124] developed PtFeCoNiCu HEA nanoparticles supported on CNT using a lithium naphthalenide-driven reduction method. This PtFeCoNiCu/CNT catalyst showed remarkable catalytic performance in the aqueous-phase hydrogenation of maleic anhydride to succinic acid, with a mass activity significantly higher than that of traditional Pt/CNT catalyst. The enhanced activity and stability were attributed to the synergy between the various metals, along with the formation of a stable and well-dispersed HEA structure, further confirming the benefits of using HEA catalysts in complex reactions. Further expanding on the role of structural design in HEA catalysts, Lu et al.[125] synthesized PtPdCoCuNi HEA nanoparticles via a colloidal approach and investigated their catalytic performance for nitrobenzene hydrogenation. The PtPdCoCuNi/SiO_2 catalyst demonstrated a yield of aniline that is 2.11 times higher than that of the PtPd/SiO_2 catalyst, even at room temperature. The exceptional performance is attributed to the formation of isolated Pt and Pd sites within the HEA structure, which facilitated enhanced interaction with nitrobenzene and improved hydrogenation activity. This work reinforced the concept that high-entropy alloying in catalysts not only boosts catalytic activity but also allows for the fine-tuning of active sites for specific reactions. In the field of coal conversion, a recent study by Wang et al.[126] reported a synergistic catalyst system comprising a PtPdCoNiCu/C HEA and $H_4SiW_{12}O_{40}$ for the low-temperature hydrogenolysis of C–O bonds in coal-derived compounds. The key innovation lies in the system's ability to efficiently cleave C–O bonds under exceptionally mild conditions (50 °C, 0.1 MPa H_2), achieving near-complete conversion (99.8%) of benzyl phenyl ether to toluene and phenol while effectively suppressing aromatic ring over-hydrogenation. Mechanistic studies revealed that the introduction of $H_4SiW_{12}O_{40}$ drastically reduces the apparent activation energy from 86.4 kJ/mol to 31.6 kJ/mol,

View Article Online
DOI: 10.1039/D6CC01653G

which is attributed to a hydrogen spillover effect that significantly accelerates the reaction rate. Furthermore, the catalyst demonstrated excellent stability over multiple cycles and was successfully applied to the hydrogenolysis of real low-rank coal, showcasing a promising pathway for the high-value utilization of coal resources under mild conditions.

In broader electrochemical synthesis and hydrogenation/dehydrogenation reactions, Pt-based HEAs should be designed to combine site isolation, tunable adsorption strength, and controlled multistep reaction pathways within a single catalyst surface. This means that Pt should not always be maximally exposed. Instead, isolated or diluted Pt motifs embedded in a multimetal environment may be more effective for suppressing side reactions and enhancing chemoselectivity. Accordingly, a practical design principle is to use high-entropy alloying to assign different neighboring elements to distinct catalytic roles, such as reactant activation, intermediate stabilization, or product desorption, while maintaining sufficient electrical conductivity and structural stability.

4. Mechanistic Understanding of Pt-Based HEAs in Electrocatalysis

4.1 Advanced Characterization and Mechanistic Analysis of Pt-Based HEAs

Theoretical calculations provide a valuable perspective for understanding the catalytic mechanisms of Pt-based HEAs by linking local Pt-M motifs to adsorption energies, reaction pathways, and reaction barriers.[127] However, theoretical calculation alone is insufficient to fully describe these systems, because many current DFT studies are constrained by small supercells, limited configurational sampling, and the difficulty of capturing dynamic structural evolution under realistic operating conditions. Consequently, theoretical results often represent only part of

View Article Online
DOI: 10.1039/D6CC01653G

the structural complexity of real HEA surfaces.[128] A comprehensive mechanistic understanding therefore requires the combination of theoretical calculations with advanced characterization, particularly local and operando techniques that can experimentally resolve coordination environments, electronic states, and surface reconstruction behavior.[129]

Conventional long-range structural probes such as XRD provide the first evidence for single-phase solid-solution formation, lattice distortion, and crystal strain-key structural signatures underpinning the continuous tuning of the d-band center in HEAs. For instance, FeCoNiCuIr HEA nanoparticles were verified by XRD and TEM/HRTEM to have a single-phase FCC structure with uniform size, and these HEAs exhibited excellent performance in alkaline OER.[130] Furthermore, a study on the synthesis of PtPdRhRuCu HEA confirmed, through characterizations such as HAADF-STEM and XRD, mesoporous nanospheres with uniform mixing of all components and the formation of a single lattice (without obvious phase separation/enrichment), which provided a structural basis for their subsequent high catalytic activity.[131]

Surface-sensitive techniques such as XPS further provide essential information on oxidation states, surface segregation, and inter-element charge transfer. This information is crucial for understanding the mechanisms of HEAs, such as multi-site distribution, electronic synergy, adsorption/desorption behaviors of intermediates, and poison-resistance. In fact, in some studies adopting "HEA core-shell" structures or surface modification (e.g., nitrogen doping), XPS has been employed to confirm the composition of the Pt shell/HEA core, as well as the presence and chemical states of surface N or other doping elements.[86] This thereby sheds light on the regulation of electronic structure, the optimization of intermediate adsorption energy, and long-term catalytic

View Article Online
DOI: 10.1039/D6CC01653G

stability.[132]

XAS including both X-ray absorption near edge structure (XANES) and extended X-ray absorption fine structure (EXAFS), has become one of the most powerful tools for probing the local coordination environment, oxidation states, and electronic structure of HEA electrocatalysts under realistic conditions. Owing to the element-specific and long-range-disorder-insensitive nature of XAS, it provides critical information that cannot be obtained from XRD or TEM, particularly for multimetallic HEAs containing complex bond configurations. Early work by Yao et al. demonstrated that carbothermal-shock synthesis can produce single-phase Pt-Fe-Co-Ni-Cu HEA nanoparticles. XANES and EXAFS analyses revealed compressed Pt-M bond lengths and decreased Pt L_3-edge white-line intensity, indicating electronic redistribution and modified d-band occupation responsible for enhanced ORR performance.[49] Building on this information, Chen et al. applied multi-edge EXAFS to ultrasmall ordered HEA/HEI nanoparticles and quantified coordination numbers and bond-length distributions. Their results showed that ordered-disordered differences in local atomic environments directly map onto variations in ORR mass activity.[133] Similarly, Feng et al. engineered structurally ordered HEI/HEA architectures and used XAS to identify element-specific coordination perturbations induced by compositional tuning, which correlated strongly with Pt utilization and fuel-cell performance.[134]

Across multiple studies, EXAFS-derived parameters such as broadened bond-length distributions and increased mean-square relative displacement (σ^2) have emerged as quantitative indicators of lattice distortion and local disorder, which are key structural features that contribute to broadened adsorption-energy distributions and enhanced electrocatalytic kinetics in HEAs.[135,136] To bridge

View Article Online
DOI: 10.1039/D6CC01653G

static structural fingerprints with working-state behavior, several groups conducted in situ/operando XAS, showing that Pt-based HEAs maintain robust Pt-M coordination during ORR, HER, or cycling conditions, while displaying reversible changes in oxidation state and bond lengths. Importantly, catalysts showing more stable operando coordination demonstrate superior durability.[137] XAS has also enabled structural validation of unconventional HEA motifs, such as HCP Pt-group HEAs where multi-edge measurements confirmed atomic mixing and unique coordination geometries that enhance alkaline HER performance.[138] Finally, systematic reviews that integrate XAS with microscopy and theoretical studies have identified practical strategies, such as analyzing multiple absorption edges, fitting multiple coordination shells, and carefully interpreting σ^2 values. These studies show that XAS is essential for connecting the local atomic and electronic structure of a catalyst with how it interacts with reaction intermediates, which ultimately determines its catalytic activity and stability.[139]

4.2 Fundamental Origins of Activity and Stability in Pt-Based HEAs

The superior electrocatalytic performance of Pt-based HEAs is believed to originate from the coupling of several structural and electronic effects that collectively govern the adsorption and conversion of reaction intermediates. One contributing factor is electronic structure regulation, particularly the modulation of Pt-centered d states through alloying. The incorporation of additional metallic elements tends to modify the local coordination environment of Pt, induce some degree of charge redistribution between neighboring atoms, and influence the filling and energy position of the surface d states. In high-entropy alloys, the wide compositional space and the possibility to gradually vary elemental proportions may enable a nearly continuous tuning of the d-band center and associated adsorption energetics. However, it should be noted that this tunability

View Article Online
DOI: 10.1039/D6CC01653G

does not necessarily extend to every multi-component system and may be more readily realized in alloys that retain a single-phase solid-solution character with relatively uniform elemental mixing. As a consequence of these electronic modifications, the adsorption strengths of key intermediates such as H, OH, O, OOH, and CO* can often be shifted toward more favorable values. In practice, such electronic regulation might be reflected in the shift of the d-band center, modification of the density of states near the Fermi level, or redistribution of electron density at Pt–M interfaces. These changes are generally considered important because they can directly influence the activation barriers and turnover kinetics of elementary steps in HER, HOR, ORR, and small-molecule electrooxidation.

A second important mechanism is multi-site synergy and ensemble cooperation. In Pt-based multimetallic systems, different surface atoms or atomic ensembles can preferentially mediate different reaction steps. Pt-rich sites often provide favorable adsorption for hydrogen-containing intermediates, whereas more oxophilic components can facilitate water dissociation, OH* formation, or the oxidative removal of poisoning species. In this way, neighboring atoms do not simply dilute Pt, but can participate cooperatively in a division of catalytic labor. Such bifunctional or ensemble effects are especially important in reactions involving coupled proton transfer and oxygenated intermediates, such as HER in alkaline media, HOR, FAOR, MOR, and related electrooxidation processes.

In addition, lattice distortion and local strain effects further contribute to catalytic optimization. By alloying elements with different atomic radius, electronegativity, and bonding preference, their incorporation into a common lattice perturbs interatomic distances and orbital overlap, thereby

View Article Online
DOI: 10.1039/D6CC01653G

modifying the electronic states and adsorption behavior of surface atoms. Local strain can weaken excessively strong binding of poisoning species or over-stabilized intermediates, and also lowers kinetic barriers for intermediate conversion. These effects are often closely coupled with electronic regulation and cannot be considered independently, since local coordination, charge transfer, and strain collectively define the catalytic behavior of each surface site.

At the same time, enhanced poison tolerance and operational stability are frequently observed in Pt-based multimetallic catalysts. Through local electronic tuning and the introduction of oxophilic neighboring atoms, strongly adsorbed poisons such as CO* may bind less strongly or be removed more easily through assisted oxidation. Likewise, multicomponent alloying can suppress rapid particle coarsening, phase separation, or loss of active surface motifs during long-term electrochemical operation, thereby contributing to improved durability.

Collectively, these electronic, structural, multi-site, and stability-enhancing effects endow Pt-based HEAs with outstanding electrocatalytic behavior, yet they do not fully capture what distinguishes HEAs from conventional low- and medium-entropy alloys. Therefore, the presence of d-band-center shifts, charge redistribution, or multi-site synergy alone should not be regarded as a unique mechanistic signature of HEAs. More fundamentally, the distinctive value of Pt-based HEAs does not lie simply in stronger electronic tuning or more pronounced multimetal synergy, since such effects can also be realized in carefully designed low entropy alloys (LEAs) and medium-entropy alloys. Instead, the primary advantage of Pt-based HEAs stems from their high configurational entropy, which stabilizes an exceptionally wide variety of local atomic environments within a single-phase crystalline lattice. In this sense, HEAs should be viewed not

View Article Online
DOI: 10.1039/D6CC01653G

merely as more complex multimetallic alloys, but as catalytic systems in which local structural heterogeneity itself becomes a functional resource. This feature leads to a catalytic mode that differs from that of many LEAs and medium-entropy alloys. In lower-entropy alloys, performance optimization is often centered on identifying a limited number of favorable Pt-M interactions or a relatively well-defined active motif. By contrast, Pt-based HEAs are less dependent on one idealized active site and more capable of operating through a distributed ensemble of diverse near-optimal sites. Different local motifs may contribute to different elementary steps, different intermediates, or even different reaction pathways. Therefore, the advantage of HEAs is not simply that the average adsorption energy can be tuned, but that a broad population of catalytically competent sites can coexist and function collectively on the same surface.

Furthermore, the durability of Pt-based HEAs should not be interpreted only by resistance to elemental leaching or surface reconstruction. Under realistic electrochemical conditions, especially for nanoscale catalysts, partial dissolution of non-noble elements and local structural reconstruction are inevitable. Therefore, their stability advantage is more appropriately attributed to enhanced tolerance to electrochemical reconstruction rather than only to the classical sluggish diffusion effect. Owing to their complex surface and subsurface environment, Pt-based HEAs can distribute degradation pathways over a broader range of local atomic configurations, retard catastrophic segregation or collapse, and preserve catalytically competent motifs after partial reconstruction. In addition, the statistical redundancy of diverse near-optimal active sites allows HEAs to maintain catalytic function even when some local motifs are lost during operation. This ability to sustain functional catalytic heterogeneity under dynamic operating conditions is likely a key origin of their frequently observed long-term durability.

View Article Online
DOI: 10.1039/D6CC01653G

This interpretation is strongly supported by advanced characterization. Operando XAS often shows that local oxidation states and coordination numbers evolve under potential bias, yet part of the Pt–M framework remains preserved or reversibly perturbed.[135,136] Identical-location TEM and high-resolution STEM reveal changes in particle morphology, shell composition, or near-surface contrast after cycling, consistent with selective dissolution and reconstruction rather than catastrophic collapse.[137] ICP-based elemental analyses also commonly indicate early-stage leaching of non-noble elements followed by a more stabilized composition profile at longer time. These observations collectively suggest that the most durable Pt-HEAs are not necessarily those that remain structurally unchanged, but those that reconstruct in a controlled and catalytically favorable way.[139]

Overall, the most characteristic advantage of Pt-based HEAs is that they introduce a distribution-based catalytic paradigm: instead of relying on one optimized composition or one dominant active site, they create a statistically rich landscape of local structures, site functions, and evolutionary pathways within a single alloy particle. This capacity to combine configurational diversity, distributed catalytic function, and dynamic resilience is what most clearly distinguishes Pt-based HEAs from conventional LEAs and medium-entropy alloys in electrocatalysis.

5. Summary and outlook

Pt-HEAs have emerged as a versatile electrocatalyst platform because they combine the intrinsic activity of Pt with multielement-induced local coordination diversity, broadened adsorption-energy distributions, and enhanced tolerance to poisoning and structural degradation. In addition

View Article Online
DOI: 10.1039/D6CC01653G

to conventional alloy design, the high-entropy strategy has recently been extended to phosphides and other non-metallic compound systems.[140] This trend provides a new direction for the structural design of high-performance electrocatalysts. Compared with conventional binary or ternary Pt alloys, Pt-HEAs are especially attractive for reactions in which multiple elementary steps must be coordinated on neighboring sites, such as alkaline HER, HOR, ORR under realistic durability constraints, and small-molecule oxidation reactions. At the same time, the present review also highlights an important limitation: the catalytic value of Pt-HEAs should not be framed solely in terms of “Pt saving”, because many reported Pt-HEAs still bury a substantial fraction of Pt atoms in the bulk and therefore do not yet match the atom-utilization efficiency of single-atom Pt catalysts or some advanced low-Pt core-shell/intermetallic systems. Thus, the future of Pt-HEAs lies not only in increasing compositional complexity, but in learning how to position Pt atoms where they are catalytically most useful.

The first priority is therefore to move from bulk-random multimetal nanoparticles toward surface-confined, ultrathin, or atomically dispersed Pt-HEA motifs. Several promising strategies can be envisioned. One is to construct Pt-enriched skins or near-surface Pt ensembles on high-entropy subsurfaces, so that the surface maintains high Pt utilization while the multimetal framework still tunes adsorption energetics. A second strategy is to develop ultrathin HEA architectures, such as nanoframes, nanowires, hollow structures, or two-dimensional metallenes, in which a much larger fraction of metal atoms is exposed at the surface. Thirdly, the most powerful strategy is to combine the logic of single-atom catalysis with high-entropy coordination engineering, that is, to build single-atom-like Pt sites embedded in or surrounded by high-entropy environments. This direction is already becoming experimentally realistic. A recent work on high-entropy-alloyed single-atom

View Article Online
DOI: 10.1039/D6CC01653G

Pt shows that Pt can be retained at only 2.3 at% while still delivering high methanol oxidation activity and strong CO tolerance, precisely because the high-entropy coordination shell around Pt actively assists poison removal.[117] Similarly, recent studies on high-entropy metallenes show that atomically thin high-entropy architectures can maximize atom exposure while preserving multimetal synergy.[141] These examples suggest that the next generation of Pt-HEAs should aim not merely for lower average Pt content, but for maximally exposed, electronically tuned, and functionally differentiated Pt sites.

The second priority is the data-driven exploration of the enormous compositional space of Pt-HEAs. Because the number of possible local atomic motifs on HEA surfaces is effectively combinatorial, and empirical trial-and-error optimization is unlikely to be efficient. Therefore, artificial intelligence and machine learning can play a transformative role. Recent studies have shown that local-environment-aware electronic descriptors can be used to predict catalytic activity in HEAs more effectively than composition-only descriptions, while machine-learning models trained on adsorption energies offer a practical route to rapidly screen vast numbers of local configurations.[142-143] In the future, the most productive workflow will likely couple calculation of phase diagrams (CALPHAD) or thermodynamic phase prediction, DFT or cluster-based sampling of representative motifs, and active-learning or Bayesian-optimization frameworks that iteratively propose the next most informative compositions for experiment. Importantly, artificial intelligence and machine learning should not only target activity, but should be trained as a multi-objective design tool that simultaneously considers Pt loading, phase stability, segregation tendency, poison tolerance, and durability under operating conditions. In this way, computational screening can help

View Article Online
DOI: 10.1039/D6CC01653G

identify not only the “best composition”, but the best trade-off surface among activity, stability, and noble-metal economy.

Finally, future work should benchmark Pt-HEAs more rigorously against medium-entropy alloys, lower-entropy Pt alloys, and advanced low-Pt catalyst architectures. This is crucial not to diminish the importance of Pt-HEAs, but to clarify where their truly distinctive value lies. In descriptor-dominated reactions, simpler low-Pt catalysts may remain highly competitive in Pt utilization. By contrast, in multistep electrocatalytic reactions that require neighboring-site cooperation, poison tolerance, and dynamically stable reconstructed surfaces, Pt-HEAs may offer more fundamental advantages. The long-term goal should therefore be evolving Pt-HEAs from compositionally complex materials into precisely engineered catalytic platforms, in which Pt is not merely diluted, but strategically positioned, electronically regulated, and maximally utilized.

Author contributions

Yehao Li: data curation, investigation, visualization, writing–original draft, review & editing. Zhuyin Sui: visualization, writing–review & editing. Jinghe Zheng: writing–review & editing. Hongzhi Cui: supervision, writing–review & editing. Zhenhua Yan: writing–review & editing. Kun Jiang: supervision, writing–review & editing. Leigang Li: conceptualization, supervision, validation, funding acquisition, writing–original draft, review & editing.

Data availability

No primary research results, software or code have been included and no new data were generated or analysed as part of this review.

View Article Online
DOI: 10.1039/D6CC01653G

Conflicts of interest

There are no conflicts of interest to declare.

Acknowledgements

The authors acknowledge the financial support from the Natural Science Foundation of Shandong Province (ZR2024MB065), Taishan Scholar of Youth Plan (tsqn202211072), Yantai Science and Technology Bureau (2024JMRH004), Taishan Scholar of Climbing Plan (tspd20230603), National Natural Science Foundation of China (22472038, 52331004, 22472038), Major-Special Science and Technology Project in Shandong Province (2023ZLGX05), and Fundamental Research Fund for Central University (202141027).

References

1 A. Raza, J. Z. Hassan, U. Qumar, A. Zaheer, Z. U. D. Babar, V. Iannotti and A. Cassinese, *Mater. Today Adv.*, 2024, **22**, 100488.

2 M. Zhou, H.-L. Wang and S. Guo, *Chem. Soc. Rev.*, 2016, **45**, 1273–1307.

3 K. Jiang, D. Zhao, S. Guo, X. Zhang, X. Zhu, J. Guo, G. Lu and X. Huang, *Sci. Adv.*, 2017, **3**, e1601705.

4 B. Y. Xia, H. B. Wu, N. Li, Y. Yan, X. W. (David) Lou and X. Wang, *Angew. Chem. Int. Ed.*, 2015, **54**, 3797–3801.

5 M. Luo, Y. Sun, X. Zhang, Y. Qin, M. Li, Y. Li, C. Li, Y. Yang, L. Wang, P. Gao, G. Lu and S. Guo, *Adv. Mater.*, 2018, **30**, 1705515.

6 J.-W. Yeh, S.-K. Chen, S.-J. Lin, J.-Y. Gan, T.-S. Chin, T.-T. Shun, C.-H. Tsau and S.-Y. Chang, *Adv. Eng. Mater.*, 2004, **6**, 299–303.

7 D. B. Miracle and O. N. Senkov, *Acta Mater.*, 2017, **122**, 448–511.

8 E. J. Pickering and N. G. Jones, *Int. Mater. Rev.*, 2016, **61**, 183–202.

9 Y. Zhang, T. T. Zuo, Z. Tang, M. C. Gao, K. A. Dahmen, P. K. Liaw and Z. P. Lu, *Prog. Mater. Sci.*, 2014, **61**, 1–93.

10 Y. Xin, S. Li, Y. Qian, W. Zhu, H. Yuan, P. Jiang, R. Guo and L. Wang, *ACS Catal.*, 2020, **10**, 11280–11306.

View Article Online
DOI: 10.1039/D6CC01653G

11 M.-H. Tsai and J.-W. Yeh, *Mater. Res. Lett.*, 2014, **2**, 107–123.

12 K.-Y. Tsai, M.-H. Tsai and J.-W. Yeh, *Acta Mater.*, 2013, **61**, 4887–4897.

13 B. Cantor, I. T. H. Chang, P. Knight and A. J. B. Vincent, *Mater. Sci. Eng. A*, 2004, **375–377**, 213–218.

14 X. Huang, G. Yang, S. Li, H. Wang, Y. Cao, F. Peng and H. Yu, *J. Energy Chem.*, 2022, **68**, 721–751.

15 K. Wang, R. Chen, H. Yang, Y. Chen, H. Jia, Y. He, S. Song and Y. Wang, *Adv. Funct. Mater.*, 2024, **34**, 2310683.

16 G. Feng, F. Ning, J. Song, H. Shang, K. Zhang, Z. Ding, P. Gao, W. Chu and D. Xia, *J. Am. Chem. Soc.*, 2021, **143**, 17117–17127.

17 L. Luo, R. Tang, L. Su, J. Kou, X. Guo, Y. Li, X. Cao, J. Cui and S. Gong, *Energy Storage Mater.*, 2024, **72**, 103773.

18 J. Chen, A. Wu, Y. Zhang, Y. Xie, H. Zheng and W. Teng, *Front. Mater.*, 2025, **12**, 1613997.

19 W. Wang and Y. Tong, *Mater. Today Energy*, 2026, **55**, 102174.

20 L. Miao, Y. Cheng, Y. Liu, X. Li, L. Zhang and W. Wang, *J. Alloys Compd.*, 2024, **984**, 173951.

21 T. Chen, F. Ning, J. Qi, G. Feng, Y. Wang, J. Song, T. Yang, X. Liu, L. Chen and D. Xia, *iScience*, 2023, **26**, 105890.

22 H. Qi, F. Lu, Q. Li, Q. Wu, Z. Kang, Y. Hou, L. Su, S. Li, Z. Huang and G. Feng, *Adv. Funct. Mater.*, 2025, e19434.

23 C. Meng, X. Wang, Z. Li, C. Wu, L. Chang, R. Liu and W. Pei, *Mater. Adv.*, 2024, **5**, 719–729.

24 Z. Shi, L. Wang, Y. Huang, X. Y. Kong and L. Ye, *Mater. Chem. Front.*, 2024, **8**, 179–191.

25 A. M. Sadeq, R. Z. Homod, A. K. Hussein, H. Togun, A. Mahmoodi, H. F. Isleem, A. R. Patil and A. H. Moghaddam, *Sci. Total Environ.*, 2024, **939**, 173622.

26 Y. Nakaya and S. Furukawa, *Chem. Sci.*, 2024, **15**, 12644–12666.

27 W. Li, T. Wang, X. Chu, H. Lv, X. Cheng, Y. Zhou and X. Li, *Mater. Today Energy*, 2024, **43**, 101580.

28 Z. Liang, Y. Yang, Z. Tao, R. Gao, Y. Chen and P. Li, *J. Mater. Chem. A*, 2025, **13**, 25195–25212.

29 R. Boukhchina, M. Hamdi, S. El Alimi, *AIMS Energy*, 2025, **13**, 696–731.

30 X. Zhang, Y. Liu, X. Zhao, Z. Cheng and X. Mu, *Energy Fuels*, 2024, **38**, 19236–19252.

31 Q. Wang and Y. Yao, *npj Comput. Mater.*, 2025, **11**, 91.

32 Y. Zhang, D. Wang and S. Wang, *Small*, 2022, **18**, 2104339.

33 W. Wan, K. Liang, P. Zhu, P. He and S. Zhang, *J. Mater. Sci. Technol.*, 2024, **178**, 226–246.

34 J. Zhu, X. Yu, M. Guo, Z. Chen and B.-J. Ni, *Adv. Funct. Mater.*, 2026, **36**, e22077.

35 L. Wang, L. Wang, X. Meng and F.-S. Xiao, *Adv. Mater.*, 2019, **31**, 1901905.

36 L. Fu, H. N. Nam, J. Zhou, Y. Kang, K. Wang, Z. Zhou, Y. Zhao, L. Zhu, R. Nandan, M. Eguchi, Q. M. Phung, T. Yokoshima, K. Wu and Y. Yamauchi, *ACS Nano*, 2024, **18**, 27617–27629.

37 M. A. Chandran, P. Dutta, P. Singh, A. K. Singh and B. L. V. Prasad, *Adv. Funct. Mater.*, 2025, **35**, 2418644.

38 Y. Saso, Y. Kang, L. Fu, K. Yagi, J. You, Y. Asakura and Y. Yamauchi, *Chem. Sci.*, 2025, **16**, 21836–21841.

39 J. Zheng, Y. Li, W. Xu, B. Sun, T. Xu, S. Liu, X. Zhu, Y. Liu, S. Zhang, M. Ge and X. Yuan, *Inorg. Chem.*, 2024, **63**, 20697–20704.

40 Y. Zhang, S. G. Ma and J. W. Qiao, *Metall. Mater. Trans. A*, 2012, **43**, 2625–2630.

41 S. Tahir, N. Shkodich, B. Eggert, J. Lill, O. Gatsa, M. Flimelová, E. Adabifiroozjaei, N. M. Bulgakova, L. Molina-Luna, H. Wende, M. Farle, A. V. Bulgakov, C. Doñate-Buendía and B. Gökce, *ChemNanoMat*, 2024, **10**, e202400064.

42 J. Johny, Y. Li, M. Kamp, O. Prymak, S.-X. Liang, T. Krekeler, M. Ritter, L. Kienle, C. Rehbock, S. Barcikowski and S. Reichenberger, *Nano Res.*, 2022, **15**, 4807–4819.

43 C. Guo, X. Hu, X. Han, Y. Gao, T. Zheng, D. Chen, X. Qiu, P. Wang, K. Xu, Y. Chen, R. Zhou, M. Zong, J. Wang, Z. Xia, J. Hao and K. Xie, *J. Am. Chem. Soc.*, 2024, **146**, 18407–18417.

44 Y. Lu, K. Huang, X. Cao, L. Zhang, T. Wang, D. Peng, B. Zhang, Z. Liu, J. Wu, Y. Zhang, C. Chen and Y. Huang, *Adv. Funct. Mater.*, 2022, **32**, 2110645.

45 C. E. Park, G. H. Jeong, V. Maheskumar, J. Theerthagiri and M. Y. Choi, *J. Mater. Chem. A*, 2024, **12**, 21744–21757.

46 Y. Yu, Q. Wang, X. Li, Q. Xie, K. Xu, S. Zhang, H. Zhang, M. Gong and W. Lei, *Nano Mater. Sci.*, 2025, **7**, 400–408.

47 J.-H. Cha, S.-H. Cho, D.-H. Kim, D. Jeon, S. Park, J.-W. Jung, I.-D. Kim and S.-Y. Choi, *Adv. Mater.*, 2023, **35**, 2305222.

48 H. Ye, J. Su, G. Yang, L. Zhou, Y. Xie, X. Zhan, J. Tian and X. Tong, *Mater. Today Commun.*, 2025, **45**, 112365.

49 Y. Yao, Z. Huang, P. Xie, S. D. Lacey, R. J. Jacob, H. Xie, F. Chen, A. Nie, T. Pu, M. Rehwoldt, D. Yu, M. R. Zachariah, C. Wang, R. Shahbazian-Yassar, J. Li and L. Hu, *Science*, 2018, **359**, 1489–1494.

50 Z. Huang, Y. Peng, L. Xing, M. Xu, M. Fang, H. Xie, J. Li, Y. Zhou, P. Wu, N. Wang, C. Tang, M. Wu, L. Wang, S. Ye and L. Du, *Appl. Catal. B-Environ. Energy*, 2025, **363**, 124775.

51 H. Qiao, M. T. Saray, X. Wang, S. Xu, G. Chen, Z. Huang, C. Chen, G. Zhong, Q. Dong, M. Hong, H. Xie, R. Shahbazian-Yassar and L. Hu, *ACS Nano*, 2021, **15**, 14928–14937.

52 S. Gao, S. Hao, Z. Huang, Y. Yuan, S. Han, L. Lei, X. Zhang, R. Shahbazian-Yassar and J. Lu, *Nat. Commun.*, 2020, **11**, 2016.

View Article Online
DOI: 10.1039/D6CC01653G

53 P. Zhao, Q. Cao, W. Yi, X. Hao, J. Li, B. Zhang, L. Huang, Y. Huang, Y. Jiang, B. Xu, Z. Shan and J. Chen, *ACS Nano*, 2022, **16**, 14017–14028.

54 P. Zhao, X. Hao, H. Pi, Y. Qi, B. Zhang, C. Lei, J. Wang, N. Zhou, X. Chen, D. Kan, B. Xu, G. Zhang, J. Chen, W. Yi and Q. Cao, *Sci. Adv.*, 2025, **11**, eadq8537.

55 S. Wang, Q. Liu, S. Li, F. Huang and H. Zhang, *ACS Nano*, 2024, **18**, 5040–5050.

56 Y. Zhang, Z. Wang, L. Wang and L. Zong, *Small*, 2024, **20**, 2400892.

57 X. Cui, Y. Liu, X. Wang, X. Tian, Y. Wang, G. Zhang, T. Liu, J. Ding, W. Hu and Y. Chen, *ACS Nano*, 2024, **18**, 2948–2957.

58 Y. Wang, Y. Zhang, P. Xing, X. Li, Q. Du, X. Fan, Z. Cai, R. Yin, Y. Yao and W. Gan, *Adv. Mater.*, 2024, **36**, 2402391.

59 Y. Zou, L. Jing, J. Zhang, S. Luo, L. Wang, Y. Li, R. Goei, K. W. Tan and A. I. Yoong Tok, *J. Mater. Chem. A*, 2024, **12**, 5668–5678.

60 J. Ahn, S. Park, D. Oh, Y. Lim, J. S. Nam, J. Kim, W. Jung and I.-D. Kim, *ACS Nano*, 2023, **17**, 12188–12199.

61 P. Kunal and T. J. Toops, *Catalysts*, 2020, **10**, 991.

62 N. Hashimoto, R. Kitaura, K. Mori and H. Yamashita, *Chem. Lett.*, 2024, **53**, upad055.

63 J. B. Khan, P. K. Panda, P.-C. Yang, C.-T. Hsieh, Y. A. Gandomi, W.-R. Liu and J.-K. Chang, *Int. J. Hydrog. Energy*, 2024, **53**, 999–1008.

64 P. K. Panda, H.-Y. Huang, P. Dash, C.-T. Hsieh, J.-K. Chang and W.-R. Liu, *Int. J. Hydrog. Energy*, 2025, **111**, 536–545.

65 C. Ni, S. Guo, C. Butler and J. G. C. Veinot, *Nanoscale*, 2025, **17**, 6072–6078.

66 H. Zhao, M. Liu, Q. Wang, Y. Li, Y. Chen, Y. Zhu, Z. Yue, J. Li, G. Wang, Z. Zou, Q. Cheng and H. Yang, *Energy Environ. Sci.*, 2024, **17**, 6594–6605.

67 Y. Yang, Z. Jia, Q. Wang, Y. Liu, L. Sun, B. Sun, J. Kuang, S. Dai, J. He, S. Liu, L. Duan, H. Tang, L.-C. Zhang, J. J. Kruzic, J. Lu and B. Shen, *Energy Environ. Sci.*, 2024, 17, 5854–5865.

68 C. Wang, J. Zhang, K. Miao, M. Long, S. Lai, S. Zhao and X. Kang, *Adv. Mater.*, 2024, **36**, 2400433.

69 Z. Fu, P. Huang, X. Wang, W. Liu, L. Kong, K. Chen, J. Li and Y. Chen, *Adv. Energy Mater.*, 2025, **15**, 2500744.

70 Z. Li, H. Zhong, X. Liu, F. Chiang, R. Li, H. Chen, X. Wang, C. Wan, Y. Wu, H. Wang, S. Jiang, X. Zhang and Z. Lu, *Adv. Mater.*, 2025, **37**, e10703.

71 H. Wang, X. Wang, F. Gao, J. Chen, X. Ren, Z. Shen, K. Wang, F. Qi, Y. Liu, Y. Gao, Y. Yang, D. Wang, Z. Li, W. Cui and H. Pan, *Adv. Mater.*, 2026, **38**, e14269.

72 Z. Hu, K. Chen, Y. Zhu, B. Liu and J. Shen, *Small*, 2024, **20**, 2309819.

73 X. Li, J. Cao, G. Chen, J. Xie, C. Gu, X. Li, F. C. Walsh, Y. Wang and W. Hu, *ACS Nano*, 2025, **19**, 7851–7863.

View Article Online
DOI: 10.1039/D6CC01653G

74 Y. Yao, X.-K. Gu, D. He, Z. Li, W. Liu, Q. Xu, T. Yao, Y. Lin, H.-J. Wang, C. Zhao, X. Wang, P. Yin, H. Li, X. Hong, S. Wei, W.-X. Li, Y. Li and Y. Wu, *J. Am. Chem. Soc.*, 2019, **141**, 19964–19968.

75 Y. Zhu, M. Klingenhof, C. Gao, T. Koketsu, G. Weiser, Y. Pi, S. Liu, L. Sui, J. Hou, J. Li, H. Jiang, L. Xu, W.-H. Huang, C.-W. Pao, M. Yang, Z. Hu, P. Strasser and J. Ma, *Nat. Commun.*, 2024, **15**, 1447.

76 H. Chen, C. Guan and H. Feng, *ACS Appl. Nano Mater.*, 2022, **5**, 9810–9817.

77 M. Niu, Q. Guan, W. Yuan, C. X. Guo, D. Cao, C. M. Li, L. Y. Zhang and X. S. Zhao, *Chem. Eng. J.*, 2024, **503**, 158465.

78 X. Ma, Y. Zhou, S. Zhang, W. Lei, Y. Zhao and C. Shan, *Small*, 2025, **21**, 2411394.

79 P. Zhang, X. Hui, Y. Nie, R. Wang, C. Wang, Z. Zhang and L. Yin, *Small*, 2023, **19**, 2206742.

80 C. Zhan, Y. Xu, L. Bu, H. Zhu, Y. Feng, T. Yang, Y. Zhang, Z. Yang, B. Huang, Q. Shao and X. Huang, *Nat. Commun.*, 2021, **12**, 6261.

81 R. Nandan, H. Nara, H. N. Nam, Q. M. Phung, Q. P. Ngo, J. Na, J. Henzie and Y. Yamauchi, *Adv. Sci.*, 2024, **11**, 2402518.

82 H. Li, F. Yang, G. Wang, L. Guan, F. Lai, N. Zhang and T. Liu, *ACS Nano*, 2025, **19**, 14434–14444.

83 X. Ma, S. Zhang, Y. Zhou, W. Lei, Y. Zhai, Y. Zhao and C. Shan, *J. Mater. Chem. A*, 2024, **12**, 8862–8868.

84 Y. Sun, W. Zhang, Q. Zhang, Y. Li, L. Gu and S. Guo, *Matter*, 2023, **6**, 193–205.

85 W. Jiao, Z. Ren, Z. Cui, C. Ma, Z. Shang, G. Chen, R. Lu, T. Gan, Z. Wang, Y. Xiong and Y. Han, *Nat. Commun.*, 2025, **16**, 883.

86 X. Zhao, H. Cheng, X. Chen, Q. Zhang, C. Li, J. Xie, N. Marinkovic, L. Ma, J.-C. Zheng and K. Sasaki, *J. Am. Chem. Soc.*, 2024, **146**, 3010–3022.

87 Y. Yu, F. Xia, C. Wang, J. Wu, X. Fu, D. Ma, B. Lin, J. Wang, Q. Yue and Y. Kang, *Nano Res.*, 2022, **15**, 7868–7876.

88 Y. Wang, X.-Y. Zhang, H. He, J.-J. Chen and B. Liu, *Adv. Energy Mater.*, 2024, 14, 2470034.

89 H. Kuang, Z. Xu, X. Tan, K. Yu and C. Chen, *Small*, 2024, **20**, 2308421.

90 J.-F. Huang and P.-K. Tseng, *Chem. Sci.*, 2018, **9**, 6134–6142.

91 H. Jin, Z. Xu, Z.-Y. Hu, Z. Yin, Z. Wang, Z. Deng, P. Wei, S. Feng, S. Dong, J. Liu, S. Luo, Z. Qiu, L. Zhou, L. Mai, B.-L. Su, D. Zhao and Y. Liu, *Nat. Commun.*, 2023, **14**, 1518.

92 S. Wang, A. Lu and C.-J. Zhong, *Nano Converg.*, 2021, **8**, 4.

93 N.-T. Suen, S.-F. Hung, Q. Quan, N. Zhang, Y.-J. Xu and H. M. Chen, *Chem. Soc. Rev.*, 2017, **46**, 337–365.

94 S. Choi, S.-J. Kim, S. Han, J. Wang, J. Kim, B. Koo, A. A. Ryabin, S. Kunze, H. Hyun, J. Han, S.-C. Haw, K. H. Chae, C. H. Choi, H. Kim and J. Lim, *ACS Catal.*, 2024, **14**, 15096–15107.

DOI: 10.1039/D6CC01653G

95 S. Zhang, C. Tan, R. Yan, X. Zou, F.-L. Hu, Y. Mi, C. Yan and S. Zhao, *Angew. Chem. Int. Ed.*, 2023, **62**, e202302795.

96 T. Munawar, S. Fatima, A. Bashir, M. Rafaqat, J. Fan, M. M. Alam, M. Hussien, S. A. Khan, F. Iqbal and C.-F. Yan, *Int. J. Hydrog. Energy*, 2025, **144**, 536–547.

97 T. Reier, M. Oezaslan and P. Strasser, *ACS Catal.*, 2012, **2**, 1765–1772.

98 S. Geng, L. Wang, W. Yan, C. Zhan, Y. Li, X. Huang and L. Bu, *Nano Lett.*, 2025, **25**, 1010–1018.

99 M. Liu, Z. Zhao, X. Duan and Y. Huang, *Adv. Mater.*, 2019, **31**, 1802234.

100 L. Zhang, S. Jiang, W. Ma and Z. Zhou, *Chin. J. Catal.*, 2022, **43**, 1433–1443.

101 T. Shen, S. Chen, R. Zeng, M. Gong, T. Zhao, Y. Lu, X. Liu, D. Xiao, Y. Yang, J. Hu, D. Wang, H. L. Xin and H. D. Abruña, *ACS Catal.*, 2020, **10**, 9977–9985.

102 X. Hu, Z. Xiao, W. Wang, L. Bu, Z. An, S. Liu, C. Pao, C. Zhan, Z. Hu, Z. Yang, Y. Wang and X. Huang, *J. Am. Chem. Soc.*, 2023, **145**, 15109–15117.

103 A. Cuesta, G. Cabello, M. Osawa and C. Gutiérrez, *ACS Catal.*, 2012, **2**, 728–738.

104 C. Zhan, L. Bu, H. Sun, X. Huang, Z. Zhu, T. Yang, H. Ma, L. Li, Y. Wang, H. Geng, W. Wang, H. Zhu, C.-W. Pao, Q. Shao, Z. Yang, W. Liu, Z. Xie and X. Huang, *Angew. Chem. Int. Ed.,* 2023, **62**, e202213783.

105 F. Si, S. Wang, Y. Zhang, R. Xue, Y. Lv, G. Chen and D. Gao, *Chem. Eng. J.*, 2024, **494**, 153213.

106 W. Cheng, C. Sun, W. Liu and Z. Wang, *Langmuir*, 2024, **40**, 2343–2351.

107 T. Shen, D. Xiao, Z. Deng, S. Wang, L. An, M. Song, Q. Zhang, T. Zhao, M. Gong and D. Wang, *Angew. Chem. Int. Ed.*, 2024, **63**, e202403260.

108 X. Zuo, R. Yan, L. Zhao, Y. Long, L. Shi, Q. Cheng, D. Liu and C. Hu, *J. Mater. Chem. A*, 2022, **10**, 14857–14865.

109 R. Yu, Y. Zhang, S. Deng, R. Zhu, S. Zhang, J. Zhang, Y. Zhao and Z. Xia, *Catalysts*, 2024, **14**(1), 60.

110 J. Huang, Y. Liu, M. Xu, C. Wan, H. Liu, M. Li, Z. Huang, X. Duan, X. Pan and Y. Huang, *Nano Lett.*, 2019, **19**, 5431–5436.

111 K. Siddharth, Z. Xing, F. Xiao, S. Zhu, L. Zhang, F. Pan and M. Shao, *Chem. Asian J.*, 2020, **15**, 2174–2180.

112 Y. Lv, L. Lin, R. Xue, P. Zhang, F. Ma, T. Gan, J. Zhang, D. Gao, X. Zheng, L. Wang, Y. Qin, H. Zhao, Y. Dong, Y. Wang and Y. Zhu, *Adv. Energy Mater.*, 2024, **14**, 2304515.

113 X. Lao, X. Liao, C. Chen, J. Wang, L. Yang, Z. Li, J. Ma, A. Fu, H. Gao and P. Guo, *Angew. Chem. Int. Ed.*, 2023, **62**, e202304510.

114 M. Hu, J. Li, T. Liu, Z. Wu and Y. Du, *J. Colloid Interface Sci.*, 2024, **675**, 481–487.

115 Y. Wang, H. Meng, R. Yu, J. Hong, Y. Zhang, Z. Xia and Y. Wang, *Angew. Chem. Int. Ed.*, 2025, **64**, e202420752.

View Article Online
DOI: 10.1039/D6CC01653G

116 J. Yang, D. Si, L. Yang, H. Chen, R. He, C. Wang, W. Huang, F. Kang, Z. Liu, Y. Xiao, T. Wang, Z. Deng, J. Ge, Z. Hu, A. Cabot, J. Hou, L. Wang, A. K. Cheetham and T. Tian, *Angew. Chem. Int. Ed.*, 2025, **64**, e202518458.

117 M. Liu, Z. Zhang, C. Li, S. Jin, K. Zhu, S. Fan, J. Li and K. Liu, *Nat. Commun.*, 2025, **16**, 6359.

118 J. Chang, G. Wang, C. Li, Y. He, Y. Zhu, W. Zhang, M. Sajid, A. Kara, M. Gu and Y. Yang, *Joule*, 2023, **7**, 587–602.

119 Z. Li, R. Wu, L. Zhao, P. Li, X. Wei, J. Wang, J. Chen and T. Zhang, *Nano Res.*, 2021, **14**, 3795–3809.

120 M. Shi, D. Bao, S. Li, B. Wulan, J. Yan and Q. Jiang, *Adv. Energy Mater.*, 2018, **8**, 1800124.

121 Z. Yu, X. Wei, J. Xu, Y. Li, A. Araujo, J. Faria, R. Dunin-Borkowski and L. Liu, *ACS Appl. Energy Mater.*, 2021, **4**, 1593–1600.

122 W. Liu, W. You, Y. Gong and Y. Deng, *Energy Environ. Sci.*, 2020, **13**, 917–927.

123 J. Luo, X. Li, Y. Ye, T. Zhou, W. Wu, H. Li, Q. Yang, H. Yan and J. Zeng, *Angew. Chem. Int. Ed.*, 2025, **64**, e202419093.

124 N. Zhang, X. Chen, S. Liu, J. Meng, M. Armbrüster and C. Liang, *ACS Appl. Mater. Interfaces*, 2023, **15**, 23276–23285.

125 F. Lu, K. Lu, G. Zhao, S. Zhou, B. He, Y. Zhang, J. Xu, Y. Li, X. Liu and L. Chen, *RSC Adv.*, 2022, **12**, 19869–19874.

126 H. Wang, Z. Huang, X. Chen, J. Ma, Y. Wang and C. Liang, *Fuel*, 2025, **393**, 135002.

127 G. Cao, S. Yang, J.-C. Ren and W. Liu, *Nat. Commun.*, 2025, **16**, 1251.

128 J. Cai and H. Zhu, *Commun. Mater.*, 2025, **6**, 118.

129 M. J. Marks, P. Gyenes and R. K. Pittkowski, *Electrochimica Acta*, 2026, **557**, 148495.

130 C. Cai, Z. Xin, X. Zhang, J. Cui, H. Lv, W. Ren, C. Gao and B. Cai, *Catalysts*, 2022, **12**, 1050.

131 A. Li, N. Qureshi and V. Maheshwari, *Nanoscale*, 2025, **17**, 20020–20043.

132 V. M. Jiménez-Arévalo, P. Martin, M. F. Sepúlveda, M. I. Azocar, X. Zhou, F. M. Galleguillos Madrid, C. G. Ramirez, J. H. Zagal and M. Páez, *Mater. Des.*, 2025, **258**, 114633.

133 T. Chen, C. Qiu, X. Zhang, H. Wang, J. Song, K. Zhang, T. Yang, Y. Zuo, Y. Yang, C. Gao, W. Xiao, Z. Jiang, Y. Wang, Y. Xiang and D. Xia, *J. Am. Chem. Soc.*, 2024, **146**, 1174–1184.

134 G. Feng, F. Ning, Y. Pan, T. Chen, J. Song, Y. Wang, R. Zou, D. Su and D. Xia, *J. Am. Chem. Soc.*, 2023, **145**, 11140–11150.

135 X. Han, G. Wu, S. Zhao, J. Guo, M. Yan, X. Hong and D. Wang, *Matter*, 2023, **6**, 1717–1751.

136 J.-T. Ren, L. Chen, H.-Y. Wang and Z.-Y. Yuan, *Chem. Soc. Rev.*, 2023, **52**, 8319–8373.

View Article Online
DOI: 10.1039/D6CC01653G

137 M. Li, F. Lin, S. Zhang, R. Zhao, L. Tao, L. Li, J. Li, L. Zeng, M. Luo and S. Guo, *Sci. Adv.*, 2024, **10**, eadn2877.

138 T.-H. Hu, C.-Y. Wu, Z. Y. He, Y. Chen, L.-C. Hsu, C.-W. Pao, J.-T. Lin, C.-W. Chang, S.-C. Lin, R. Osmundsen, L. Casalena, K. H. Lin, S. Zhou and T.-H. Yang, *Adv. Sci.*, 2025, **12**, 2409023.

139 L. Sun, K. Wen, G. Li, X. Zhang, X. Zeng, B. Johannessen and S. Zhang, *ACS Mater. Au*, 2024, **4**, 547–556.

140 J. Zhu, J. Ruan, W. Wu, Y. Huang, X. Liu, Z. Chen and B.-J. Ni, *Energy Environ. Mater.*, 2025, **0**, e70178.

141 S. Han, L. Xu, C. Ma, W. Cao and Q. Lu, *J. Mater. Chem. A*, 2025, **13**, 28019–28025.

142 D.-H. Mok, H. Li, G. Zhang, C. Lee, K. Jiang and S. Back, *Nat. Commun.*, 2023, **14**, 7303.

143 D.-H. Mok, Y. Yan, G. Yu, Y. Li, K. Jiang and S. Back, *ACS Catal.*, 2026, DOI: 10.1021/acscatal.5c07832.

View Article Online
DOI: 10.1039/D6CC01653G

Data Availability Statement

No primary research results, software or code have been included and no new data were generated or analysed as part of this review.